Louisiana Transportation Research Center

Final Report 650

Load Rating of Existing Continuous Stringers on Louisiana's Bridges

by

C. Shawn Sun
Louisiana Tech University

Daniel G. Linzell
Jay A. Puckett
University of Nebraska-Lincoln

4101 Gourrier Avenue | Baton Rouge, Louisiana 70808
(225) 767-9131 | (225) 767-9108 fax | www.ltrc.lsu.edu

TECHNICAL REPORT STANDARD PAGE

1. Title and Subtitle
   Load Rating of Existing Continuous Stringers on Louisiana's Bridges
2. Author(s)
   C. Shawn Sun, Daniel G. Linzell, and Jay A. Puckett
3. Performing Organization Name and Address
   Civil Engineering Program
   Louisiana Tech University
   Ruston, LA 71272
4. Sponsoring Agency Name and Address
   Louisiana Department of Transportation and Development
   P.O. Box 94245
   Baton Rouge, LA 70804-9245
5. Report No.
   FHWA/LA.19/650
6. Report Date
   October 2021
7. Performing Organization Code
   LTRC Project Number: 18-4ST
   SIO Number: DOTLT1000222
8. Type of Report and Period Covered
   Final Report
   06/2018 – 4/2021
9. No. of Pages
   277
10. Supplementary Notes
    Conducted in Cooperation with the U.S. Department of Transportation, Federal Highway Administration
11. Distribution Statement
    Unrestricted. This document is available through the National Technical Information Service, Springfield, VA 21161.
12. Key Words
    Moment gradient factor, load rating, continuous stringers
13. Abstract

Some of Louisiana's bridges built in the 1950s and 1960s used two-girder or truss systems, in which floor beams are carried by main members and continuous (spliced) stringers are supported by the floor beams. The main members are either two edge (fascia) girders or trusses. Stringer bottom flanges are in compression at the negative moment region, which could result in lateral torsional buckling. When the continuous stringers are load-rated using AASHTOWare Bridge Rating ™ analysis software, C_b is calculated in accordance with the *AASHTO LRFD Bridge Design Specifications*, which does not properly account for the bracing effect of non-composite deck and therefore underestimates the flexural strength. As a result, the rating may become low enough to require restrictive load posting or even closure. This issue affects bridges that are key parts of Louisiana's highway system. The current load rating would cause expensive (and possibly unnecessary) bridge rehabilitation or replacement with significant disruption for the traveling public. This project reassesses the methodology behind load rating the stringers, with efforts focusing on more realistic values for C_b. The project objective was to evaluate the capacity of the aforementioned bridges built with continuous stringers and to develop a new approach for rating those stringers by more accurately representing moment gradients using C_b.

Project Review Committee

Each research project will have an advisory committee appointed by the LTRC Director. The Project Review Committee is responsible for assisting the LTRC Administrator or Manager in the development of acceptable research problem statements, requests for proposals, review of research proposals, oversight of approved research projects, and implementation of findings.

LTRC appreciates the dedication of the following Project Review Committee Members in guiding this research study to fruition.

LTRC Administrator/Manager

Walid R. Alaywan, Ph.D., P.E.
Senior Structures Research Engineer

Members

Dana Feng, Ph.D., P.E.
Mark Bucci, P.E.
Nick Fagerburg, P.E.
Alden Allen, P.E.
Kelly Kemp, P.E.
William Metcalf, P.E.
Kian Yap, P.E.
Michael Boudreaux, P.E.
Art Aguirre, P.E.

Directorate Implementation Sponsor

Christopher P. Knotts, P.E.
DOTD Chief Engineer

Load Rating of Existing Continuous Stringers on Louisiana's Bridges

By
C. Shawn Sun
Civil Engineering Program
Louisiana Tech University
Ruston, LA 71272

Daniel G. Linzell
Department of Civil Engineering
University of Nebraska-Lincoln
Lincoln, NE 68588

Jay A. Puckett
Durham School of Architectural Engineering and Construction
University of Nebraska-Lincoln
Omaha, NE 68182

LTRC Project No. 18-4ST
SIO No. DOTLT1000222

conducted for
Louisiana Department of Transportation and Development
Louisiana Transportation Research Center

October 2021

Abstract

Some of Louisiana's bridges built in the 1950s and 1960s used two-girder or truss systems in which floor beams are carried by main members and continuous (spliced) stringers are supported by the floor beams. The main members are either two edge (fascia) girders or trusses. Stringer bottom flanges are in compression at the negative moment region, which could result in lateral torsional buckling. When the continuous stringers are load-rated using AASHTOWare Bridge Rating™ analysis software, C_b is calculated in accordance with the *AASHTO LRFD Bridge Design Specifications*, which does not properly account for the bracing effect of non-composite deck and therefore underestimates the flexural strength. As a result, the rating may become low enough to require restrictive load posting or even closure. This issue affects bridges that are key parts of Louisiana's highway system. The current load rating would cause expensive (and possibly unnecessary) bridge rehabilitation or replacement with significant disruption for the traveling public. This project reassesses the methodology behind load rating the stringers, with efforts focusing on more realistic values for C_b. The project objective was to evaluate the capacity of the aforementioned bridges built with continuous stringers and to develop a new approach for rating those stringers by more accurately representing moment gradients using C_b.

Acknowledgments

The investigators would like to thank the Louisiana Transportation Research Center (LTRC) and the Louisiana Department of Transportation and Development (DOTD) for funding this project. The investigators are grateful to the Project Review Committee Members for their guidance and support. Special thanks go to Walid R. Alaywan, Ph.D., for his leadership and project management.

Implementation Statement

This project proposes a more realistic moment gradient factor for the rating of continuous stringers via improving the estimated capacity of continuous stringers on floor beams. The work provides an improved approach for load rating that mitigates unnecessary posting or rehabilitation while allowing better allocation of resources and maintaining safety. The findings are a candidate for inclusion in the DOTD rating manual.

Table of Contents

List of Tables

List of Figures

Introduction

Some of the Louisiana's bridges built in the 1950s and 1960s used two-girder or truss systems in which floor beams are carried by main members and continuous (spliced) stringers are supported by the floor beams. The main members are either two edge (fascia) girders (Figure 1) or trusses (Figure 2). In accordance with *Bridge Design and Evaluation Manual* by the Louisiana Department of Transportation and Development (DOTD) [1], all bridges shall be rated using the Load and Resistance Factor Rating (LRFR) method as specified in the American Association of State Highway Officials (AASHTO) *Manual for Condition Evaluation and Load Resistance Factor Rating (LRFR) of Highway Bridges*, referred to as the MBE [2]. LRFR is consistent with the *AASHTO LRFD Bridge Design Specifications* (LRFD Specifications) via use of a reliability-based limit state philosophy and extends the provisions of the LRFD Specifications to load rating [3]. The general LRFR rating equation (MBE Eq. 6A. 4.2.1-1) is given as:

$$RF = \frac{\emptyset_c \emptyset_s \emptyset R_n - (\gamma_{DC})(DC) - (\gamma_{DW})(DW) \pm (\gamma_P)(P)}{(\gamma_L)(LL+IM)} \quad (1)$$

In the context of this research project, stringers shall be evaluated for the strength, service, and fatigue limit states subject to various loads. As-designed bridge ratings shall include the inventory and operating ratings for the HL-93 and the inventory rating for the LADV-11 truckloads. If the inventory rating for the HL-93 is less than 1.0, additional rating for all legal trucks shall be provided. State legal load rating trucks include the LA Type 3, LA Type 3-S2, AASHTO Type 3-3, LA Type 6, and LA Type 8 vehicles. Specialized hauling vehicle ratings use the Notional Rating Load (NRL) as the screening vehicle. If the NRL rating factor is less than 1.0, additional ratings for posting vehicles SU4, SU5, SU6, and SU7 are needed.

In Equation (1), R_n is the nominal flexural resistance of the stringers. When the flexural resistance of an I-section stringer is determined, both local buckling and lateral torsional buckling (LTB) are accounted for in the LRFD Specifications. LTB may often control the resistance used for load rating. The LRFD Specifications provide LTB resistance as derived for uniform, major-axis bending moment. A moment gradient factor, C_b, is applied to account for the effects of variable moment along an unbraced length. The LTB resistance is capped at F_{max} or M_{max}, as illustrated by the dashed line in Figure 3 [3]. R_n is given by the following equation, where F_{nc} represents the nominal flexural resistance of a member:

$$F_{nc} = C_b \left[1 - \left(1 - \frac{F_{yr}}{R_h F_{yc}}\right)\left(\frac{L_b - L_p}{L_r - L_p}\right)\right] R_b R_h F_{yc} \leq R_b R_h F_{yc} \quad (2)$$

As shown in this equation, C_b directly affects the estimated flexural strength of the stringer, and therefore, the load rating.

AASHTOWare Bridge Rating (BrR) and Bridge Design (BrD) are mandated as software to be used for DOTD projects. BrR can perform superstructure load rating in accordance with the MBE and LRFD Specifications and, as a result, provides the default analytical engine for LRFR. BrR can address various structures, including girder-floor stringer-stringer configurations and truss-floor stringer-stringer configurations. When stringers are load rated, C_b is calculated in accordance with the *AASHTO LRFD Bridge Design Specifications*, which does not account for the bracing effect of non-composite deck properly and therefore underestimates the flexural strength. As a result, the rating may be low enough to require restrictive live load posting or even closure. This issue affects bridges that are key elements of the Louisiana's highway system. Current continuous stringer load ratings based on this approach could result in expensive (and possibly unnecessary) bridge rehabilitation or replacement that costs hundreds of millions of dollars and causes significant disruption to the traveling public. Therefore, there is an immediate need for re-assessment of the methodology behind load rating continuous stringers, with efforts focusing on developing more realistic values for C_b.

Figure 1. Sample floor system, fascia girder

Figure 2. Sample floor system, truss

Figure 3. Generalized I-section flexural resistance curves [3]

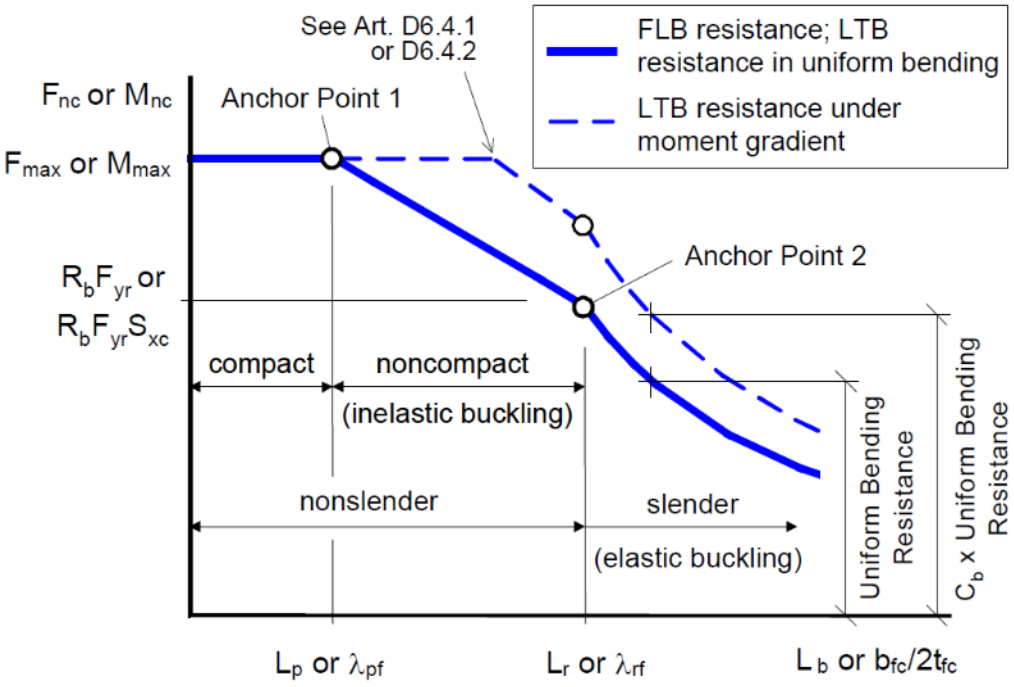

Literature Review

The research team conducted a literature review of relevant domestic and international guidelines and specifications as well as other publications. The team collected the information by accessing available sources, including the Transportation Research Board's Transportation Research Information Services (TRIS) database and other databases such as Web of Science. The focus of this research is related to I-shaped stringers having doubly symmetric sections and primarily subject to vertical loading. Several significant references associated with the development of C_b and lateral bracing provided by bridge decks are discussed herein.

Moment Gradient Factor Cb

Several specifications and codes are presented, including the *AASHTO LRFD Bridge Design Specifications*, the *AISC Steel Construction Manual*, the *Canadian Highway Bridge Design Code,* the *Australian Steel Code*, the *British Standards Structural Use of Steelwork in Building*, and the *Japanese Standard Specifications for Steel and Composite Structures*. In addition, work by several significant researchers is included. Each section presents relevant background discussions and equations for the moment gradient factor followed by definitions of primary parameters.

1) AASHTO LRFD Bridge Design Specifications, Eighth Edition, 2017 [3]

LTB equations in the *AASHTO LRFD Bridge Design Specifications* give predictions close to mean LTB resistances from uniform bending experimental tests conducted by Galambos and Ravindra in 1978 [4]. For members subject to a moment gradient, the factor is included primarily following research work performed by Salvadori [5]. For continuous stringers supported by floor beams, C_b can be greater than 1.0 using Equation (3).

$$C_b = 1.75 - 1.05\left(\frac{f_1}{f_2}\right) + 0.3\left(\frac{f_1}{f_2}\right)^2 \leq 2.3 \qquad (3)$$

where,

f_1= stress without consideration of lateral bending at the brace point opposite to the one corresponding to f_2, calculated as the intercept of the most critical assumed linear stress variation passing through f_2 and either f_{mid} or f_0, whichever produces the smaller value of

C_b. When variation in the moment along the entire length between the brace points is concave in shape, $f_1 = f_0$ (Figure 4); otherwise, $f_1 = 2f_{mid} - f_2 \geq f_0$.

f_2 = largest compressive stress without consideration of lateral bending at either end of the unbraced length of the flange under consideration, calculated from the critical moment envelope value. f_2 shall be due to the factored loads and shall be taken as positive. If the stress is zero or tensile in the flange under consideration at both ends of the unbraced length, f_2 shall be taken as zero.

Figure 4. Examples f_1 calculations, concave moment diagrams [3]

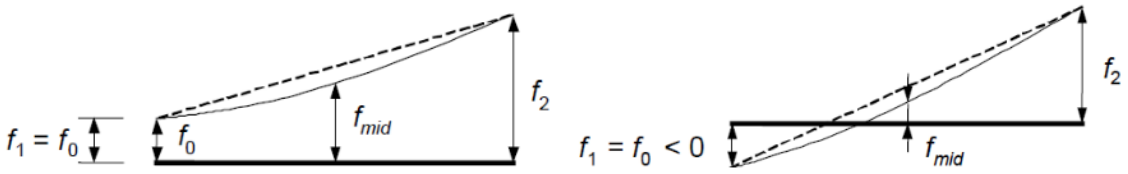

Case 1) f_0 and f_2 have the same sign

Case 2) f_0 and f_2 have the opposite sign

It is convenient and always conservative to use extreme moment values to compute the stresses in Equation (3). However, strict application of C_b would require consideration of concurrent moments along the unbraced length. This would necessitate calculation of: 1) the maximum possible value of f_2 at the brace point having the higher compressive stress using the critical moment envelope value, along with calculation of f_0 and f_{mid} using concurrent moments; and 2) the maximum possible compressive value of f_{mid} using the critical moment envelope value, along with the calculation of f_0 and f_2 using the concurrent moments. The use of the concurrent moments normally provides a larger value of C_b, which is likely more accurate when determining flexural resistance.

2) AISC Steel Construction Manual, 2017 [6]

The *AISC Steel Construction Manual* provides the lateral-torsional buckling modification factor, C_b, for non-uniform moment diagrams primarily based on the research work by Kirby and Nethercot with slight modifications [7]. C_b is determined as follows:

$$C_b = \frac{12.5M_{max}}{2.5M_{max}+3M_A+4M_B+3M_C} \quad (4)$$

where,

M_{max} = absolute value of maximum moment in the unbraced segment;

M_A = absolute value of moment at quarter point of the unbraced segment;

M_B = absolute value of moment at center of the unbraced segment; and

M_C = absolute value of moment at three-quarter point of the unbraced segment.

This equation is applicable to linear and nonlinear moment diagrams. It provides a more accurate solution for unbraced lengths in which the moment diagram deviates substantially from a straight line, such as the case of a fixed-end stringer with no lateral bracing within the span, subjected to a uniformly distributed transverse load.

3) Canadian Highway Bridge Design Code, S6-14 [8]

In accordance with the *Canadian Highway Bridge Design Code*, structural sections shall be designated as Class 1, 2, 3, or 4 depending on width-to-thickness ratios of the elements that make up the cross-section and on loading conditions. A Class 1 section is one that will attain the plastic moment capacity, adjusted for the presence of axial force if necessary, and permit subsequent redistribution of bending moment. A Class 2 section is one that will attain the plastic moment capacity, adjusted for the presence of axial force if necessary, but not necessarily permit subsequent moment redistribution. A Class 3 section is one that will attain the yield moment capacity, adjusted for the presence of axial force if necessary. A Class 4 section is one in which the slenderness of the elements making up the cross-section exceeds the limits of Class 3.

For Class 1 and Class 2 sections subjected to bending about their major axes that are laterally unbraced over a length, L, the factored resistance, M_r, shall be calculated as:

$$M_r = 1.15\emptyset_s M_p \left[1 - \frac{0.28M_p}{M_u}\right] \leq \emptyset_s M_p \text{ when } M_u > 0.67M_p \quad (5)$$

or

$$M_r > \emptyset_s M_u \text{ when } M_u \leq 0.67M_p \quad (6)$$

where,

M_p = plastic moment resistance; and
M_u = critical elastic moment of a laterally unbraced stringer.

For doubly symmetric sections,

$$M_u = \frac{w_2\pi}{L}\sqrt{E_s I_y G_s J + \left[\frac{\pi E_s}{L}\right]^2 I_y C_w} \quad (7)$$

The moment gradient factor, $w_2 = \frac{4M_{max}}{\sqrt{M_{max}^2+4M_a^2+7M_b^2+4M_c^2}} \leq 2.5$ (8)

where,

M_{max} = maximum absolute value of factored moment in the unbraced segment;
M_a = factored bending moment at one-quarter point of the unbraced segment;
M_b = factored bending moment at midpoint of the unbraced segment; and
M_c = factored bending moment at three-quarter point of the unbraced segment.

For a Class 3 section, the factored resistance, M_r, can be calculated similarly to Eqs. (5) and (6) by replacing M_p by M_y, Where M_y is the yield moment.

4) Australian Steel Code AS4100 [9]

The flexural resistance curve for stringers in the Australian code is an approximate lower-bound fit to LTB test data. The nominal lateral buckling moment strength, M_b, of an I-section is given by

$$M_b = \alpha_m \alpha_s M_p \quad (9)$$

where,

M_p = major axis full plastic moment;
α_m = moment modification factor which allows for non-uniform moment distributions ($\alpha_m = 1.0$ for uniform bending); and
α_s = slenderness reduction factor, which allows for the effects of elastic buckling, initial crookedness and twist, and residual stresses.

$$\alpha_s = 0.6\left\{\sqrt{\left[\left(\frac{M_{px}}{M_{yz}}\right)^2 + 3\right]} - \frac{M_{px}}{M_{yz}}\right\} \leq 1.0 \quad (10)$$

where,

M_{yz} = elastic buckling moment of a simply supported stringer in uniform bending given by

$$M_{yz} = \sqrt{\frac{\pi^2 E I_y}{L^2}\left(GJ + \frac{\pi^2 E I_w}{L^2}\right)} \quad (11)$$

where,

E and G = Young's and shear moduli of elasticity;
I_y, J, and I_W = minor axis second moment of area, the uniform torsion section constant; and the warping section constant, respectively; and
L = length of the stringer.

AS4100 provides Equation (12) to determine an equivalent uniform moment factor or moment modification factor, α_m, for stringers where β is the ratio of the two end moments. It also allows simple approximation using Equation (13) that applies to any bending moment distribution.

$$\alpha_m = 1.75 + 1.05\beta + 0.3\beta^2 \leq 2.5 \quad (12)$$

$$\alpha_m = \frac{1.7M_m}{\sqrt{(M_2)^2+(M_3)^2+(M_4)^2}} \leq 2.5 \quad (13)$$

where,

M_m = maximum design bending moment;
M_2, M_4 = design bending moments at the quarter points; and
M_3 = design bending moment at the midpoint of the segment.

5) British Standards Institution (BSI), Structural Use of Steelwork in Building, BS 5950-1:2000 [10]

In the British code, the flexural resistance of I-stringers with equal flanges should satisfy the following:

$$M_x \leq M_b/m_{LT} \text{ and } M_x \leq M_{cx} \quad (14)$$

where,

M_b = buckling resistance moment;
M_{cx} = major axis moment capacity of the cross section;
M_x = maximum major axis moment in the segment; and
m_{LT} = equivalent uniform moment factor for lateral torsional buckling.

$$m_{LT} = 0.2 + \frac{0.15M_2+0.5M_3+0.15M_4}{M_{max}} \geq 0.44 \quad (15)$$

All moments are taken as positive. The moment M_2 and M_4 are the values at the quarter points, M_3 is the value at mid-length and M_{max} is the maximum moment in the segment (Figure 5).

Figure 5. Illustration of moments at various locations

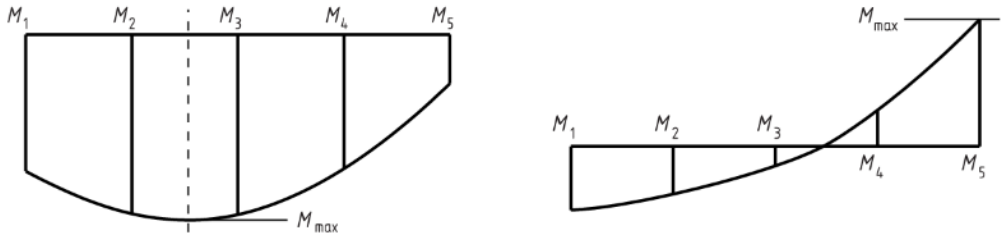

6) Japanese Standard Specifications for Steel and Composite Structures, 2007 [11]

The bending resistance of steel members in the Japanese specification is determined based on the nominal bending resistance corresponding to classification of a cross section, considering influence of the initial deflection, residual stress, and elastic lateral torsional buckling. The bending resistance is directly related to the slenderness ratio of the stringer, which depends on the parameter M_E as specified in Equation (16). M_E accounts for an equivalent moment factor, C_{b1}.

$$M_E = \frac{C_{b1}\pi^2 EI_y}{l^2}\left[C_{b2}h_t + C_{b3}\beta_z + \sqrt{(C_{b2}h_t + C_{b3}\beta_z)^2 + \frac{1}{\gamma}\frac{I_w}{I_y}\left(1 + \frac{l^2 GJ}{\pi^2 EI_w}\right)}\right] \quad (16)$$

$$\gamma = 1 - \frac{I_y}{I_x} \quad (17)$$

where,

M_E = Elastic transverse torsional buckling moment of a simply supported stringer. When the loading condition is different from this, eigenvalue analysis for elastic buckling may be used to obtain the transverse torsional buckling moment;

I_y, I_z = Moment of inertia with respect to the weak and strong axes, respectively;
J = St. Venant's torsion constant;
I_w = Warping torsion constant;
L = Length of a simply supported stringer for out-of-plane deformation;
C_{b1} = Equivalent moment factor;

$$C_{b1} = \frac{1.0}{0.6+0.4\beta} \leq 2.5 \quad (18)$$

$$\beta = \frac{M_2}{M_1} \tag{19}$$

M_1, M_2 = Bending moments at each end of member, where $M_1 \geq M_2$. The sign of the bending moment is to be taken as positive when compressive stress occurs in the flange;
h_t = Distance between the position at which load acts (height) and the shear center. The sign shall be taken as positive when the position at which the load acts is closer to the tension side in bending than the shear center;
C_{b2} = Coefficient for correcting the effect of the position at which the load acts on the stringer according to the loading condition;
β_z = Coefficient expressing the asymmetry of the cross section; and
C_{b3} = Coefficient for correcting the effect of the asymmetric cross section according to the loading condition.

7) Research by Lopez et al. [12]

Lopez et al. proposed a closed form expression for the equivalent uniform moment factor, C_1, applicable to any moment distribution. The proposed formula incorporates end support conditions through a parameter related to the lateral torsional buckling length of the stringer. For a general moment diagram, the coefficient C_1 may be obtained by:

$$C_1 = \frac{\sqrt{\sqrt{k}A_1 + \left[\frac{(1-\sqrt{k})A_2}{2}\right]^2} + \frac{(1-\sqrt{k})A_2}{2}}{A_1} \tag{20}$$

where k depends on the lateral bending and warping condition coefficients k_1 and k_2:

$$k = \sqrt{k_1 k_2} \tag{21}$$

and A_1 and A_2 are given by:

$$A_1 = \frac{M_{max}^2 + \alpha_1 M_1^2 + \alpha_2 M_2^2 + \alpha_3 M_3^2 + \alpha_4 M_4^2 + \alpha_5 M_5^2}{(1+\alpha_1+\alpha_2+\alpha_3+\alpha_4+\alpha_5) M_{max}^2} \tag{22}$$

$$A_2 = \left| \frac{M_1 + 2M_2 + 3M_3 + 2M_4 + M_5}{9M_{max}} \right| \tag{23}$$

where,

$$\alpha_1 = 1 - k_2; \quad \alpha_2 = 5\frac{k_1^3}{k_2^2}; \quad \alpha_3 = 5\left(\frac{1}{k_1} + \frac{1}{k_2}\right); \quad \alpha_4 = 5\frac{k_2^3}{k_1^2}; \; \alpha_5 = 1 - k_1 \tag{24}$$

In Eqs. (22) and (23), M_{max} is the maximum moment, and M_1, M_2, M_3, M_4, and M_5 are the values of the moment at different sections of the stringer, each of them with the corresponding sign.

8) Research by Subramanian and White [13]

The LTB curves in AASHTO [3] and AISC [6] are based in large part on unified provisions proposed by White [14], which were in turn based largely on experimental data compiled by White and Jung [15] and White and Kim [16]. A recent study by Subramanian et al. demonstrated that rolled I-stringers may exhibit an inelastic C_b effect. This essentially means that, when the inelastic LTB strength is scaled by the modification factor C_b (where C_b is developed based on elastic buckling formulations), strength estimates tend to be higher than the true inelastic LTB strength under a moment gradient. Subramanian et al. concluded that when the maximum moment in a span occurs at a braced location, the proposed LTB model for uniform moment, along with current handling of C_b in the AASHTO and AISC, is satisfactory and no modifications were proposed for such cases. When the maximum moment occurs within an unbraced segment of the stringer, it was shown that the current AISC specification moment modifier in the inelastic LTB region can be as much as 20% not conservative. The SABRE2 computational tool was also developed to implicitly and rigorously capture moment gradient effects based on applied loading as well as any unbraced length end-restraint effects.

9) Research by Helwig et al. [17]

Helwig et al. suggested multiplying the original equation for C_b from Kirby and Nethercot by the terms $1.4^{2y/h}$ to account for the effects of load height within the cross-section and by R to account for effects of I-section monosymmetry and reverse curvature bending in prismatic members. The term $1.4^{2y/h}$ considers destabilizing or tipping effect of loads applied transversely to the top flange, or the stabilizing or restoring effect of loads applied transversely to the bottom flange. If one or more intermediate braces are provided within an ordinary or cantilever span in which the ends are prevented from twisting, load height effects do not need to be considered in the calculation of C_b.

$$C_b = \frac{12.5M_{max}}{2.5M_{max}+3M_A+4M_B+3M_C}\left(1.4^{2y/h}\right)R \tag{25}$$

where,

$M_{\max}$ = absolute value of the maximum moment within the unbraced length;
M_A, M_B, and M_C = absolute values of the moments at the 1/4, middle, and 3/4 points of

the unbraced segment;
y = distance from the mid-depth of the cross section to the point of the load application, which is taken as negative for downward loads applied above mid-depth and positive for downward loads applied below mid-depth;
h = distance between the compression and tension flange centroids; and
R = 1.0 for beams with single-curvature bending.

For reverse-curvature bending,

$$R = 0.5 + 2\left(\frac{I_{y\,Top}}{I_y}\right)^2 \quad (26)$$

where,

$I_{y\,Top}$ = moment of inertia of the top flange about an axis in the plane of the web; and
I_y = moment of inertia of the entire section about an axis in the plane of the web.

10) Research by Salvadori [18]

Beginning with the 1961 AISC Manual and continuing through the 1986 AASHTO LRFD Specifications, Equation (27) was used to adjust lateral-torsional buckling equations for variations in the moment diagram within an unbraced length.

$$C_b = 1.75 + 1.05\left(\frac{M_1}{M_2}\right) + 0.3\left(\frac{M_1}{M_2}\right)^2 \leq 2.3 \quad (27)$$

where,

M_1 = smaller moment at end of unbraced lengths;
M_2 = larger moment at end of unbraced lengths; and
(M_1/M_2) is positive when moments cause reverse curvature and negative for single curvature.

11) Research by Wong and Driver [19]

Wong and Driver reviewed several approaches and recommend the following quarter-point equation for use with doubly symmetric I-shaped members:

$$C_b = \frac{4M_{max}}{\sqrt{{M_{max}}^2 + 4{M_A}^2 + 7{M_B}^2 + 4{M_c}^2}} \quad (28)$$

The equation gives improved predictions for several important cases, including cases with moderately nonlinear moment diagrams. Also, the length between braces, not the distance to inflection points, is used in all cases.

12) Research by Yura and Helwig [20] [21]

Many situations arise where a stringer may be subjected to reverse curvature bending with one of the flanges continuously braced laterally by closely spaced joists and/or light gauge decking normally used for roofing or flooring systems. Although this type of lateral bracing provides significant restraint to one of the flanges, the other flange can still buckle laterally due to compression caused by the reverse curvature bending. For gravity loaded, rolled I–section stringers with the top flange laterally restrained, the following expression is applicable:

$$C_b = 3.0 - \frac{2}{3}\left(\frac{M_1}{M_0}\right) - \frac{8}{3}\left[\frac{M_{CL}}{(M_1+M_0)^*}\right] \quad (29)$$

where,

M_0 = moment at the end of the unbraced length that gives the largest compressive stress in the bottom flange;
M_1 = moment at other end of the unbraced length;
M_{CL}= moment at the middle of the unbraced length; and
$(M_0 + M_1)^* = M_0$, if M_1 is positive, causing tension on the bottom flange.

13) Research Findings in Other References

The research team studied additional references on the flexural strength accounting for lateral torsional buckling and moment gradient factor. Because the research findings in these publications are similar or comparable to those listed above, they are not described individually for brevity.

Lateral Bracing Effect of Bridge Decks

Bracing members are commonly classified as torsional (diaphragms or cross frames) or lateral (top chord, upper and lower laterals, or bridge decks). Both tests and theoretical solutions have shown that cross section distortion has a significant effect on torsional brace effectiveness [22]. A bridge deck has the potential to act as a lateral and/or torsional brace. The friction that may be mobilized at the deck-stringer interface acts as a lateral brace because it restrains lateral movement of the stringer top flange. A number of researchers concluded that, even if there is no mechanical connection between the deck

and the stringers, friction may still be adequate to develop the required deck stiffness to act as a lateral brace at the contact area of the wheel load. Therefore, if a stringer is non-composite and it is subject to positive moment, it might be considered laterally supported at the wheel load location near midspan [23].

A full-size test on a five-girder short-span bridge conducted by Vegesna and Yura showed that timber decks not positively attached to the stringers can provide lateral bracing at wheel load locations through friction [24]. Common timber decks have enough lateral bracing stiffness to permit the stringers to reach yield without buckling. It can be inferred that concrete decks provide greater lateral stiffness and have better friction resistance than timber decks.

Another study of bracing effects provided by bridge decks was completed by Kissane for the New York State Department of Transportation in 1985 [25]. The objective was to determine the effectiveness of a non-composite concrete bridge deck as a lateral brace for the compression flange of the supporting stringers without any positive shear connections. To complete the comparison, tests were completed where the physical or chemical bond between the concrete deck and the stringers was intentionally eliminated. Kissane concluded that friction resistance between the concrete deck and the stringers was sufficient to use the deck as a brace and allow the stringers to reach their full bending capacity without buckling laterally. In addition, Linzell et al. conducted field testing of a riveted through-girder bridge in Pennsylvania and identified unintended composite action under live loads [26].

When a stringer is made composite with a concrete deck slab or the top flange is fully embedded in the deck slab, the top flange is considered to be fully braced if subject to positive moment (compression on top), and therefore, LTB is not applicable. In the negative moment region, the bottom flange of the stringers is in compression and shall be evaluated for LTB resistance. In past practice, points of contraflexure sometimes have been considered as brace points when the influence of moment gradient is not included in LTB resistance equations. However, this practice sometimes can lead to a substantially not conservative estimate of the flexural resistance. The influence of moment gradient may be correctly accounted for using C_b and the effect of restraint from adjacent unbraced segments may be accounted for by using an effective length factor less than 1.0. Multiple researchers have proposed using a braced column nomograph as an acceptable analogy for obtaining the effective length of the critical stringer [27] [28].

Summary of Literature Review

The research team performed an extensive literature review of domestic and international guidelines and specifications, and numerous technical papers and reports. The focus of this literature review was on the moment gradient factor C_b for stringers that have doubly symmetric sections and are primarily subject to vertical loading. The team synthesized the literature review by including pertinent provisions in the current *AASHTO LRFD Bridge Design Specifications and* the *AISC Steel Construction Manual*. A summary of international practices referring to the Canadian, Australian, British, and Japanese design codes and specifications is included. Some significant work on the moment gradient factor by individual researchers are included as well.

Objective

The project objective was to evaluate the bending capacity of continuous stringers in two-girder or truss structures and develop a new approach for load rating these stringers. This project focuses on determining a reasonable, but not overly conservative, estimate of the moment gradient factor, C_b.

Scope

The project scope consisted of three major tasks. The first task focused on the review of domestic and international guidelines and specifications and research studies on how to realistically determine the lateral torsional buckling strength of continuous stringers by using a reasonable moment gradient factor, C_b. The focus was on doubly-symmetric stringer sections primarily subject to vertical loading. In the second task, current procedures related to load rating continuous stringers on floor beams were studied. The third, primary task intended to develop a methodology to determine a more realistic moment gradient factor. This task included lab tests that approximated behavior of stringers in a bridge while accounting for various types of bracings. Finite element analyses were conducted to simulate the behavior of the tested stringers. A representative bridge was also analyzed using a finite element model to evaluate the stringer's flexural strength.

Methodology

Current Rating Techniques

Most of the bridges in Louisiana are rated using AASHTOWare Bridge Rating (BrR) software in which the moment gradient factor is determined following the *AASHTO LRFD Bridge Design Specifications.* However, this may not account for the bracing effect of non-composite deck properly and underestimates the flexural resistance of the continuous stringer. As a result, the load rating may be overly conservative.

The DOTD provided the research team with relevant information on five representative bridges, including as-built plans and draft load rating reports. The research team developed in-house Excel spreadsheets to perform the load rating of these bridges. Table 1 summarizes the bridge number, typical floor beam spacing, and stringer section, spacing, and strength. Only HL-93 (Inventory) load was included in the ratings to examine various load rating approaches. Stringer LTB resistance was determined accounting for the moment gradient factor in accordance with the *AASHTO LRFD Bridge Design Specifications*. Analyses were also performed following other codes and standards to evaluate their calculated moment gradient factors, including the AISC Steel Construction Manual, the Canadian Highway Bridge Design Code, the Australian Steel Code, and the British Standards. In addition to the moment gradient factor, the research team studied the effect of using moment envelopes and concurrent moment approaches on load rating results.

Table 1. Representative bridges

Bridge No.	Typical Floor beam Spacing (ft.)	Controlling Stringer Section	Stringer Spacing (ft.)	Yield Strength of Stringer (ksi)
610065	24.7	W24x62	7.5	36
300330	25.0	24WF68	9.0	36
200830	19.5 /23.5	16WF50	6.5	36
201810	28.2	21WF68	5.5	33
001715	24.5	W18x40	6.0	50

In positive bending the compression flange of the stringer is laterally braced by the concrete deck slab. As a result, there is no LTB. Therefore, this study focuses on negative bending regions of the stringer over the floor beam. Regardless of whether composite

action exists between the deck slab and the stringer, the negative moment region is treated similarly except that deck reinforcement may contribute to the flexural resistance for stringers acting compositely with the deck.

Because the stringer is continuous over the floor beam, the portion near the floor beam is subject to compression in its bottom flange, which can potentially induce LTB. Once it is beyond the contraflexure points, the bottom flange of the stringer is in tension. Based on the literature review, the influence of moment gradient may be approximated using C_b. Representative bridge plans show no intermediate cross frames or diaphragms are used along the stringer spans. Therefore, a full stringer span (i.e., the distance between supporting floor beams) is taken as the unbraced length in the load rating calculations. All five bridges are analyzed and results are summarized below.

Bridge No. 610065

The process used to rate Bridge No. 610065 is representative of the procedure used for all five bridges and is discussed in detail. The bridge includes four lines of steel plate girders, floor beams, and six lines of continuous stringers. Figure 6 and Figure 7 illustrate the bridge framing plan and cross section, respectively. A typical stringer unit consists of either three or four continuous spans. A four-span unit was selected in the analysis and an interior stringer, a W24x62, was load rated for the HL-93 (Inventory rating) load. Floor beams are spaced at approximately 24 ft. – 8 5/8 in. and stringers spaced at 7 ft. – 6 in. A36 steel is used.

Figure 6. Framing plan, Bridge No. 610065

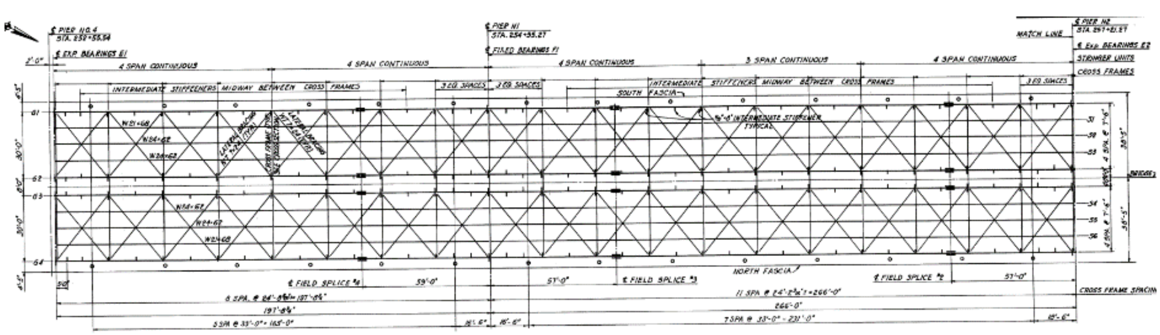

Figure 7. Cross section, Bridge No. 610065

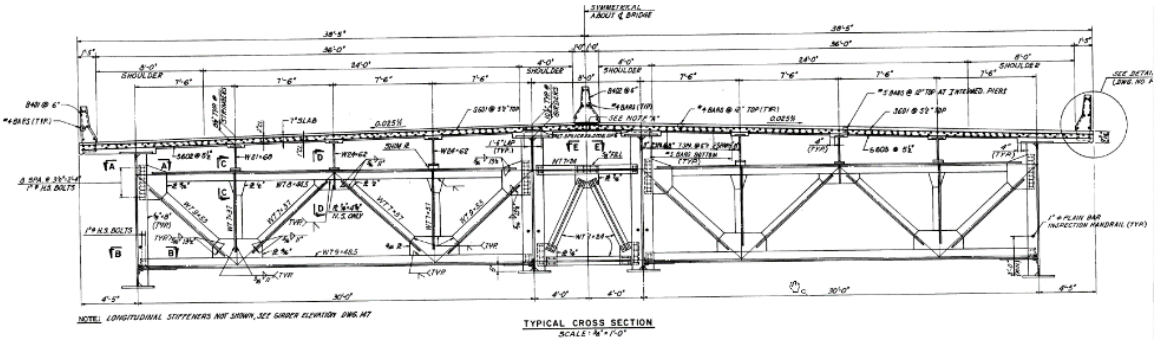

1) C_b and flexural resistance from AASHTO LRFR

The *AASHTO LRFD Bridge Design Specifications* (LRFD) provides two primary sections, Article (Art.) 6.10.8.2 and Art. A6.3.3, addressing flexural resistance of stringers under negative moment. Art. A6.3.3 is more accurate for stringers because it accounts for the ability of compact and non-compact web I-sections to develop flexural resistances greater than the yield moment.

When AASHTOWare BrR was used, the unbraced length was taken as the stringer length between adjacent floor beams. When Excel spreadsheets were employed to perform the rating following the MBE, for consistency a similar live load distribution factor to that used by AASHTOWare BrR was assumed. In addition, analyses were conducted accounting for various moment gradient factors and unbraced lengths.

The effect the moment envelope or concurrent moment values was also examined for live load analysis. Figure 8 shows the unfactored moment envelope due to HL-93 in which a pair of design tandems and a design lane load controlled over other live loads. The maximum negative moment at the first interior floor stringer is -181.5 Kip-ft. Figure 9 plots the concurrent moment under HL-93 matching maximum negative moment in Figure 8. As a result, both moment envelope and concurrent moment approaches were used to determine moment gradient coefficients and corresponding load rating factors.

Figure 8. Unfactored moment envelope due to HL-93 (unit in Kip-ft.)

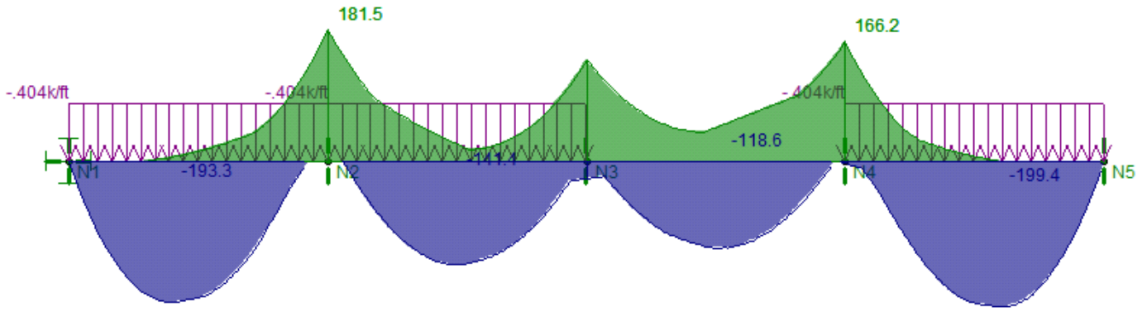

Figure 9. Unfactored concurrent moment due to HL-93 (unit in Kip-ft.)

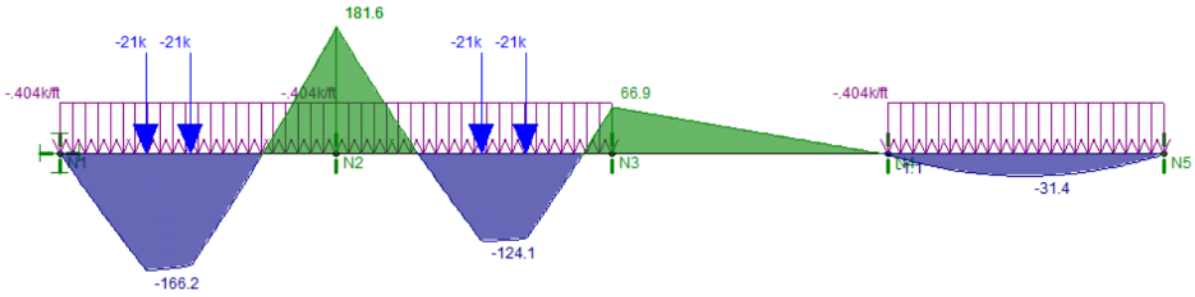

Inventory load rating factors under HL-93 are determined using AASHTOWare BrR and Excel spreadsheets assuming the full stringer span as the unbraced length. The rating factor from the spreadsheet is close to the AASHTOWare BrR result when the LRFD A6.3.3 is followed. As an old design methodology, the continuous stringers in Louisiana's bridges were likely designed assuming contraflexure points as brace points, which allowed for sufficient rating factors. Table 2 lists rating factors using both assumptions on the unbraced lengths. As shown in Table 2, when the moment gradient factor is increased, the load rating factor is increased accordingly. For illustration purpose, Figure 10 plots rating versus moment gradient factor diagrams. As expected, the moment gradient factor substantially affects resulting rating factors.

Table 2. LRFR moment gradient and load rating factors

	Use full span as unbraced length		Use contraflexure points as brace points
	Moment Envelope	Concurrent moment	Concurrent moment
C_b	1.07	1.36	1.00
RF	0.33	0.49	1.10

Figure 10. HL-93 (inventory) rating versus moment gradient factors

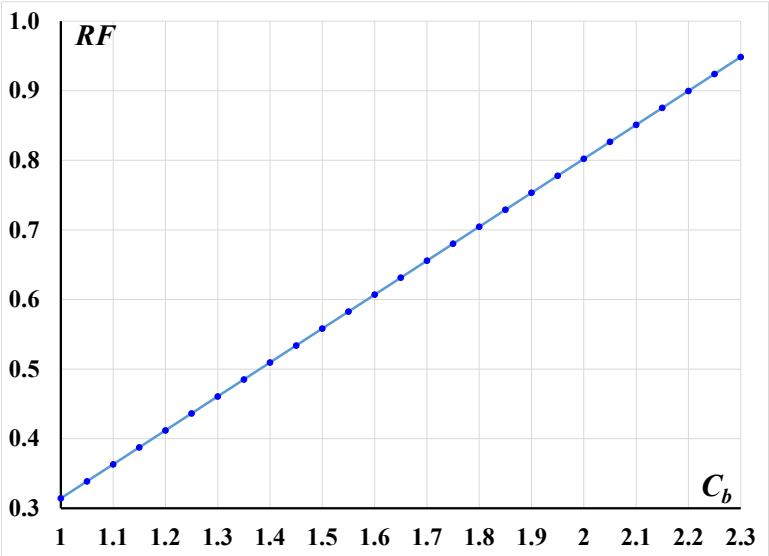

2) C_b from the AISC Steel Construction Manual, the Canadian Highway Bridge Design Code, the Australian Steel Code, and the British Standards

Because the equations for the moment gradient factor are similar in these codes and specifications, Table 3 summarizes moment gradient factors determined according to these codes and specifications and subsequent MBE rating factors. The moment gradient factors were calculated using absolute moments at relevant sections accounting for both end (exterior) and interior spans. As a result, the moment gradient factors are larger than 1.0 for all cases. Moment envelope and concurrent moment approaches are also included assuming a full stringer span as the unbraced length. The rating factors increased when the concurrent moment approach is adopted. Figure 11 plots moment gradient and rating factors based on these sources and shows generally comparable results. The British Standards appears to provide the lowest rating results, while the Australian Steel Code gives the highest rating results.

Table 3. C_b from various codes and specifications, corresponding *RF* following MBE

		Moment Envelope		Concurrent Moment	
		End span	Interior span	End span	Interior span
M_{Max}		377	377	377	377
M_A		326	127	273	52
M_B		366	267	291	213
M_C		177	186	152	155
AISC	C_b	1.20	1.60	1.39	1.95
	RF	0.41	0.61	0.51	0.78
Canada	C_b	1.18	1.64	1.42	2.00
	RF	0.40	0.63	0.52	0.80
Australia	C_b	1.23	1.83	1.50	2.39
	RF	0.43	0.72	0.56	0.99
U.K.	C_b	1.13	1.47	1.33	1.77
	RF	0.38	0.55	0.47	0.69

Note: Moment in Kip-ft.

Figure 11. Variation of *RF* as a function of C_b from various codes and specifications

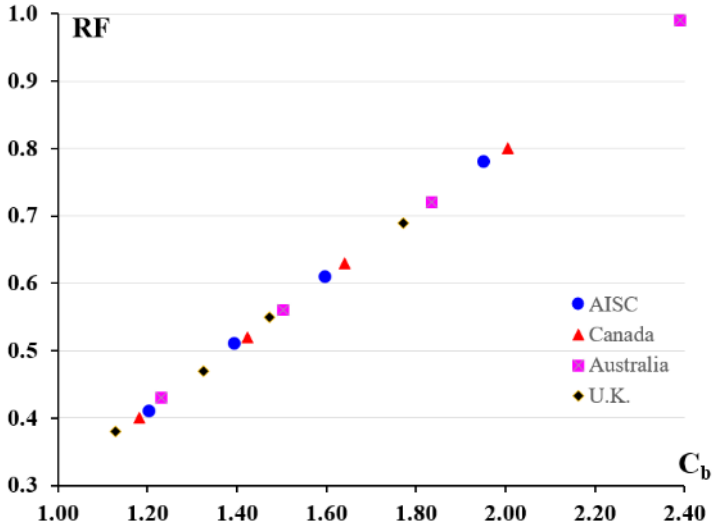

3) C_b from Yura and Helwig

Yura and Helwig studied gravity-loaded rolled I-sections in bending with the top flange laterally restrained and suggested using Eq. (29) to determine C_b. This equation is particularly applicable to the situation where a stringer is subjected to reverse curvature bending. Table 4 summarizes moments at relevant sections within an unbraced length and calculated C_b values using Eq. (29), which are significantly higher than previously reported methods. When these moment gradient factors are used for load rating corresponding rating factors exceed 1.0.

Table 4. C_b and *RF* following Yura and Helwig

	Moment Envelope		Concurrent Moment	
	End span	Interior span	End span	Interior span
M_0	-377	-377	-377	-377
M_1	0	-287	0	-157
M_{CL}	12	-23	291	213
$M_1 + M_0$	-377	-664	-377	-534
C_b	3.08	2.40	5.06	3.79
RF	1.25	1.00	1.25	1.25

Bridge No. 300330

Bridge No. 300330 includes several stringer units. A typical unit that consists of 7 continuous stringers was load rated for HL-93 (Inventory). Floor beams are spaced at 25 ft. and the stringers, 24WF68s, are spaced at 9 ft. (Figure 12 and Figure 13). Like Table 2, Table 5 lists the calculated rating factors. The rating factor can be significantly increased accounting for moment gradient. Tables 6 and 7 provide the moment gradient factors and corresponding load ratings using other codes, standards, and approaches. Because Bridge No. 300330 has comparable stringer size and floor beam spacing as Bridge No. 610065, behavioral observations are similar.

Figure 12. Framing plan, Bridge No. 300330

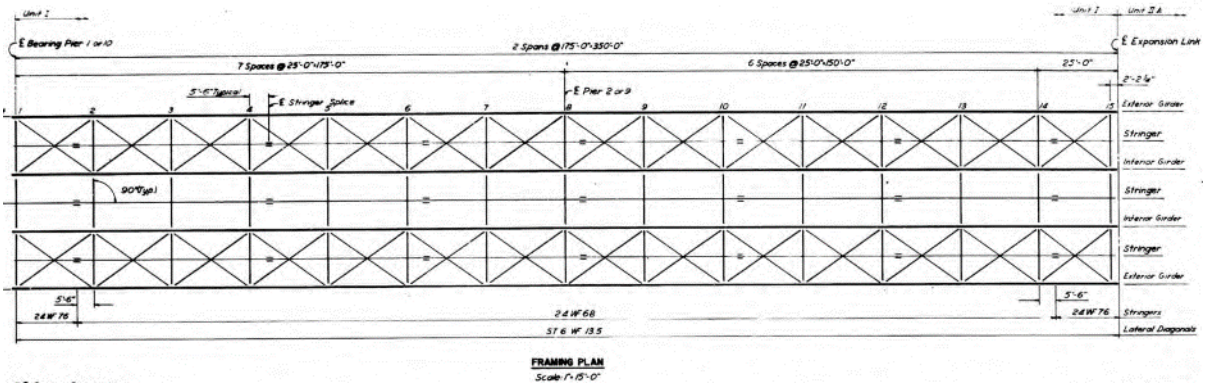

Figure 13. Cross section, Bridge No. 300330

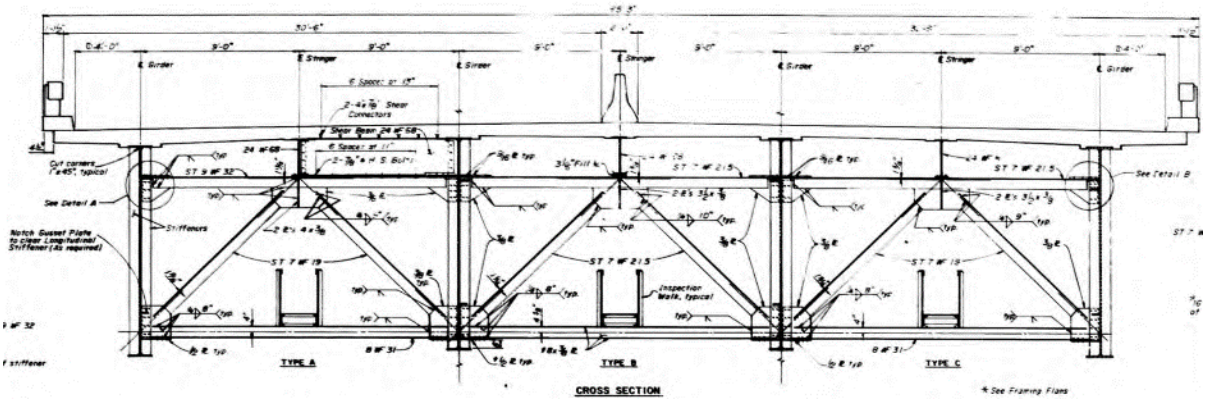

Table 5. LRFR moment gradient and load rating factors

	Follow LRFD Art. A6.3.3	
	Moment Envelope	**Concurrent moment**
C_b	1.06	1.35
RF	0.57	0.78

Table 6. C_b in accordance with the AISC, Canada, Australia, and U.K. Codes, and corresponding *RF* following the MBE

		Moment Envelope		Concurrent Moment	
		End span	**Interior span**	**End span**	**Interior span**
M_{Max}		444	444	444	444
M_A		380	145	314	60
M_B		426	305	346	249
M_C		207	208	79	169
AISC	C_b	1.21	1.64	1.51	1.99
	RF	0.68	1.00	0.90	1.21
Canada	C_b	1.19	1.69	1.47	2.04
	RF	0.67	1.03	0.87	1.21
Australia	C_b	1.24	1.90	1.59	2.46
	RF	0.70	1.19	0.96	1.21
U.K.	C_b	1.14	1.51	1.38	1.79
	RF	0.63	0.90	0.81	1.11

Table 7. C_b and RF following the research by Yura and Helwig

	Moment Envelope		Concurrent Moment	
	End span	Interior span	End span	Interior span
M_0	-444	-444	-444	-444
M_1	0	-342	0	-193
M_{CL}	-23	-22	346	249
$M_1 + M_0$	-444	-786	-444	-637
C_b	2.86	2.41	5.08	3.75
RF	1.21	1.21	1.21	1.21

Bridge No. 200830

Bridge No. 200830 includes continuous stringers supported on floor beams that are typically spaced at 23 ft. – 6 in. except at for two stringer end spans, where floor beams are spaced at 19 ft. – 6 in. The bridge cross section includes three lines of 16WF50 stringers using A36 steel (Figure 14 and Figure 15). The stringers are spaced at 6 ft. – 6 in. Like Table 2, Table 8 lists the calculated rating factors. Tables 9 and 10 provide the moment gradient factors and corresponding load ratings using other codes, standards, and approaches. Similar conclusions are drawn for this bridge to that of Bridge No. 610065.

Figure 14. Framing plan, Bridge No. 200830

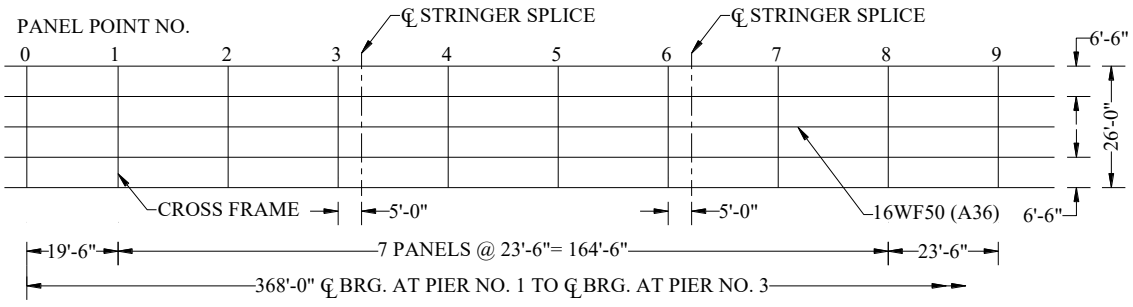

Figure 15. Cross section, Bridge No. 200830

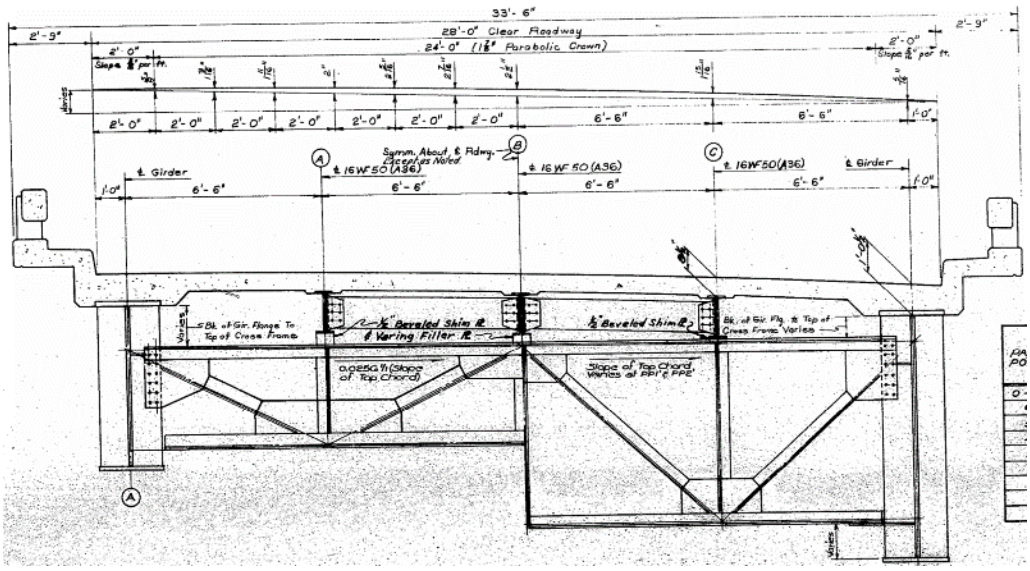

Table 8. LRFR moment gradient and load rating factors

	Follow LRFD Art. A6.3.3	
	Moment Envelope	Concurrent moment
C_b	1.00	1.12
RF	0.52	0.61

Table 9. C_b from various codes and specifications, corresponding *RF* following MBE

		Moment Envelope		Concurrent Moment	
		End span	Interior span	End span	Interior span
M_{Max}		244	268	244	268
M_A		220	159	167	131
M_B		246	245	103	203
M_C		123	146	52	9
AISC	C_b	1.16	1.31	1.82	1.76
	RF	0.63	0.73	1.08	1.04
Canada	C_b	1.14	1.30	1.93	1.64
	RF	0.61	0.73	1.14	0.96
Australia	C_b	1.18	1.40	2.04	1.89
	RF	0.64	0.79	1.14	1.13
U.K.	C_b	1.09	1.21	1.83	1.52
	RF	0.58	0.66	1.09	0.87

Table 10. C_b and RF following Yura and Helwig

	Moment Envelope		Concurrent Moment	
	End span	Interior span	End span	Interior span
M_0	-244	-268	-244	-268
M_1	0	-239	0	-162
M_{CL}	-35	-18	103	203
$M_1 + M_0$	-244	-507	-244	-430
C_b	2.62	2.31	4.13	3.86
RF	1.14	1.14	1.14	1.14

Bridge No. 201810

Bridge No. 201810 includes one girder-floor stringer-stringer span of 84 ft. – 6 in. that controls the load rating. It consists of three continuous spans of stringers supported by floor beams that are equally spaced at approximately 28 ft. – 2 in. The bridge cross section includes eight 21WF68 interior stringer lines (Figure 16 and Figure 17). The stringers are spaced at 5 ft. – 6 in. and are comprised of carbon steel with yield strength of 33 ksi. Like Table 2, Table 11 lists the calculated rating factors. Also included are tables listing the moment gradient factors and corresponding load ratings following other codes, standards, and approaches (Tables 12 and 13). Similar conclusions can be drawn for this bridge to that of Bridge No. 610065.

Figure 16. Framing plan, Bridge No. 201810

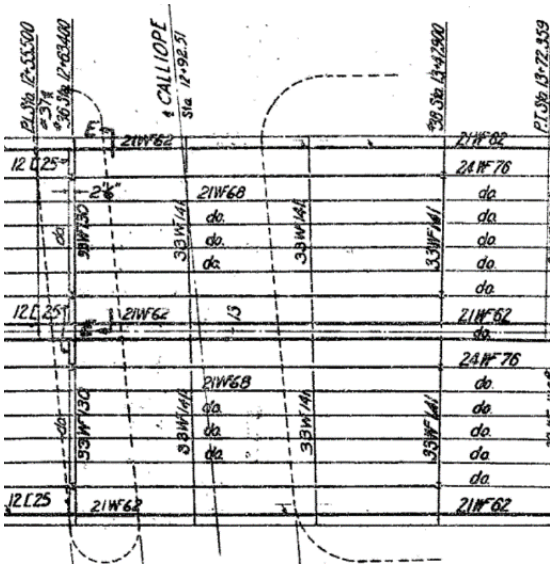

Figure 17. Cross section, Bridge No. 201810

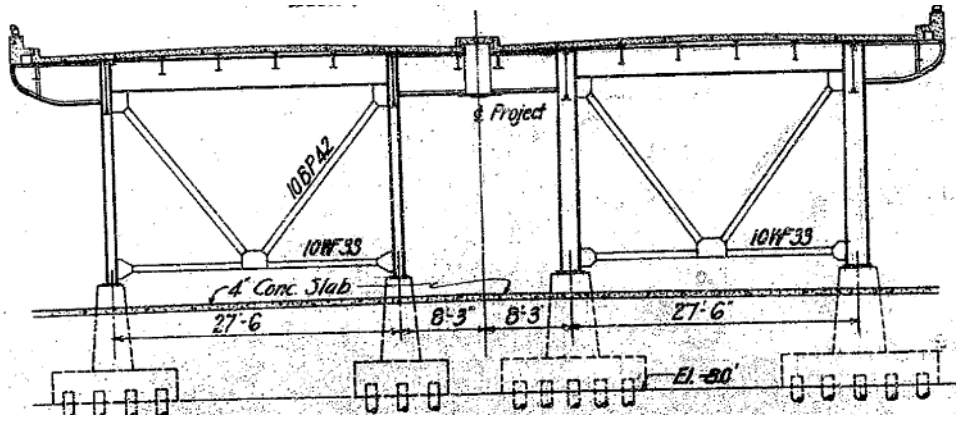

Table 11. LRFR moment gradient and load rating factors

	Follow LRFD Art. A6.3.3	
	Moment Envelope	**Concurrent moment**
C_b	1.05	1.36
RF	0.45	0.64

Table 12. C_b from various codes and specifications, corresponding *RF* following MBE

		Moment Envelope		Concurrent Moment	
		End span	**Interior span**	**End span**	**Interior span**
M_{Max}		372	372	372	372
M_A		303	140	214	38
M_B		342	214	283	205
M_C		168	158	1	96
AISC	C_b	1.25	1.74	1.72	2.16
	RF	0.58	0.87	0.86	1.06
Canada	C_b	1.24	1.86	1.59	2.16
	RF	0.57	0.95	0.78	1.06
Australia	C_b	1.30	2.10	1.78	2.50
	RF	0.61	1.06	0.91	1.06
U.K.	C_b	1.18	1.65	1.50	1.89
	RF	0.53	0.82	0.73	0.96

Table 13. C_b and RF following Yura and Helwig

	Moment Envelope		Concurrent Moment	
	End span	Interior span	End span	Interior span
M_0	-372	-372	-372	-372
M_1	0	-336	0	-156
M_{CL}	30	-23	283	205
$M_1 + M_0$	-372	-708	-372	-528
C_b	3.22	2.31	5.03	3.76
RF	1.06	1.06	1.06	1.06

Bridge No. 001715

Bridge No. 001715 includes four girder-floor stringer-stringer units. Each span consists of continuous stringers supported by floor beams with a spacing ranging from 22 ft. – 7 1/8 in. to 24 ft. – 5 3/8 in. The bridge cross section includes ten stringer lines of either W18x40 or W18x46 using A572 steel (Figure 18). The stringers are spaced at 6 ft. (Figure 19). Like Table 2, the stringer was load rated for HL-93 (Inventory) following the MBE. Table 14 lists the calculated rating factors. Also included are tables listing the moment gradient factors and corresponding load rating factors following other codes, standards, and approaches (Tables 15 and 16). Similar conclusions can be drawn for this bridge to that of Bridge No. 610065.

Figure 18. Framing plan, Bridge No. 001715

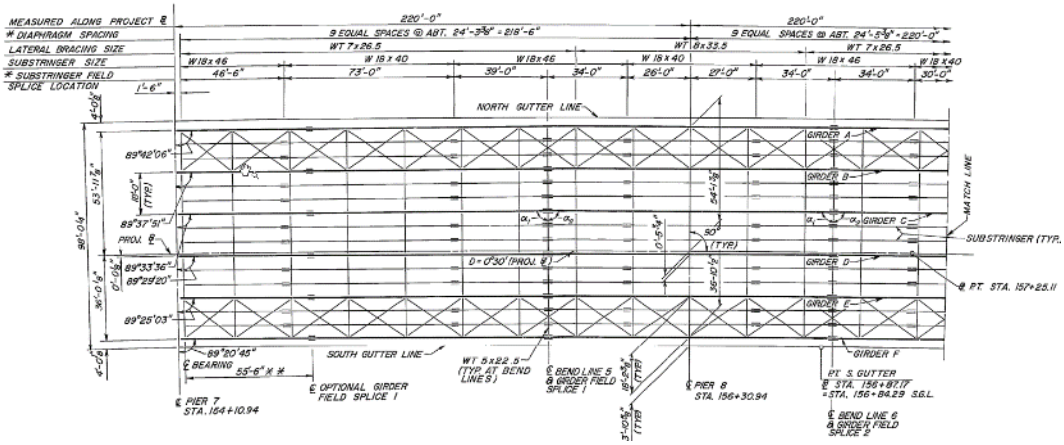

Figure 19. Cross section, Bridge No. 001715

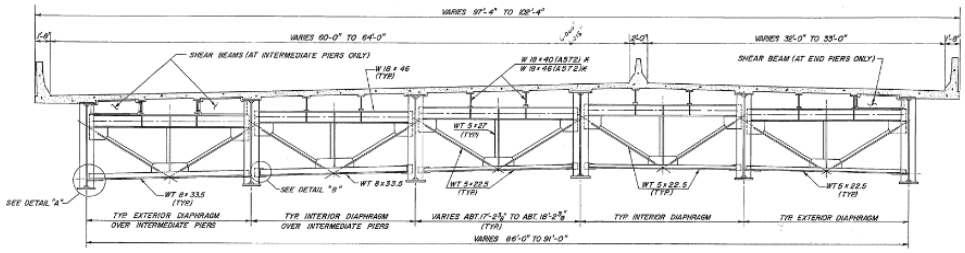

Table 14. LRFR moment gradient and load rating factors

	Follow LRFD Art. A6.3.3	
	Moment Envelope	Concurrent moment
C_b	1.00	1.36
RF	0.09	0.17

Table 15. C_b from various codes and specifications, corresponding *RF* following MBE

		Moment Envelope		Concurrent Moment	
		End span	Interior span	End span	Interior span
M_{Max}		377	377	377	377
M_A		333	167	282	55
M_B		375	277	293	214
M_C		188	192	15	163
AISC	C_b	1.18	1.51	1.57	1.92
	RF	0.13	0.20	0.21	0.29
Canada	C_b	1.15	1.56	1.46	1.98
	RF	0.12	0.21	0.19	0.30
Australia	C_b	1.20	1.71	1.57	2.33
	RF	0.13	0.24	0.21	0.38
U.K.	C_b	1.11	1.41	1.41	1.75
	RF	0.11	0.18	0.18	0.25

Table 16. C_b and *RF* following Yura and Helwig

	Moment Envelope		Concurrent Moment	
	End span	Interior span	End span	Interior span
M_0	-377	-377	-377	-377
M_1	0	-290	0	-159
M_{CL}	2	-55	293	214
$M_1 + M_0$	-377	-667	-377	-536
C_b	3.01	2.27	5.07	3.78
RF	0.53	0.37	0.83	0.70

In summary, ratings of these bridges presented the following general observations:

1) The AASHTOWare BrR software may underestimate flexural resistance of the stringer and result in a lower load rating factor in comparison to other approaches when a smaller moment gradient factor is used.
2) If the moment gradient factors are determined following the *AISC Steel Construction Manual*, the *Canadian Highway Bridge Design Code*, the *Australian Steel Code*, and the *British Standards*, these codes and standards generally produce comparable moment gradient factors that typically exceed 1.0. The British Standards appear to provide the lowest results while the Australian Steel Code gives the highest results.
3) The equation for the moment gradient factor by Yura and Helwig provides significantly higher RFs.
4) When the concurrent moments are used to conduct the load rating instead of moment envelopes, the calculated moment gradient factor is generally higher and the RF increases.

Experimental Study

This project included an experimental study of the LTB resistance of a two-span continuous steel structure, which included three lines of stringers, steel diaphragms at the end supports, and a floor beam as the interior support. A variety of lateral bracing conditions were evaluated, including steel diaphragms, timber ties located at the stringer top flanges, and a non-composite concrete deck. The steel diaphragms and timber ties were provided at variable spacing to investigate their bracing effects. To address variations in relative flexural stiffness where stringers were supported by a floor beam, tests accounted for both rigid and flexible floor beams. To account for connection restraint at this location, stringer bottom flanges were either unbolted or bolted to the floor beams. The interior stringer was subject to a vertical point load at its midspan of either one or both spans. LTB resistance of the stringer from the lab testing was compared with predicted values in accordance with the *AASHTO LRFD Bridge Design Specifications*. The study also presented comparisons between moment gradient factors calculated from collected test data and those obtained from the existing specifications and codes. As a result, the experimental study could potentially justify use of a higher moment gradient factor than that taken from *the AASHTO LRFD Bridge Design Specifications* and could increase the load rating factor for the continuous steel stringers.

The experimental study examined influence of the following factors on system performance, most notably as it related to interior stringer LTB:

1) Stringer to floor beam connection fixity.
2) Use of intermediate steel diaphragms, timber ties, and a non-composite concrete deck.
3) Stringer to floor beam relative flexural stiffness.

Data produced from the tests were used to establish experimental LTB resistances and moment gradient factors for the interior stringer. The following sections describe the test frame, test matrix, instrumentation, and test results.

Test Frame

The test frame was designed to address critical parameters from the representative bridges, including span, spacing, and size of the stringers, deck thickness, material properties, and support conditions. The basic setup was a grillage system that accommodated a variety of bracing configurations and stringer-to-floor beam relative stiffness and connection fixity conditions. The grillage system included three lines of 50-ft-long W16x31 stringers, one 25-ft-long W24x68 floor beam, and C12x20 end diagrams bolted to the stringers. Figure 20 and Figure 21 show the framing plan and a section of the grillage at the floor beam, respectively. The grillage was a two-span structure having 24-ft. spans between the centerlines of bearings. As shown in Figure 22 and Figure 23, stiff supports underneath the floor beam at different locations helped create rigid and flexible conditions. Stringers were spaced at 4 ft. and the deck was 50 ft. long by 10 ft. wide and 6 in. thick. The deck was conventionally reinforced using Grade 60 rebar. Figure 24 and Figure 25 present the deck plan and a typical section.

Figure 20. Grillage system framing plan

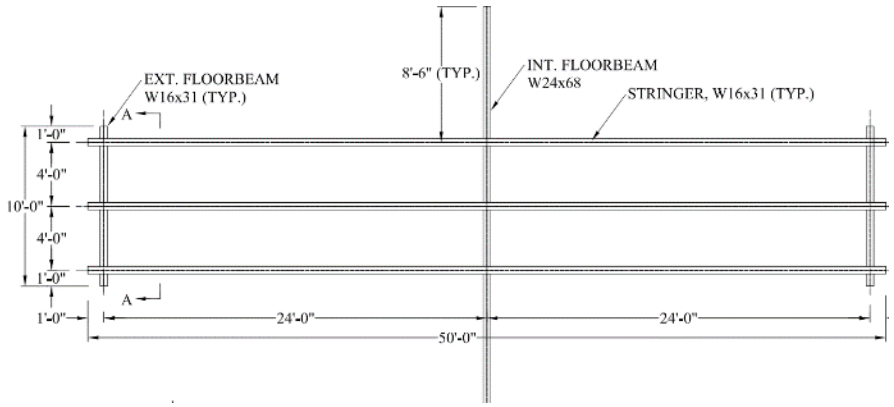

Figure 21. Grillage system section at floor beam

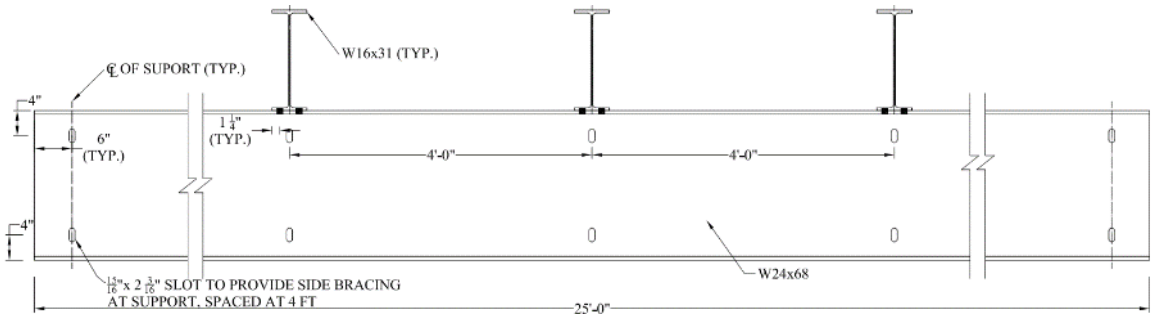

Figure 22. Test setup mimicking rigid (stiff) floor beam

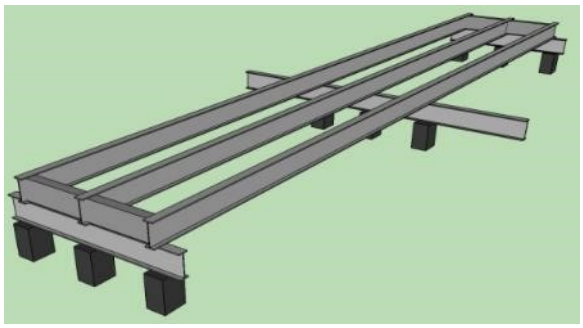

Figure 23. Test setup mimicking flexible floor beam

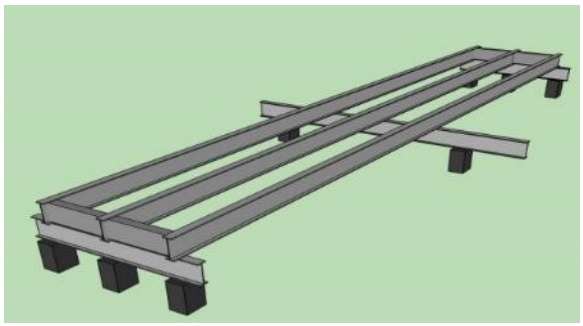

Figure 24. Deck reinforcement plan

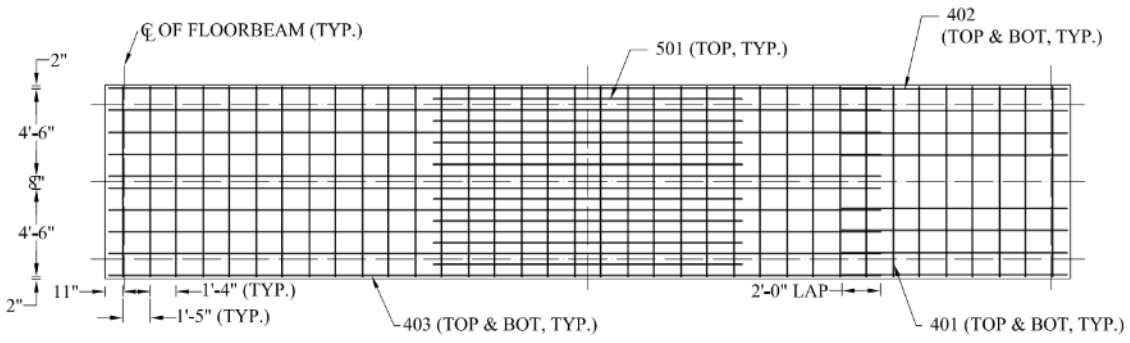

Figure 25. Deck reinforcement section

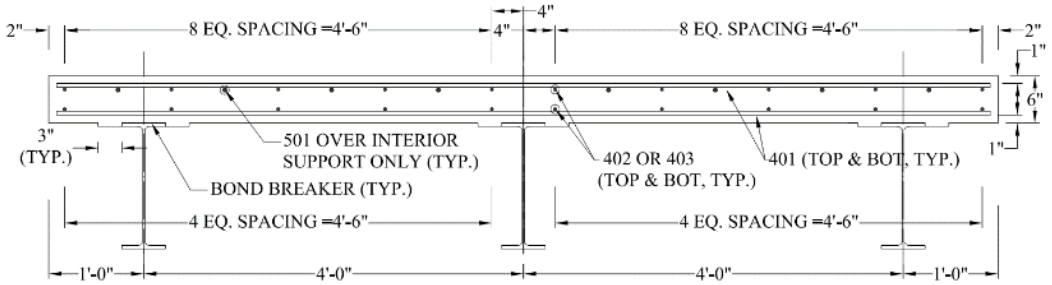

W16x31s were selected for the stringers for the following reasons: 1) the identified stringer size, including the section height and web slenderness, should be comparable to stringers in the representative bridges; and 2) the stringers were anticipated to exhibit elastic buckling behavior, which allows for repetitive tests. Grade 50 steel allows for multiple tests without yielding the stringers. Furthermore, the modulus of elasticity is the same for Grades 36 and 50. Grade 50 yield stresses vary less than Grade 36 and steel grade minimally impacts controlling $L_{b.}$ or L_r.

Test Matrix

Table 17 provides the complete test matrix, including: categories; corresponding configurations (i.e., test setups); stringer support conditions (i.e., floor beam flexural stiffness); loading and bracing conditions, including existence or absence of composite action (i.e., C or NC); and test run identification numbers. Testing is categorized into four general groups as listed below. For both balanced and unbalanced loading conditions a concentrated force is applied at the midspan. When no deck is included, the load is applied to the top flange of the interior stringer. When an unbalanced load is applied, the unloaded stringer end is tied down to avoid possible uplift. The grillage system is repeatedly used in Groups I to III tests. Group IV tests utilized a new interior stringer.

- **Group I**: It consists of test setup Nos. 1, 1A, 1B, and 1C, in which the grillage system stringer top flanges were unbraced (Figure 26). Either a rigid or flexible interior floor beam was provided. The stringer bottom flanges were either unbolted or bolted at the floor beam. When bolted, 7/8 in. diameter high-strength bolts were used. Balanced and unbalanced loads were applied. This group includes Tests 1 to 8 and serves as a baseline for comparison to other groups.
- **Group II:** It consists of setup Nos. 1’ and 1’A, in which the grillage system stringers were braced by the intermediate steel diaphragms at various locations, including the interior support, and $L/2$, $L/8$, $L/4$, and $3L/8$ away from the interior support (L = span). The diaphragms were bolted with the stringers and rigid interior support is provided for the stringers. The stringer bottom flanges were either unbolted or bolted

at the floor beam. Balanced and unbalanced loads were applied. This group includes Tests 9 to 28. Figure 27 shows an example of Group II setup.

- **Group III:** It consists of test setup Nos. 2, 2A, 2B, and 2C, in which the grillage system stringer top flanges were laterally braced by timber ties (4 x 4) and C-clamps (Figure 28). These setups were intended to represent a transition of bracing conditions between Groups I and IV. Either a rigid or flexible interior floor beam was provided. The stringer bottom flanges were either unbolted or bolted at the floor beam. Balanced loads were applied. This group includes Tests 29 to 44.

Table 17. Test matrix

Group	Test setup	NC or C	Description of boundary conditions			Load condition	Test Run #
			Interior support at center stringer	Top flange of stringer	Bottom flange of stringer		
I	No. 1	NC	Rigid	Unbraced	Unbraced	1 point load	1
						2 point loads	2
	No. 1A				Braced laterally by bolts	1 point load	3
						2 point loads	4
	No. 1B		Flexible		Unbraced	1 point load	5
						2 point loads	6
	No. 1C				Braced laterally by bolts	1 point load	7
						2 point loads	8
II	No. 1'	NC	Rigid	Diaphragms @ Int. Support	Unbraced	1 point load	9
						2 point loads	10
				Diaphragms @ L/2		1 point load	11
						2 point loads	12
				Diaphragms @ L/8 from Int. Support		1 point load	13
						2 point loads	14
				Diaphragms @ L/4 from Int. Support		1 point load	15
						2 point loads	16
				Diaphragms @ 3L/8 form Int. Support		1 point load	17
						2 point loads	18
	No. 1'A		Rigid	Diaphragms @ Int. Support	Braced laterally by bolts	1 point load	19
						2 point loads	20
				Diaphragms @ L/2		1 point load	21
						2 point loads	22
				Diaphragms @ L/8 from Int. Support		1 point load	23
						2 point loads	24
				Diaphragms @ L/4 from Int. Support		1 point load	25
						2 point loads	26
				Diaphragms @ 3L/8 form Int. Support		1 point load	27
						2 point loads	28
III	No. 2	NC	Rigid	Timber strut @ L/2, TF	Unbraced	2 point loads	29
				Timber strut @ L/3, TF		2 point loads	30
				TS @ L/4, L/2, L, L/2, L/4		2 point loads	30'
				Timber strut @ L/4, TF		2 point loads	31
				Timber strut @ L/5, TF		2 point loads	32
	No. 2A			Timber strut @ L/2, TF	Braced laterally by bolts	2 point loads	33
				Timber strut @ L/3, TF		2 point loads	34
				TS @ L/4, L/2, L, L/2, L/4		2 point loads	34'
				Timber strut @ L/4, TF		2 point loads	35
				Timber strut @ L/5, TF		2 point loads	36
				TS @ L/8, L/4, L/2, L, L/8, L/4, L/2		2 point loads	36'
	No. 2B		Flexible	Timber strut @ L/2, TF	Unbraced	2 point loads	37
				Timber strut @ L/3, TF		2 point loads	38
				Timber strut @ L/4, TF		2 point loads	39
				Timber strut @ L/5, TF		2 point loads	40
	No. 2C			Timber strut @ L/2, TF	Braced laterally by bolts	2 point loads	41
				Timber strut @ L/3, TF		2 point loads	42
				Timber strut @ L/4, TF		2 point loads	43
				Timber strut @ L/5, TF		2 point loads	44
IV	No. 3	NC Concrete slab cast to stringer top flange	Rigid	No Diaphragms	Unbraced	1 point load	45
						2 point loads	46
	No. 3A				Braced laterally by bolts	1 point load	57
	No. 3B		Flexible	No Diaphragms	Unbraced	1 point load	69
	No. 3C				Braced laterally by bolts	1 point load	81

Note: NC = non-composite; C = composite.

- **Group IV:** It consists of test setup Nos. 3, 3A, 3B, and 3C, in which a concrete deck was poured on the stringer top flanges and haunches were placed next to both sides of the stringer top flanges. The deck was intentionally made non-composite with the stringers and debonding material was applied at the stringer top flanges prior to concrete placement. Unbalanced loads were applied to all tests except one, in which both spans were loaded. This group includes Tests 45, 46, 57, 69, and 81. Figure 29 shows an example of Group IV setup.

Figure 26. Example Group I setup

Figure 27. Example Group II setup

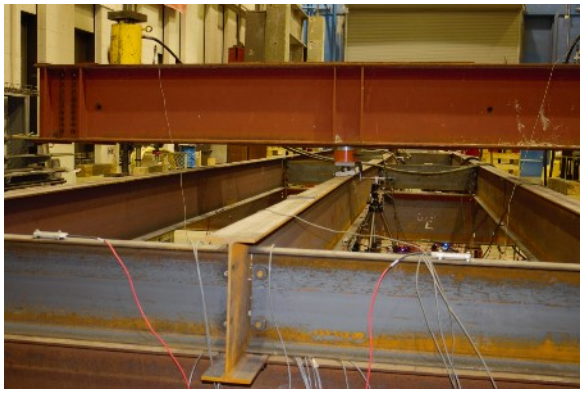

Figure 28. Example Group III setup

Figure 29. Example Group IV setup

Instrumentation

Load and pressure cells, strain gauges, and LVDTs measured applied forces and grillage response. Instrument locations are detailed in Figure 30. Strain gauges were placed at multiple sections on the interior stringer and critical exterior stringer sections to capture effects due to the primary, lateral and weak axis bending moments, torsion and axial loads. Figure 31 depicts the instrumented sections. Gauges were installed at both top and bottom flanges of the stringers. Four strain gauges were provided at critical sections and three at other sections. Additional strain gauges were provided at the top and bottom of the deck at the critical sections. LVDTs were installed at midspan of the interior stringer of both spans and were oriented to capture vertical or lateral deflections. Load cells were provided at the spreader beams that were used to apply forces to the grillage. Figure 32 and Figure 33 show LVDT and strain gauges at Loc. 10 and 4, respectively. Testing results were commonly reported at four critical locations herein. Those sections are presented in Table 18 (see Figure 30).

Figure 30. Instrumentation plan view

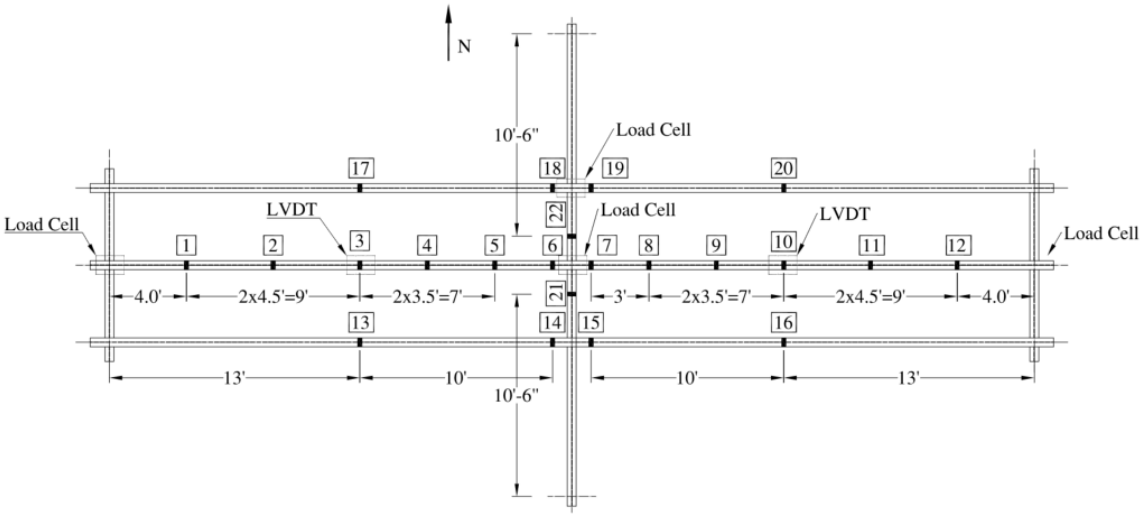

Figure 31. Instrumented sections

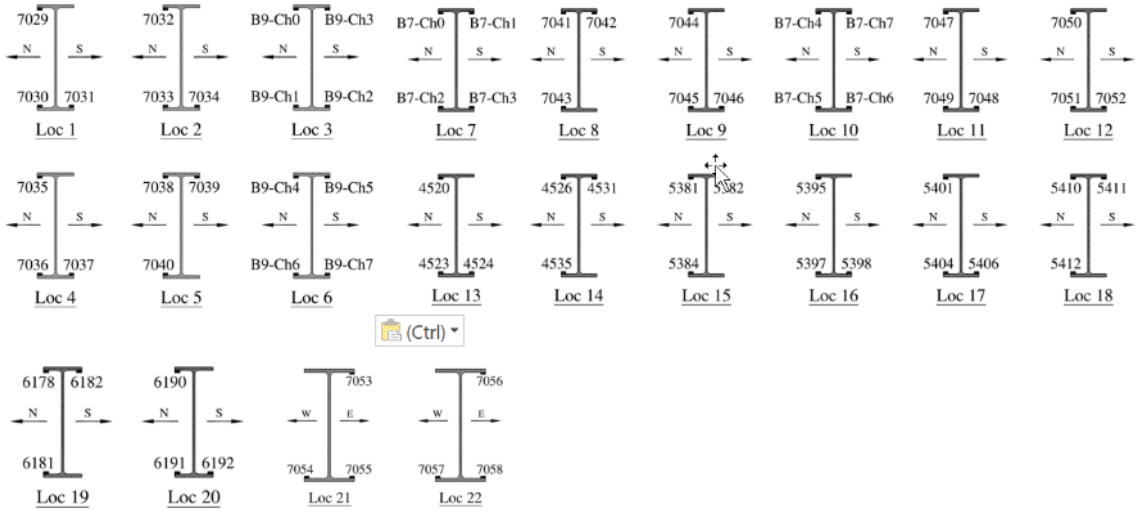

Table 18. Four critical locations

Location	Description
3	Midspan max. +M when loaded at Loc. 3 Midspan -M when loaded at Loc. 10
6	Critical -M location adjacent to floor beam
7	Critical -M location adjacent to floor beam
10	Midspan max. +M when loaded at Loc. 10 Midspan -M when loaded at Loc. 3

Figure 32. LVDT and strain gauges, Loc. 10

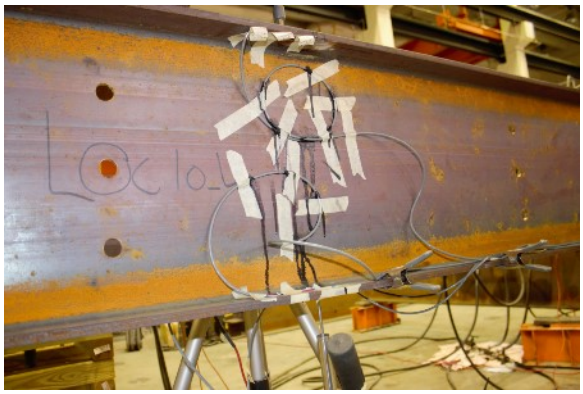

Figure 33. Strain gauge, Loc. 4

Group I Test Results

As indicated in Table 17, Group I tests were of the grillage system with no intermediate stringer bracing. Figure 34 depicts Test Run #3, showing vertical and lateral LVDTs on the interior stringer, the applied load and corresponding load cell at midspan, a supported (stiff) floor beam, and the bolted connection between the interior stringer and floor beam. Figure 35 shows LTB of the interior stringer observed during the test.

Figure 34. Test Run #3

(a) Midspan LVDTs and load cell

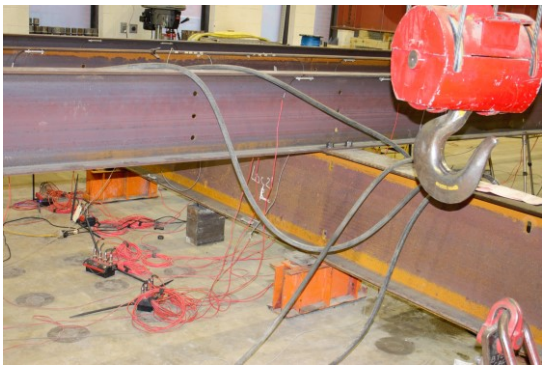

(b) Supports and bolted connection at floor beam

Figure 35. LTB of the interior stringer, Test Run #3

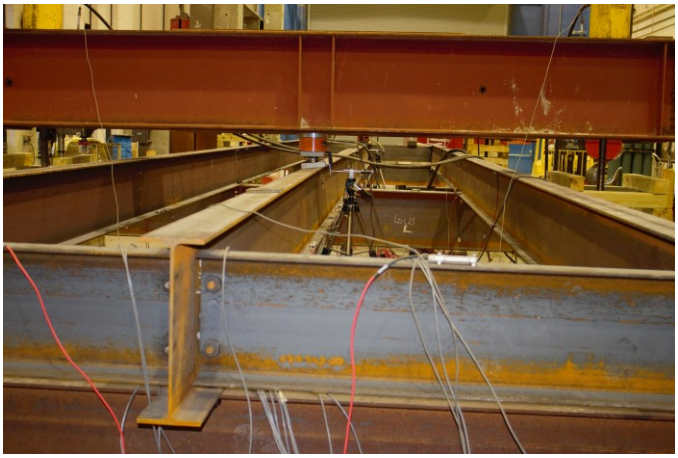

1) Effects of Spreader Beam Self-Weight

Prior to applying load testing it was of importance to establish initial conditions caused by placement of the spreader beams onto the grillage. Each spreader beam weighed approximately 3.7 kips. Figure 36 shows collected deflection data at Locs. 3 and 10. For tests that had loads applied a midspan of both spans, data was recorded as spreaders were sequentially placed onto the grillage. Measured deflections exactly matched elastic analysis results. Figure 37 illustrates collected strain data. Corresponding stresses are comparable to calculated stresses in Table 19.

Figure 36. Vertical deflections from placement of spreaders at Locs. 3 and 10

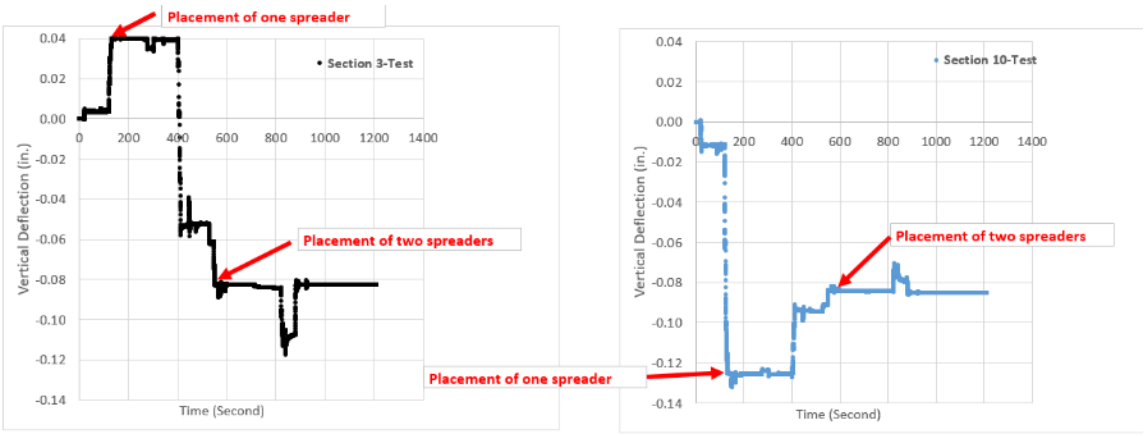

Figure 37. Strains from placement of spreaders at Locs. 3 and 10

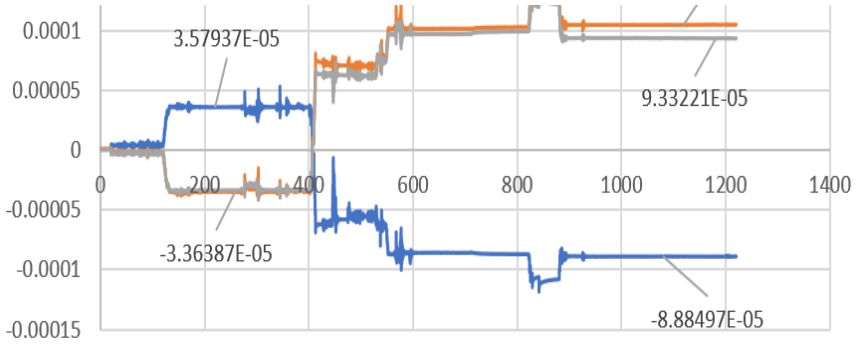

Table 19. Comparison of test and elastic analysis stresses

Gauge		Placement of One Spreader				Placement of Two Spreaders			
		From Testing		From Analysis	Ratio	From Testing	From Analysis		Ratio
		Strain (microstrain)	Stress (ksi)	Predicted stress (ksi)		Strain (microstrain)	Stress (ksi)	Predicted stress (ksi)	
Ch0	**Top**	36	1.04	1.15	90%	-89	-2.58	-2.96	87%
Ch1	**Bot.**	-34	-0.98	-1.15	85%	105	3.03	2.96	103%
Ch2	**Bot.**	-34	-0.98	-1.15	85%	93	2.71	2.96	92%

2) Test Runs #1, 3, 5, and 7 Results

As indicated in Table 17, Test Runs #1, 3, 5 and 7 were conducted to study the behavior of stringers without any bracing. They accounted for a rigid or flexible interior floor beam and the stringer bottom flanges were either unbolted or bolted at the floor beam. Figure 38 presents load-vertical deflection plots at Loc. 3 and indicates comparable vertical stiffness for all test runs. Load-lateral deflection plots in Figure 39, however, show that Test Run #3 provided the largest lateral stiffness because stringer bottom flanges were bolted to the floor beam and the floor beam was supported underneath each stringer (stiff). Test Run #1 provided the lowest lateral stiffness because stringer bottom flanges were not connected to the floor beam. Test Runs #5 and 7, both of which had flexible interior supports, exhibited lateral stiffness between Test Runs #1 and 3. Test Run #7 provided slightly higher lateral stiffness than Test Run #5 because stringer bottom flanges were bolted to the floor beam.

Figure 38. Load-vertical deflection plots, Test Runs 1, 3, 5, and 7

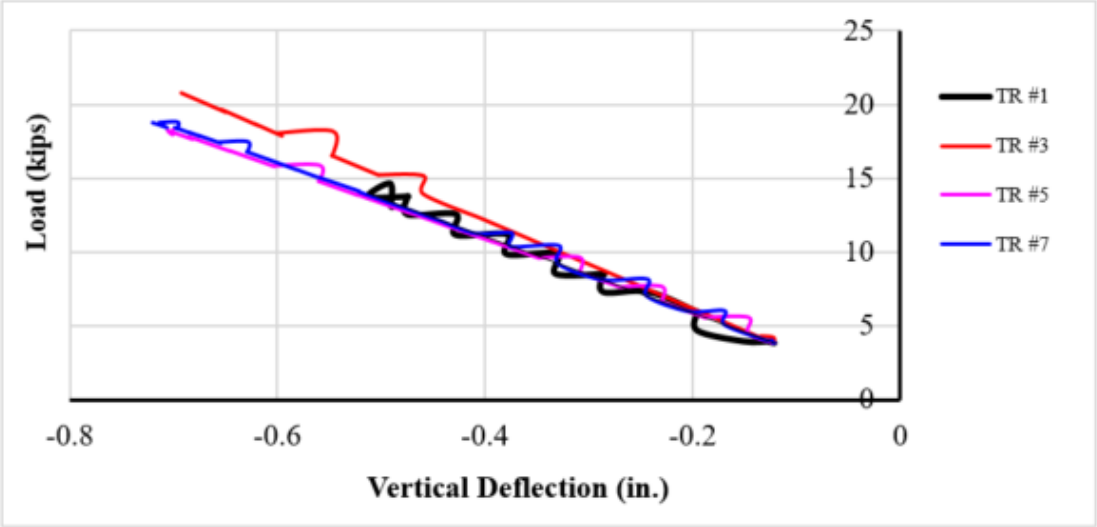

Figure 39. Load-lateral deflection plots, Test Runs #1, 3, 5, and 7

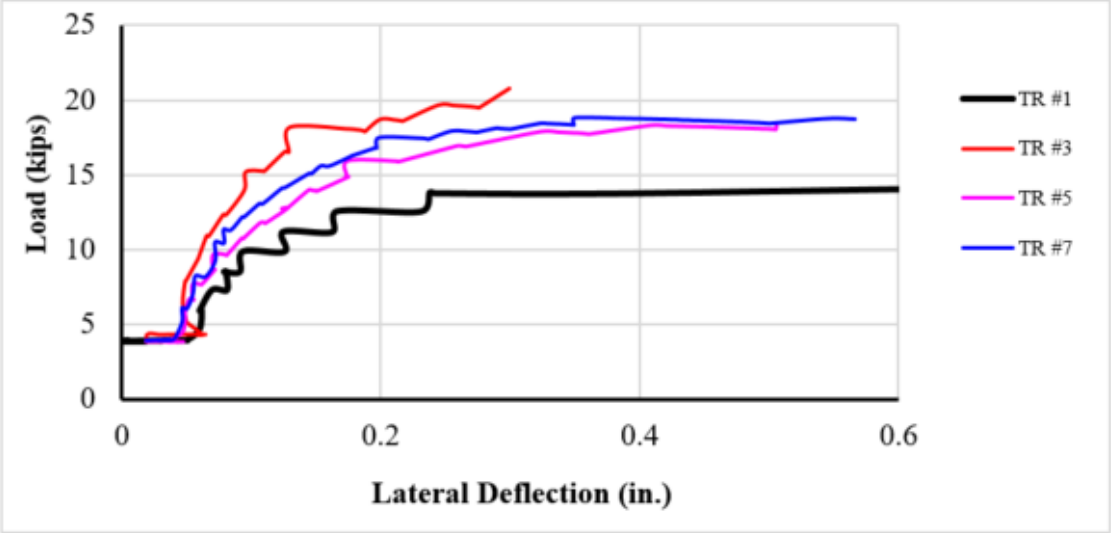

Figures 40 to 43 present load-strain plots for the four tests at Loc. 3 TN (top north), TS (top south), BN (bottom north), and BS (bottom south). Test Run #1 exhibits comparable strains to the other three test runs until it reaches its peak load, which is lower than that for the other test runs. Similar plots are provided in Figures 44 to 47 at Loc. 6 and they slightly differ for the four test runs. Test Run #1 exhibits LTB under a lower load. Similar plots are provided for Test Runs #2, 4, 6, and 8, where both spans are loaded, in Appendix I.

Figure 40. Load-strain plots at Loc. 3 TN

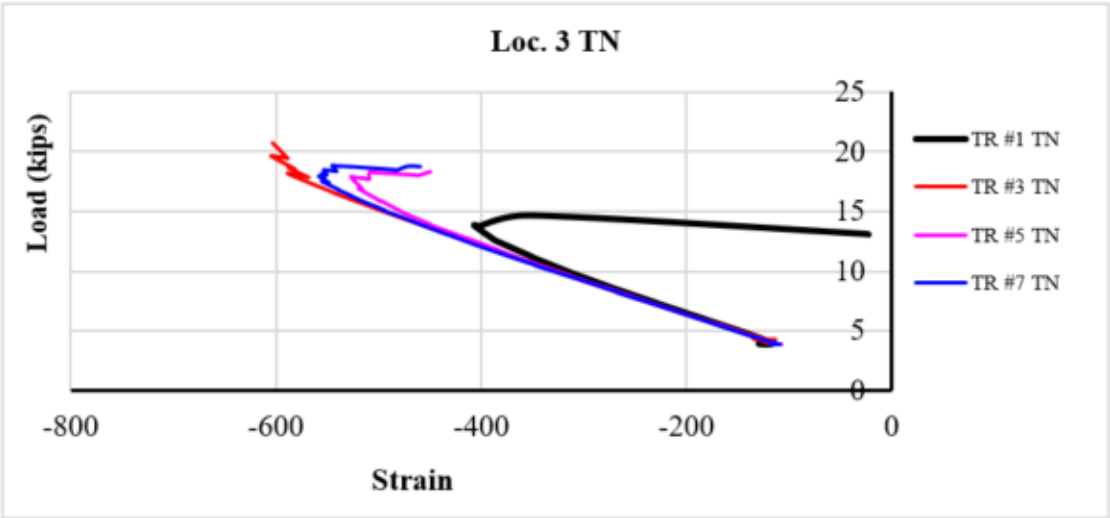

Figure 41. Load-strain plots at Loc. 3 TS

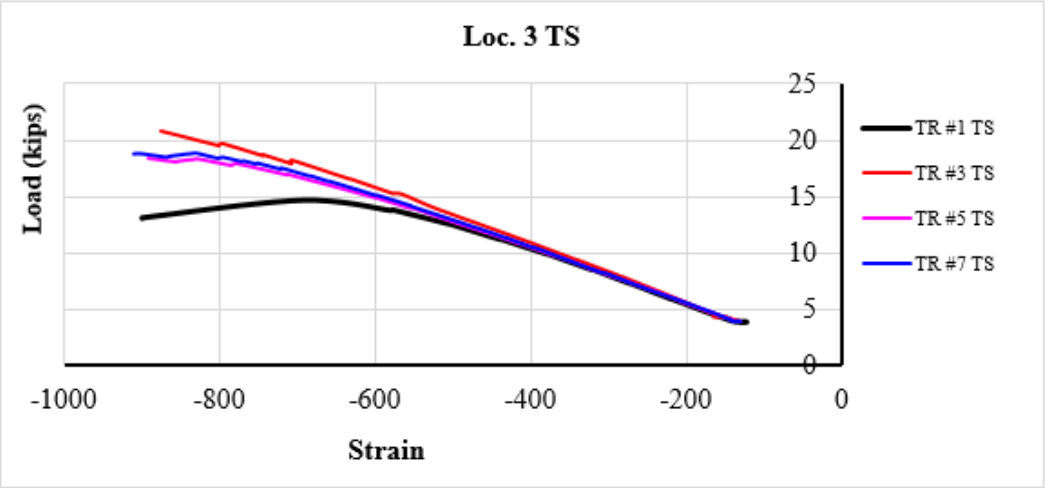

Figure 42. Load-strain plots at Loc. 3 BN

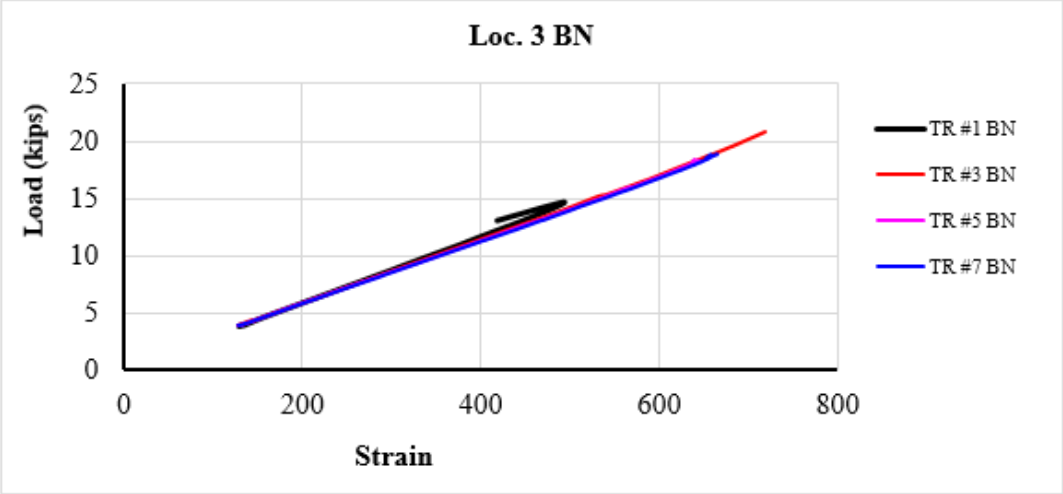

Figure 43. Load-strain plots at Loc. 3 BS

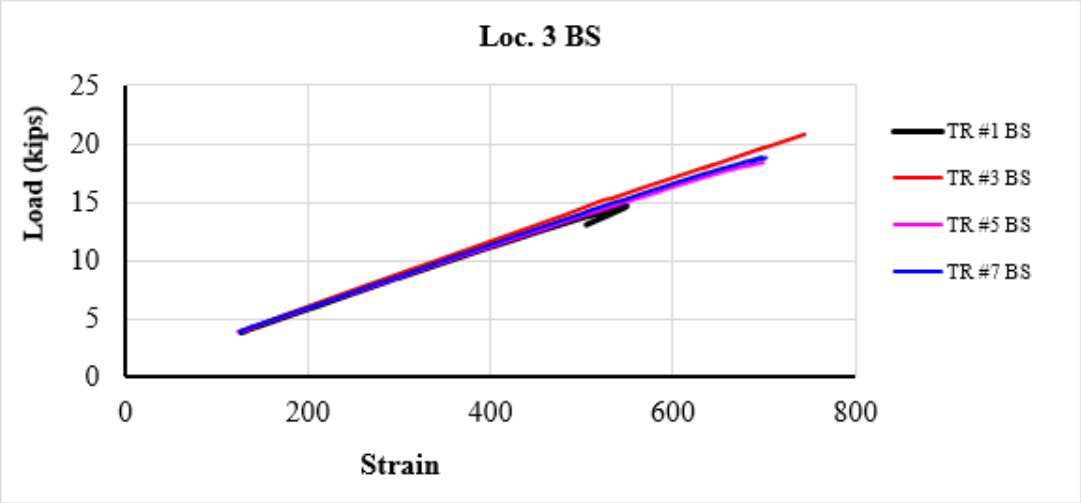

Figure 44. Load-strain plots at Loc. 6 TN

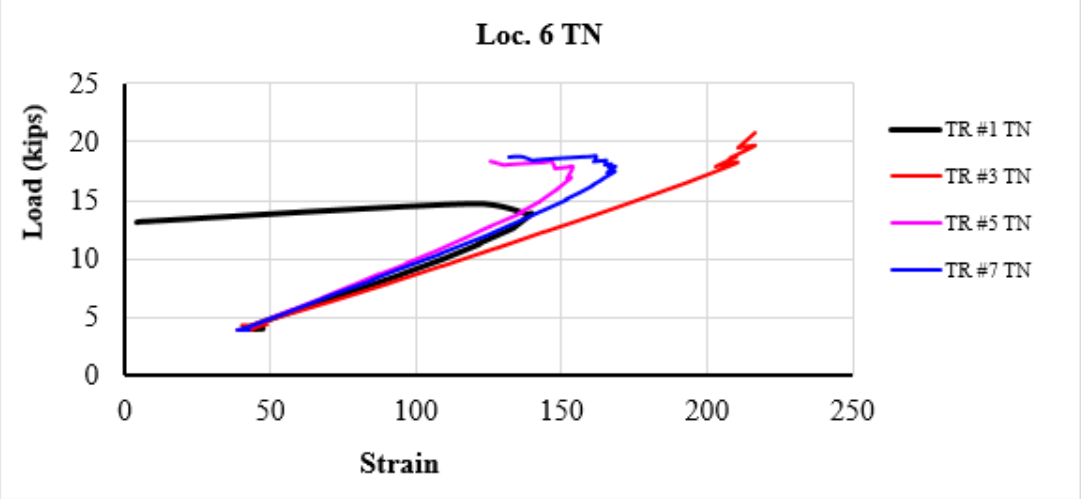

Figure 45. Load-strain plots at Loc. 6 TS

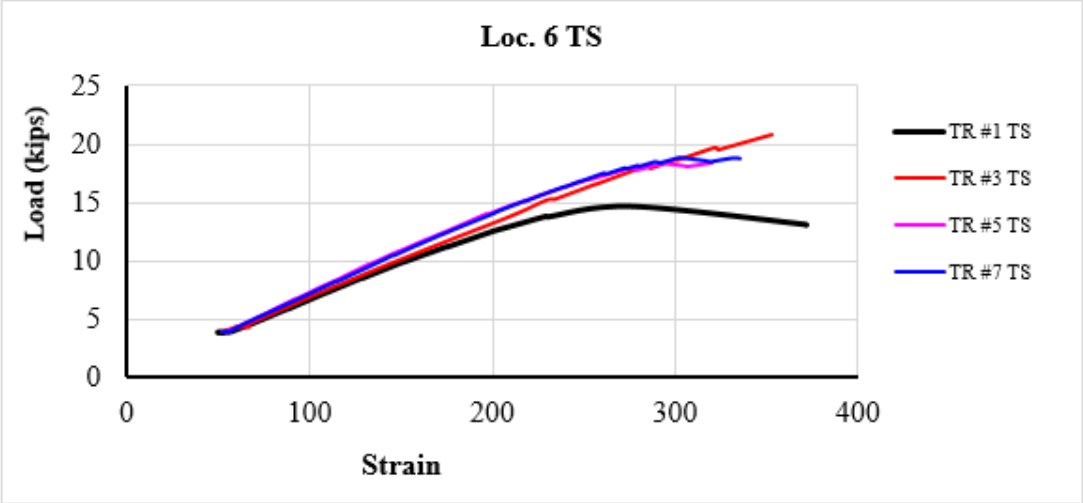

Figure 46. Load-strain plots at Loc. 6 BN

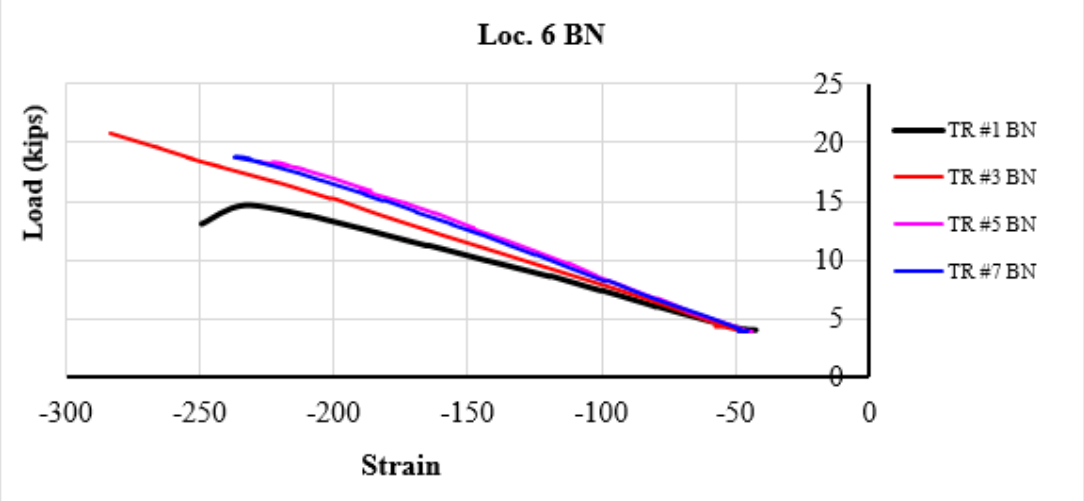

Figure 47. Load-strain plots at Loc. 6 BS

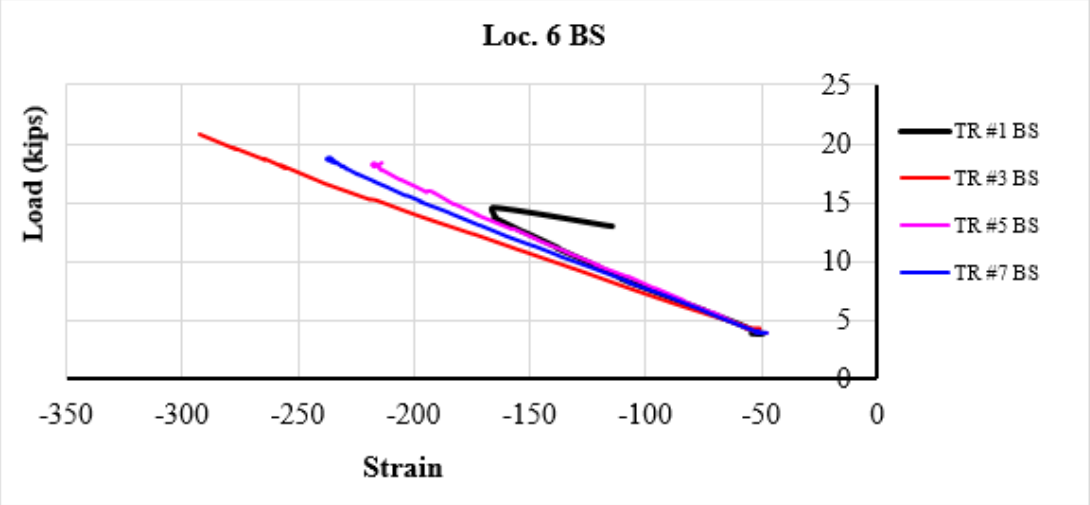

3) Stress Components Corresponding to Strain Gauge Readings

To further assess behavior at a typical section, strains were converted to stresses and values were decoupled to capture axial, primary and out-of-plane bending, and warping torsion normal stress components (Figure 48). Warping torsion results in tendency of portions of structural element to move out of plan. If the out-of-plane movement is prevented, it generates both in-plane shear stresses and stresses normal to plane. Warping torsion can be seen as a force couple to each flange.

Figure 48. Stress components

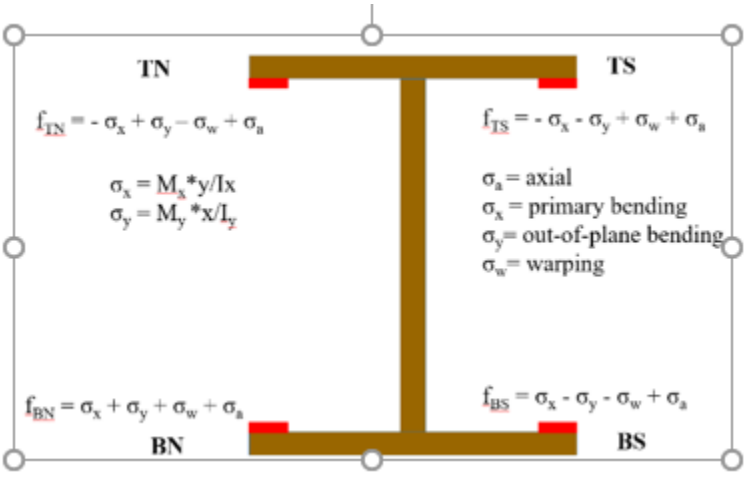

Figures 49 to 52 provide load verses stress plots for each stress component at Loc. 3 for Test Run #1. Stresses at the four gage locations at Loc. 3 are plotted. Axial stresses are

typically zero, as expected, while weak-axis bending and warping torsion stresses experience a gradual increase after peak load, indicating that LTB occurs. Note Figure 49 and Figure 50 that the magnitude and sign associated with out-of-plane bending stress σ_y and warping stress σ_w appreciably impact σ_{Total}. Figure 51 and Figure 52 indicate that out-of-plane bending and warping stresses are of similar sign and do not significantly affect σ_{Total}. Similar plots are provided at Loc. 6 in Figures 53 to 56 and stress components at other critical sections and for other test runs are provided in Appendix II.

Figure 49. Stress components, Loc. 3 TN, Test Run #1

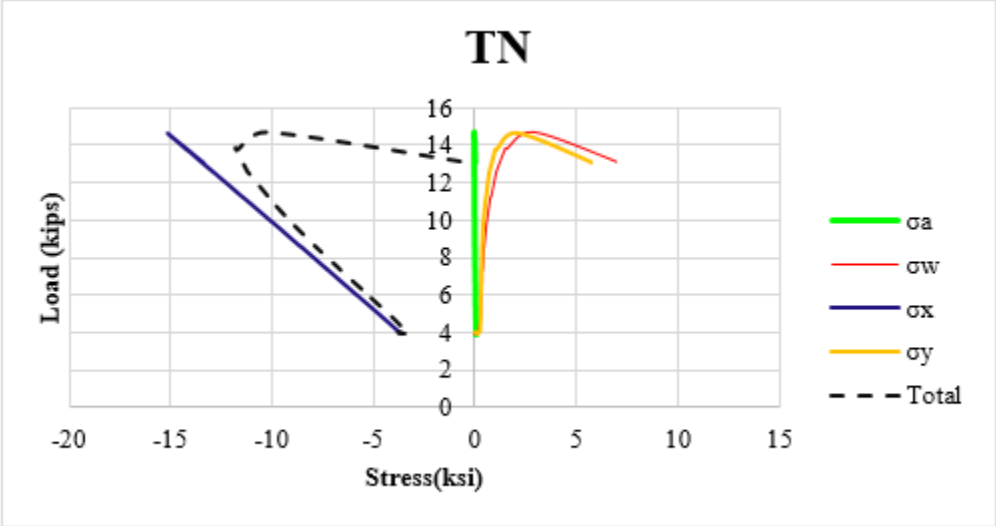

Figure 50. Stress components, Loc. 3 TS, Test Run #1

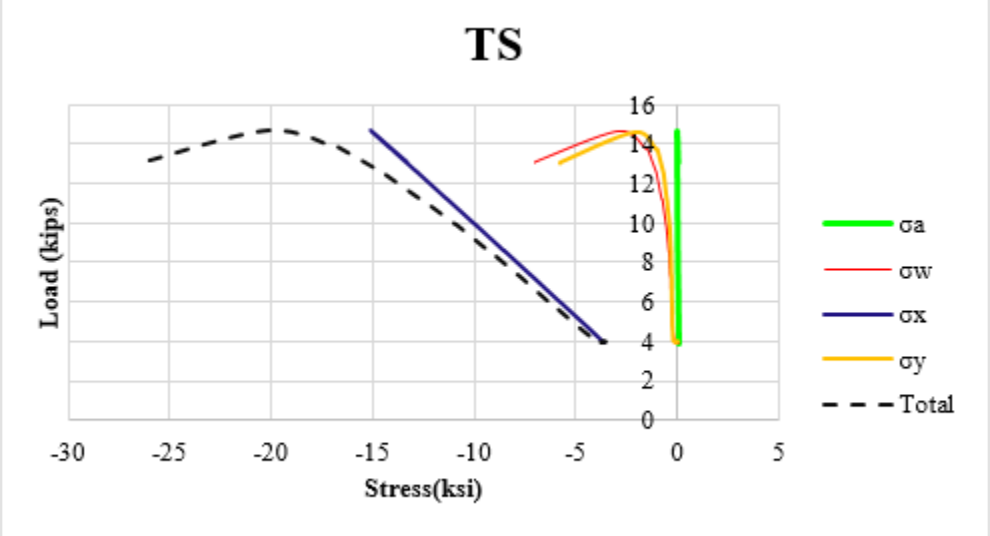

Figure 51. Stress components, Loc. 3 BN, Test Run #1

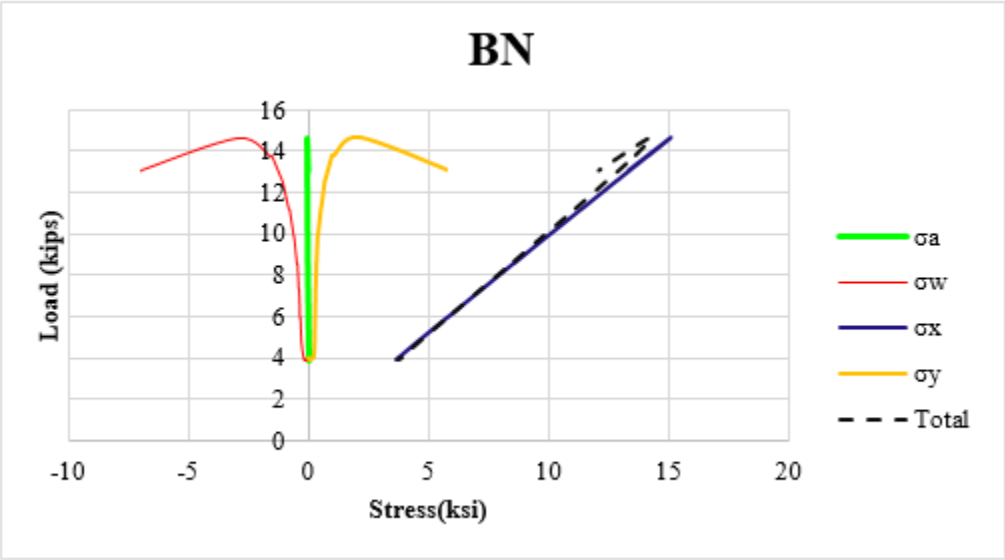

Figure 52. Stress components, Loc. 3 BS, Test Run #1

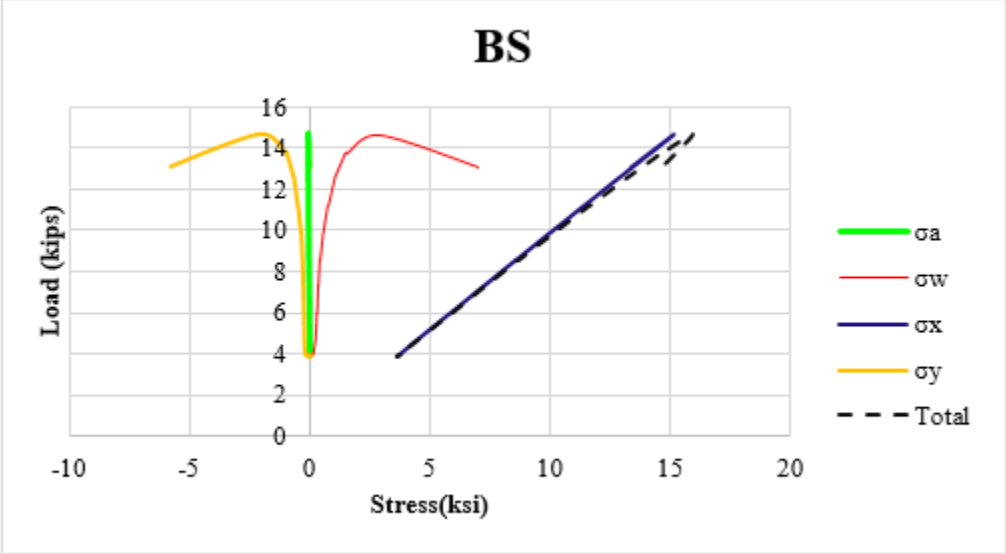

Figure 53. Stress components, Loc. 6 TN, Test Run #1

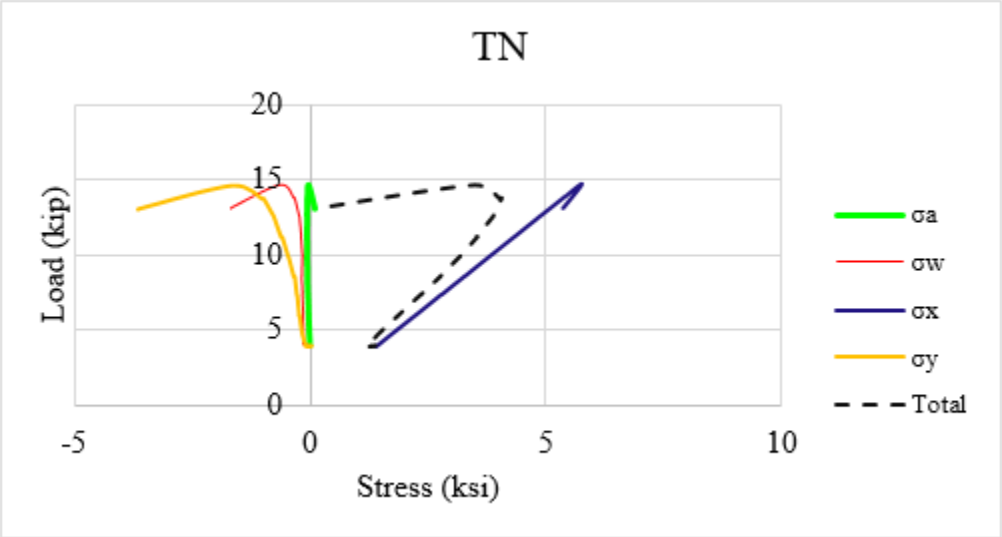

Figure 54. Stress components, Loc. 6 TS, Test Run #1

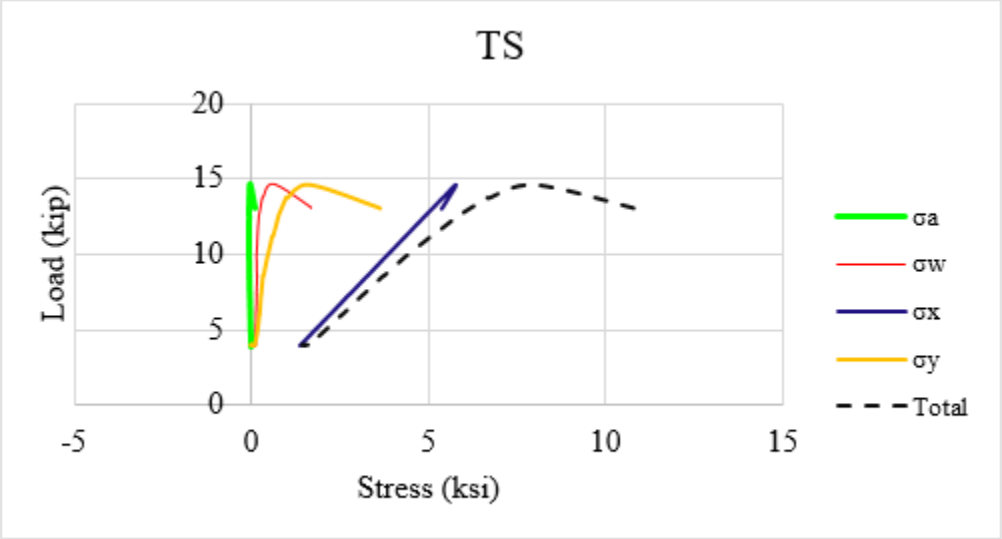

Figure 55. Stress components, Loc. 6 BN, Test Run #1

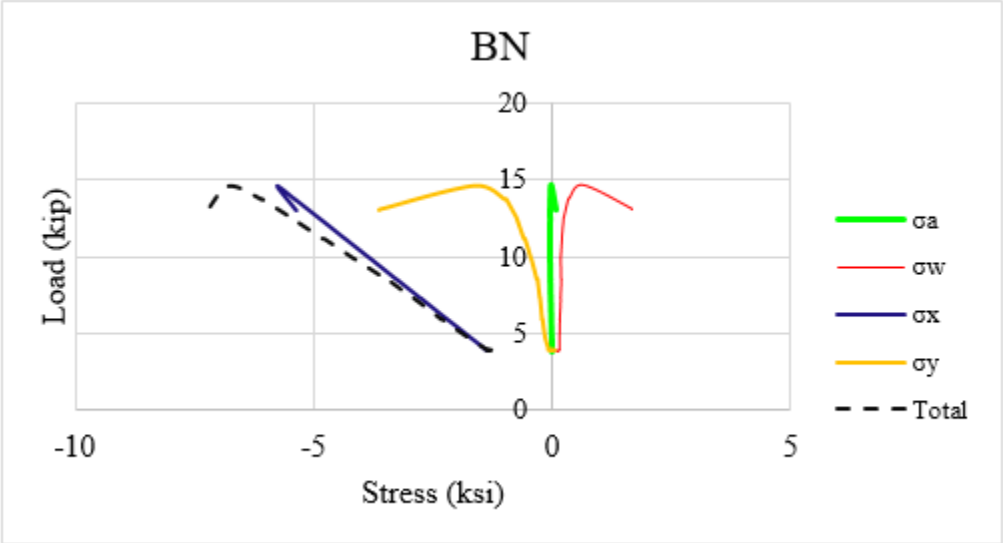

Figure 56. Stress components, Loc. 6 BS, Test Run #1

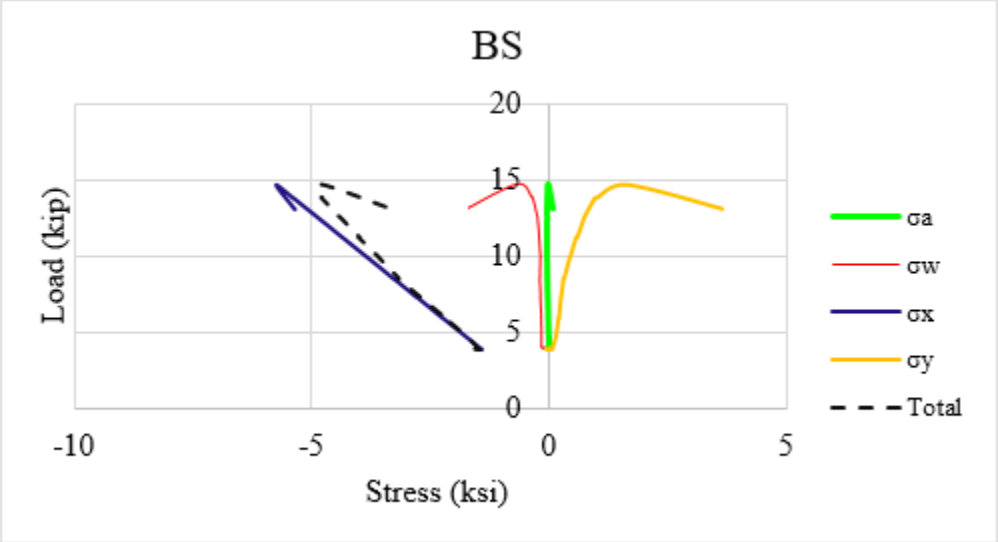

Figure 57 illustrates the effect of floor beam relative stiffness on observed response for Test Runs #1 to 8. A flexible floor beam results in approximately 10% difference for LTB resistance for most cases. Figure 58 illustrates the effect of stringer to floor beam fixity for Test Runs #1 to 8. LTB commonly occurs at higher applied load when the stringer bottom flange is connected to the floor beam.

Figure 57. Effect of floor beam relative stiffness on loading capacity

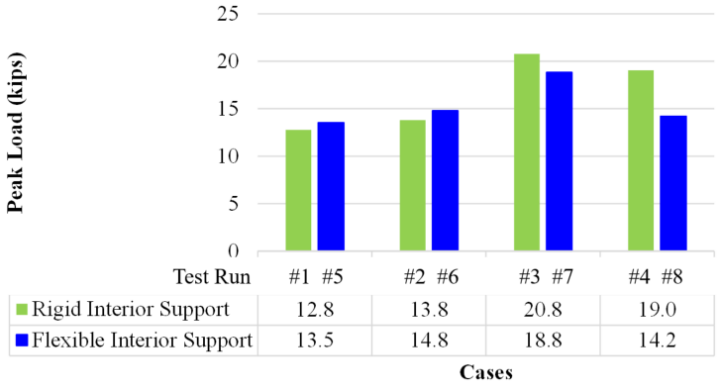

Figure 58. Effect of stringer to floor beam fixity on loading capacity

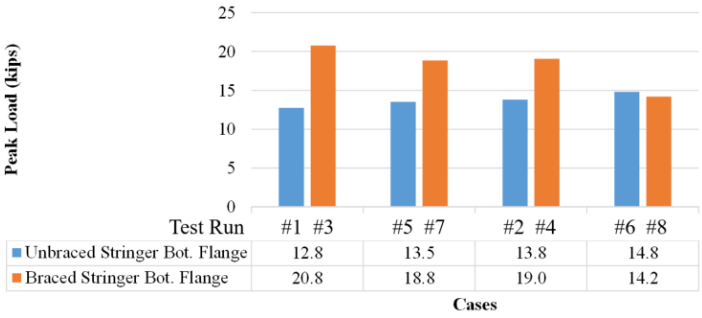

Group II Test Results – Intermediate Bracing by Diaphragms

Rigid interior supports are provided for Group II test setups, while the stringer bottom flanges are either unbraced or braced by the floor beam. Installation of intermediate steel diaphragms directly reduces the stringer's unbraced length and therefore increases its LTB resistance. Test Run #15 is taken as one example to present the testing data. Other results are provided in Appendix III. Steel diaphragms are located at a quarter span from the interior support and the interior stringer is subject to loading at one span only. Load-vertical and load-lateral deflections are shown at Locs. 3 and 10 (Figure 59). The interior stringer exhibited LTB when the load reached 24.3 kips, which resulted in approximately 0.8 in. lateral displacement near midspan. Load-stress plots at the critical section are illustrated in Figure 60.

Figure 59. Load-deflection plots of Test Run #15

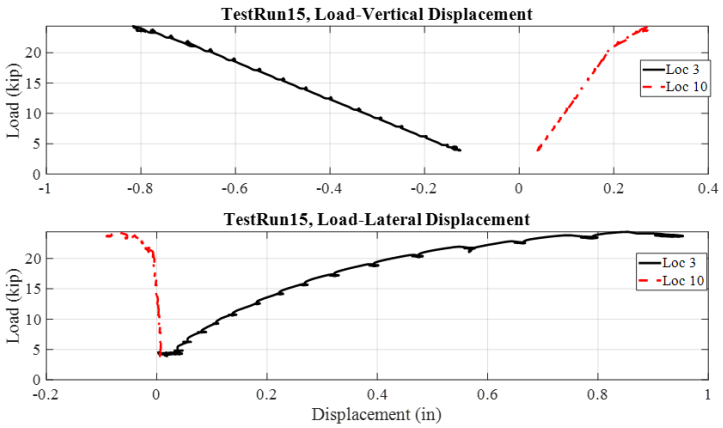

Figure 60. Load-stress plots of Test Run #15

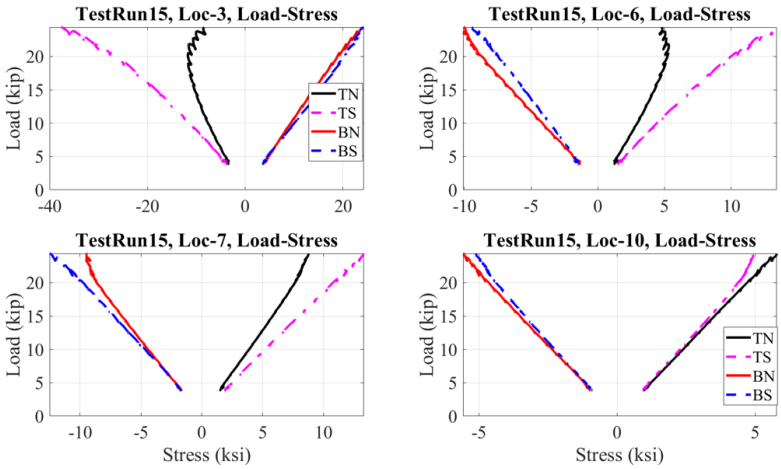

Intermediate steel diaphragms were installed at various locations to study their effect on LTB. Figure 61 illustrates buckling load capacities for unbraced lengths between 12 and 24 ft. The interior stringer is loaded at midspan of one or both spans and the stringer is bolted to the floor beam. Figure 62 is a similar comparison when the stringer bottom flange is not bolted to the floor beam. Both figures confirm that larger unbraced lengths correspond to reduced buckling loads as expected.

Figure 61. Intermediate steel diaphragm effect on LTB, stringer bolted to floor beam

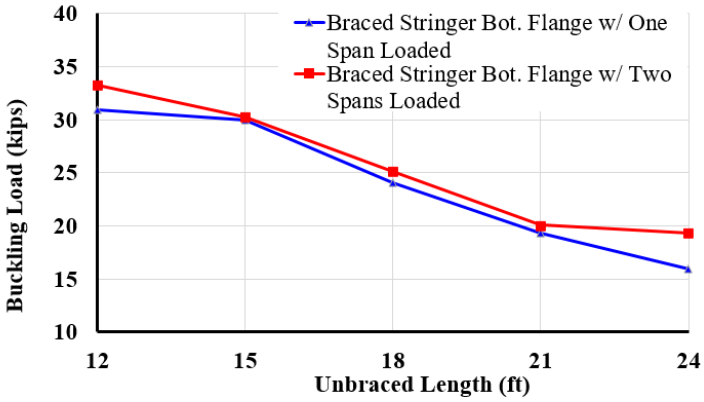

Figure 62. Intermediate steel diaphragm effect on LTB, stringer unbolted to floor beam

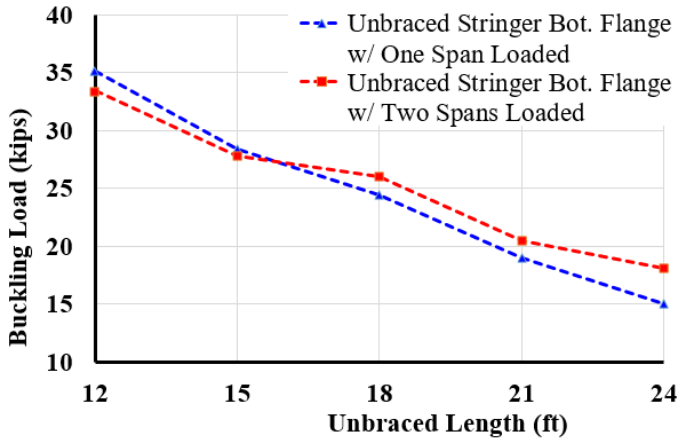

Figure 63 compares experimental LTB resistance as a function of unbraced length to those obtained from specifications and codes, including the *AASHTO LRFD Bridge Design Specifications* and *AISC Steel Construction Manual*. It shows that the calculated LTB resistance from testing data is generally lower than the predicted values using these references. Table 20 lists calculated flexural strengths and corresponding moment gradient factors obtained from selected specifications and codes to tests values for an unbraced length of 18 ft.

Figure 63. LTB resistance for various unbraced lengths

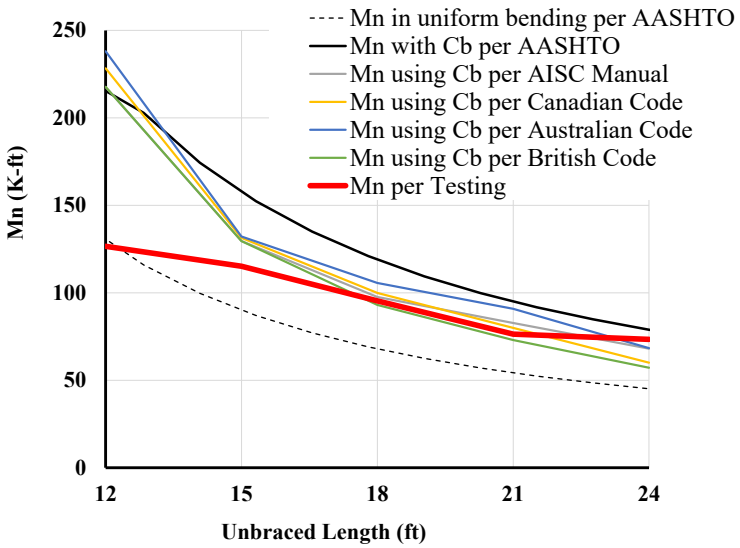

Table 20. Comparison of M_n and C_b, unbraced length of 18 ft.

Sources	M_n (Kip-ft.)	C_b
AASHTO	118.9	1.75
AISC	97.2	1.43
Canada	99.4	1.46
Australia	105.2	1.55
U.K.	92.5	1.36
Lab Testing	95.4	1.40

Group III Test Results – Intermediate Bracing Using Timber Ties

As indicated in Table 17, Group III tests were of the grillage system braced by timber ties. These ties (4”x4”) were installed on the stringer top flanges using C-clamps. Table 21 lists the descriptions of Test Run (TR) Nos. 2, and 29 to 32 that are subject to loading at both spans. Figures 64 and 65 show the load-vertical and load-lateral deflection plots. Figure 66 to 73 show the load-strain plots at both Locs. 3 and 6 corresponding to four strain gauges at each location, TN, TS, BN, and BS. Use of timber ties at midspan (TR #29) can nearly double the loading capacity as compared to the baseline (TR #2). When the stringer is braced at its midspan (TR #29), the bracing effect is more effective as compared to TR #30 (ties spaced at L/3). The bracing effects of ties in TRs #31 (ties spaced at L/4) and #32 (ties spaced at L/5) are nearly the same.

Table 21. Descriptions of Test Run #2, and 29 to 32 that are subject to loading at both spans

Test Run No.	Description of boundary conditions			
	Floor beam relative stiffness	Stringer top flange bracing		Stinger bottom flange bracing
2	Rigid	Unbraced		Unbraced
29	Rigid	Timber ties (4"x4"), connected using C-clamps	Spaced at L/2	Unbraced
30	Rigid		Spaced at L/3	Unbraced
31	Rigid		Spaced at L/4	Unbraced
32	Rigid		Spaced at L/5	Unbraced

Figure 64. Load-vertical deflection plots

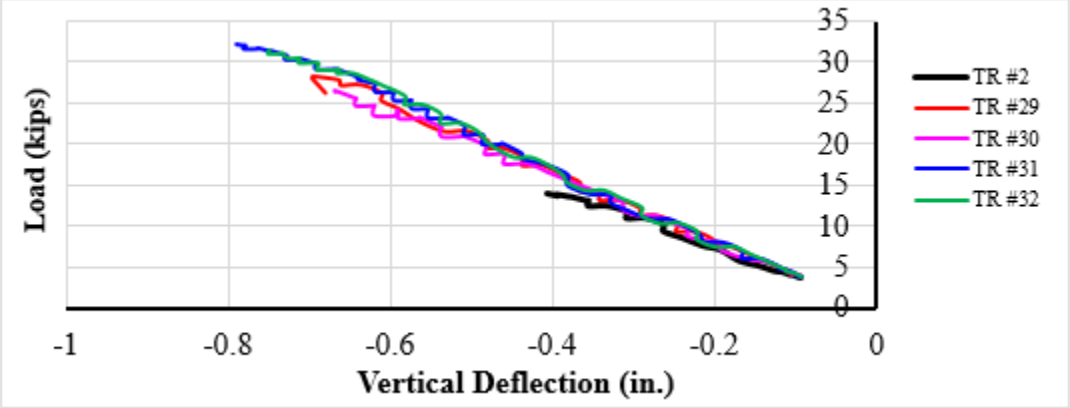

Figure 65. Load-lateral deflection plots

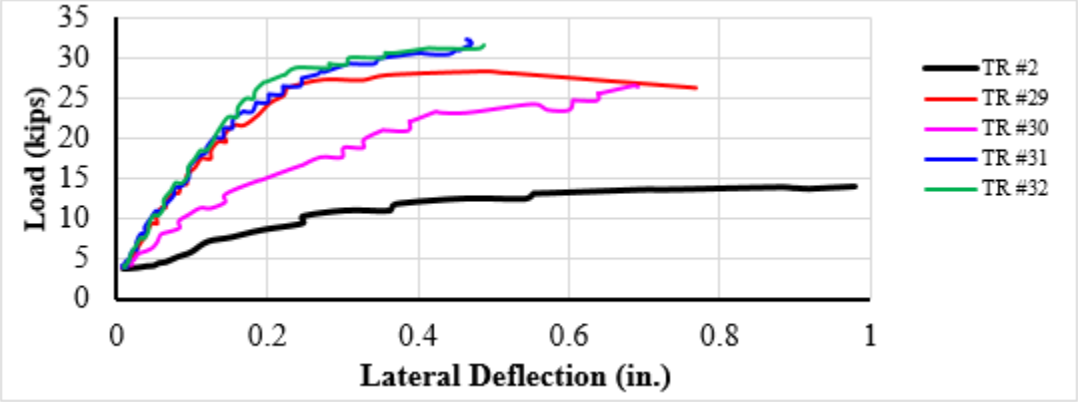

Figure 66. Load-strain plots at Loc. 3 TN

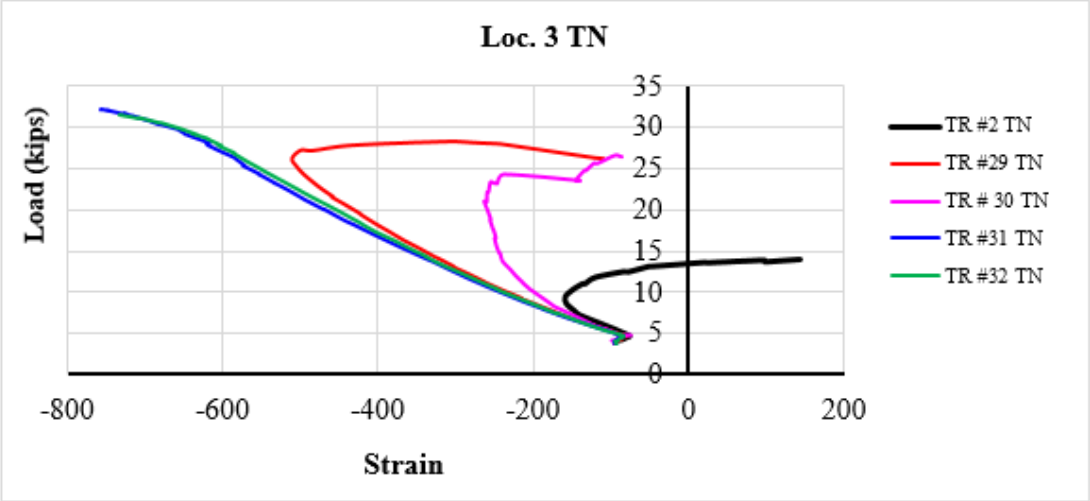

Figure 67. Load-strain plots at Loc. 3 TS

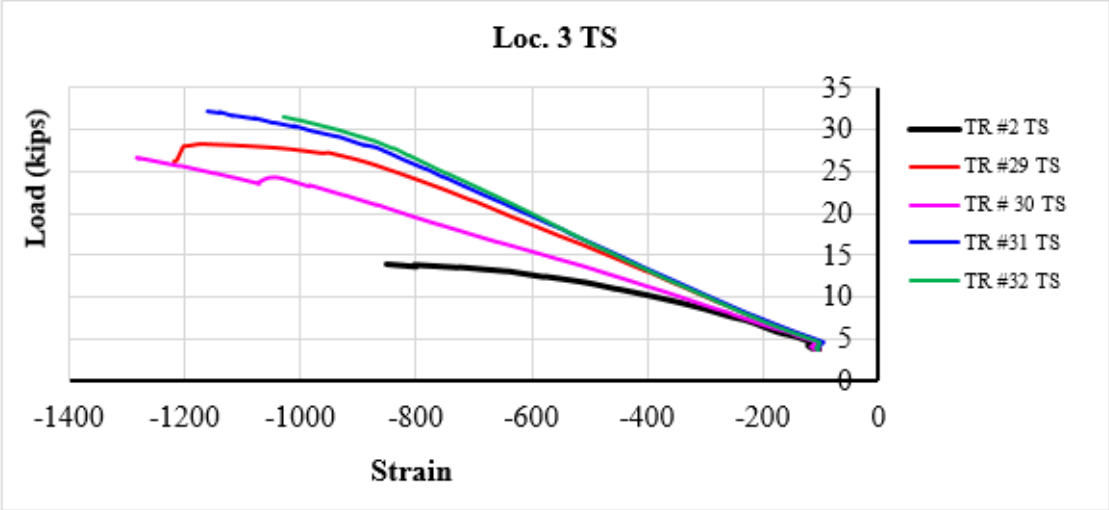

Figure 68. Load-strain plots at Loc. 3 BN

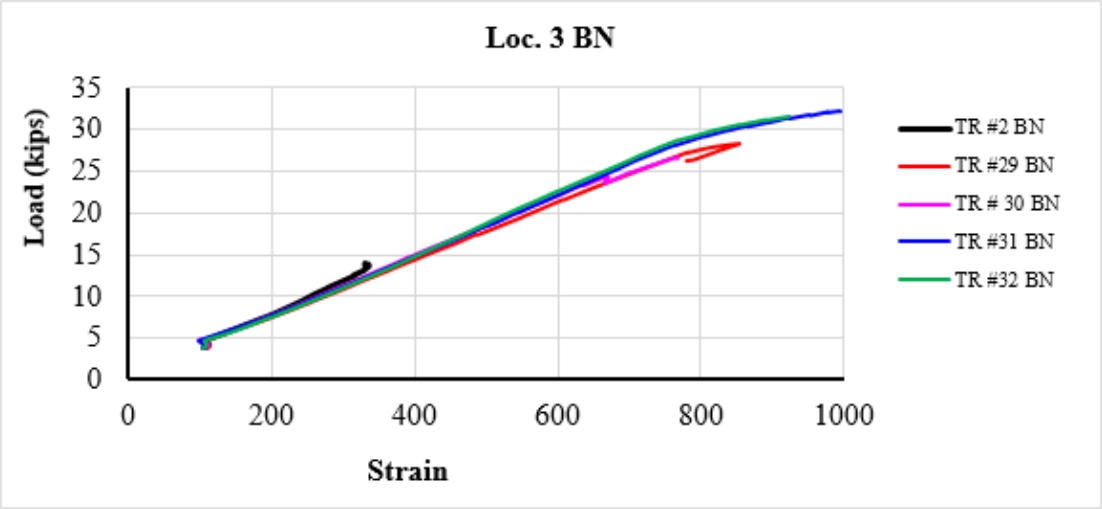

Figure 69. Load-strain plots at Loc. 3 BS

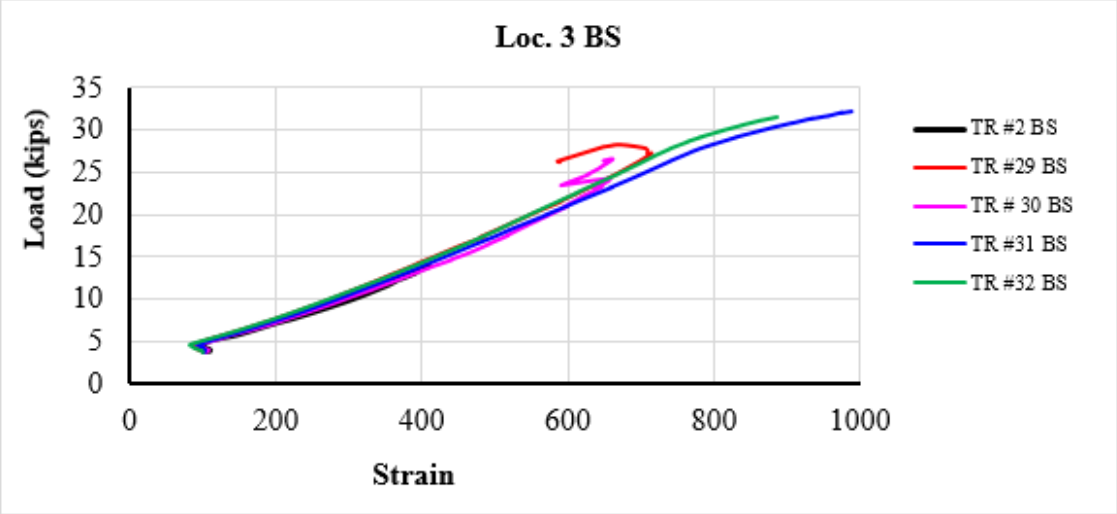

Figure 70. Load-strain plots at Loc. 6 TN

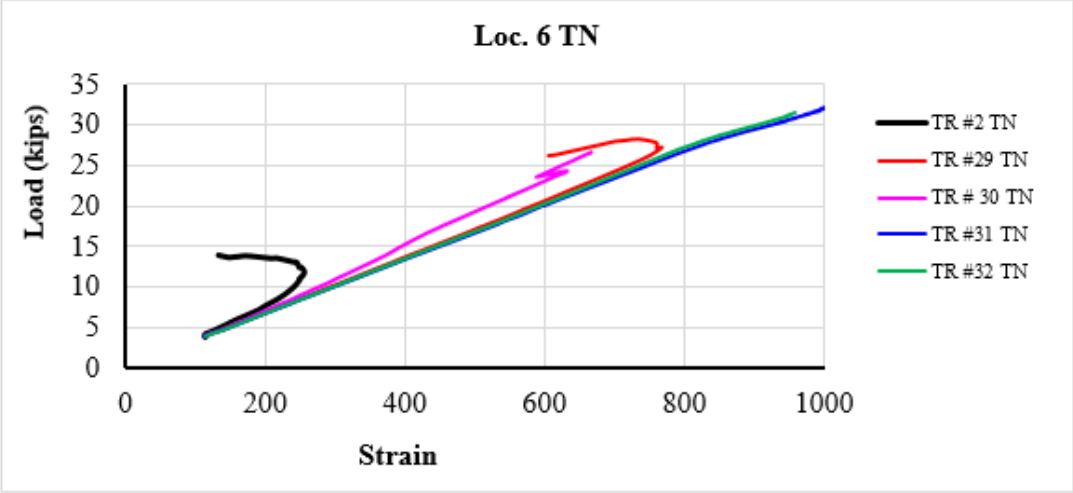

Figure 71. Load-strain plots at Loc. 6 TS

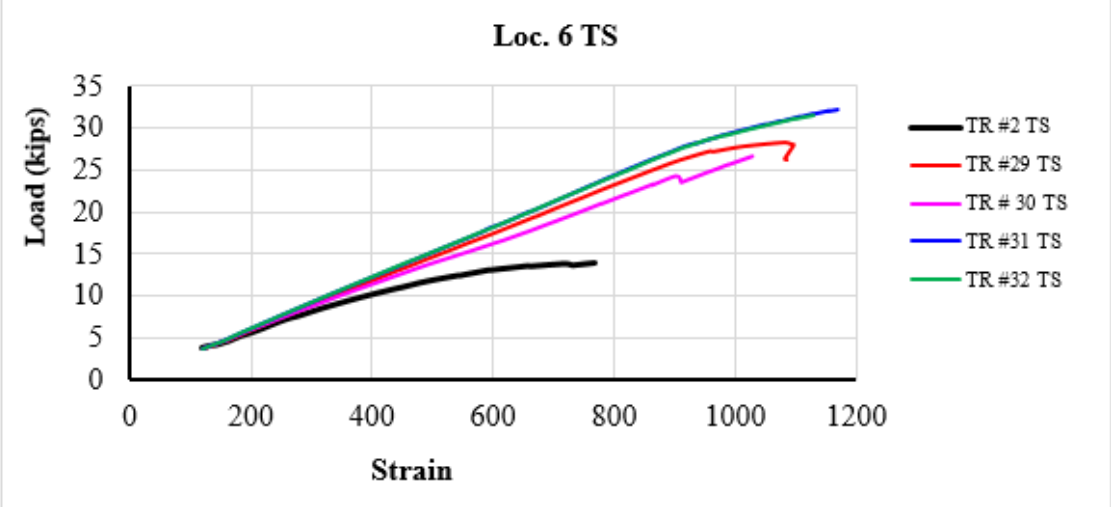

Figure 72. Load-strain plots at Loc. 6 BN

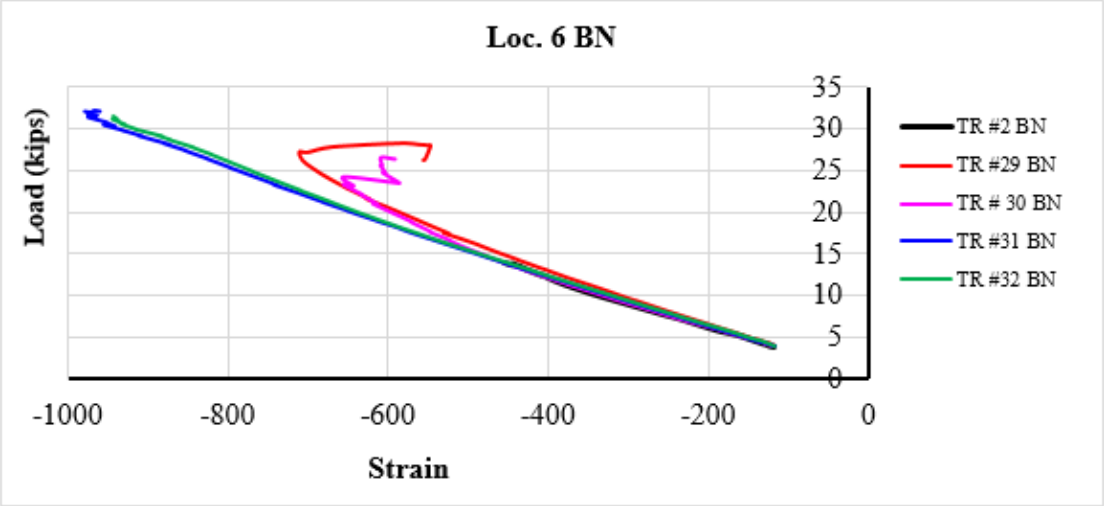

Figure 73. Load-strain plots at Loc. 6 BS

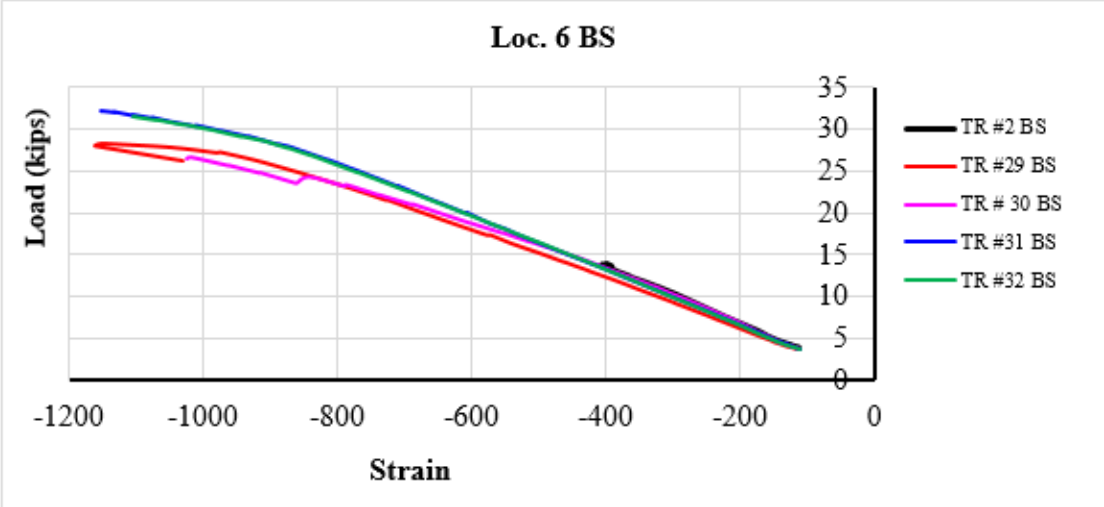

The bracing effect of timber ties is evaluated for a number of test runs involving either rigid or flexible interior supports, as shown in Figures 74 and 75. These figures plot the buckling loads versus timber tie spacing. Group III test results show that the LTB resistance can be increased significantly using minimal lateral stiffness provided by 4-in. by 4-in. timber ties and C-clamps. For example, buckling load increased by approximately 70% for all tests when timber ties were provided only at midspan. These results are expected and are consistent with the finding reported elsewhere [22].

Figure 74. Bracing effect of timber ties with rigid interior support

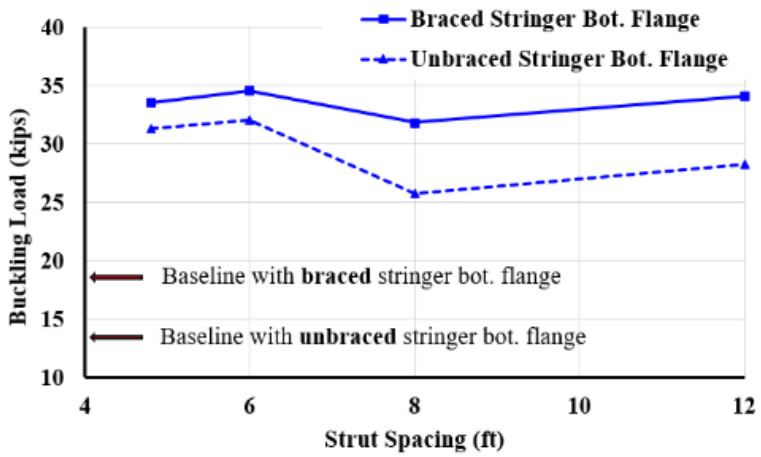

Figure 75. Bracing effect of timber ties with flexible interior support

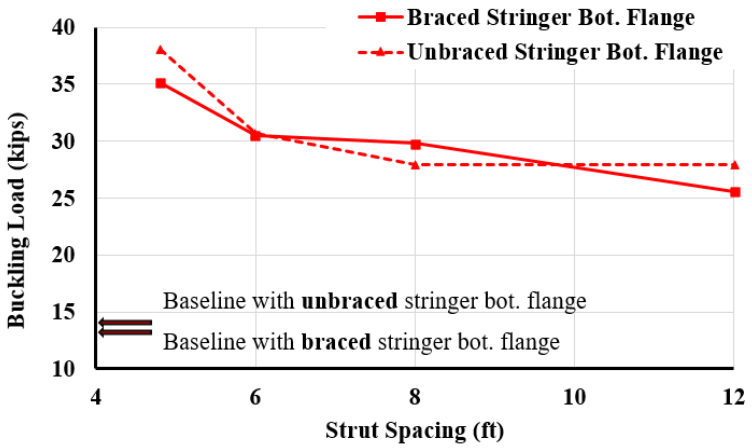

Finite Element Analyses

Finite element analysis (FEA) simulated stringer behavior while accounting for various parameters, including geometric imperfections, various bracing configurations, rigid and flexible interior supports, other loading conditions, etc. FEA was completed using ANSYS R19. A combination of static, linear Eigenvalue buckling, and non-linear buckling analyses were performed. Stringer geometry measurements were collected using laser scans prior to the tests. An initial imperfection for the interior stringer, approximately $L/1{,}500$ (L = span), was accounted for in the non-linear analysis following the critical buckling mode. The FEA model includes three lines of stringers, end diaphragms, and the floor beam (Figure 76). Also shown in Figure 76 is a non-composite concrete deck. Model boundary conditions at various supports are illustrated in Figure 77.

SHELL181 elements were used for the stringers, end and intermediate diaphragms, and floor beam. This shell element is a first-order element with 4 external nodes and no internal nodes and six degrees of freedom at each node: translations and rotations about the x, y, and z axes. Each stringer flange consists of 4 elements along its width while the stringer web is divided into 8 equal elements. A typical mesh of the stringer section is shown in Figure 78. The element size along the length of the stringer at each span is 2 in. A convergence study was performed to validate the mesh for both linear and nonlinear analyses. Figure 79 shows a comparison among three mesh types (fine, finer, and finest meshes) for Test Run #3 and indicates that the fine mesh type is sufficient to capture the stringer behavior.

The concrete deck in the linear analysis was modeled using SOLID185 elements. This is a linear 3D eight-node element with only three (translational) degrees of freedom. The deck has three layers of elements across the thickness and the element size in the transverse and longitudinal directions is 4 in. In the nonlinear analysis, the previous elements are substituted by CPT215 elements. CPT215 is a coupled physics 3D eight-node suitable for the microplane model used to capture the nonlinear behavior of the concrete.

LINK180 elements were used to represent the reinforcing bars in the concrete deck for both linear and nonlinear analyses. The element is a linear 3D spar with two nodes and only translation degrees of freedom suitable for uniaxial tension or compression. Similarly, this element was employed for the wood bracings in the appropriate tests because it best represented the test data compared to BEAM188, which resists load in bending. The selected structural steel stress-strain diagram is shown in Figure 80. This constitutive model was selected to match the yield strength based on the coupon tests (Appendix IV) and it is expected to reasonably capture the stringer LTB behavior. The elastic modulus of steel is assumed to be 29,000 ksi. The stringers and floor beam were Grade 50 steel, and the diaphragms Grade 36 steel. The concrete strength at the time of testing was approximately 5,000 psi (f'_c) based on the cylinder tests.

Linear elastic concrete properties were used for the linear analysis and the parameters were chosen to obtain the best imperfection for the stringers. A microplane model with coupled damage-plasticity was employed for the nonlinear analysis. This material model accounts for the elasticity, plasticity, damage, and nonlocal interaction of the concrete.

After numerous FEA model trials, use of a lateral spring with a stiffness of 1.0 kip/in. at the loading location best represented load assembly lateral stiffness and provided the most comparable results with test data. Observed lateral stiffness is attributable to friction between the load bearing plate and the interior stringer, and lateral stiffness of the loading

assembly largely provided by the two threaded rods used to support the spreader beam. Regarding the connection between the non-composite deck and stringers, initial model trials assumed no friction along any direction while the deck was explicitly constrained (only in the lateral direction) to the top flange of the stringers at discrete point along the length. After comparing with the testing results, the lateral constraint was abandoned and a frictional interface with a coefficient of 0.1 was selected along both transverse and longitudinal directions because it best matched the testing data.

Figure 76. FEA model

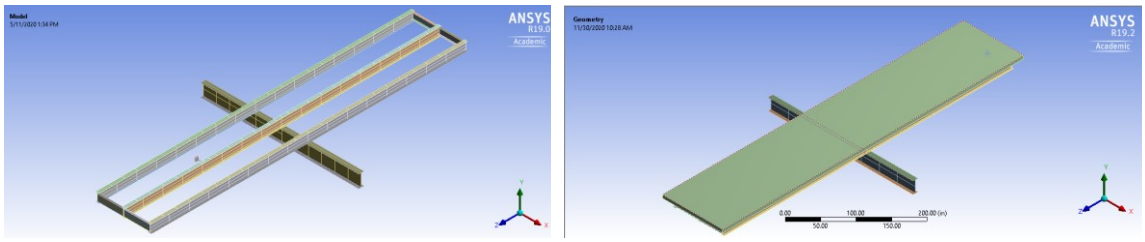

(a) Model without deck (b) Model with non-composite deck

Figure 77. Boundary conditions

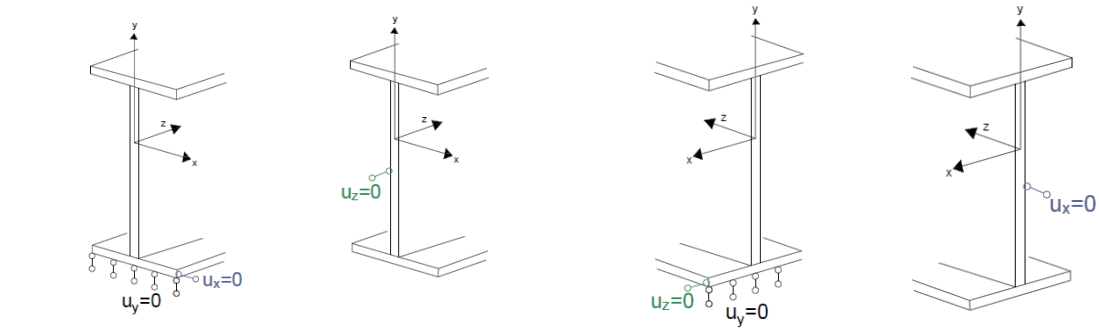

End support at all stringers

Interior support at all stringers

End support at floor beam

Midspan of the floor beam

Figure 78. Typical mesh in FEA

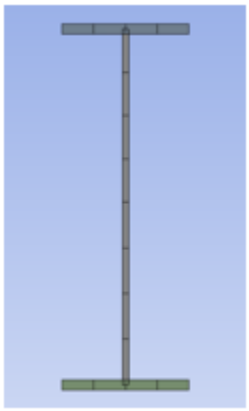

Figure 79. FEA mesh sensitivity study

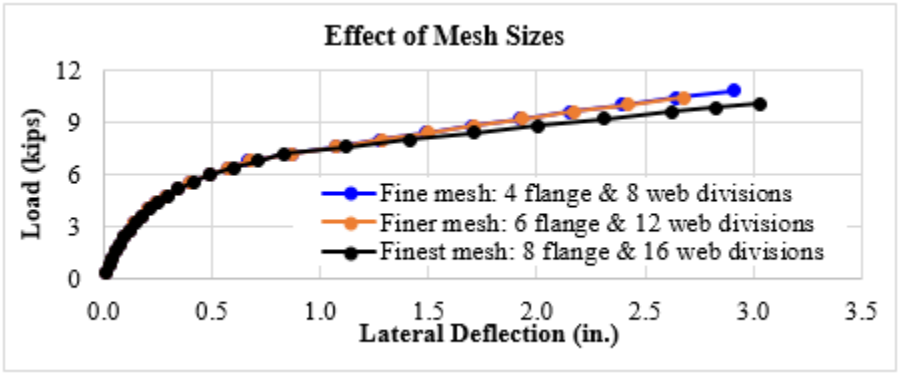

Figure 80. Selected stress-strain diagram for structural steel

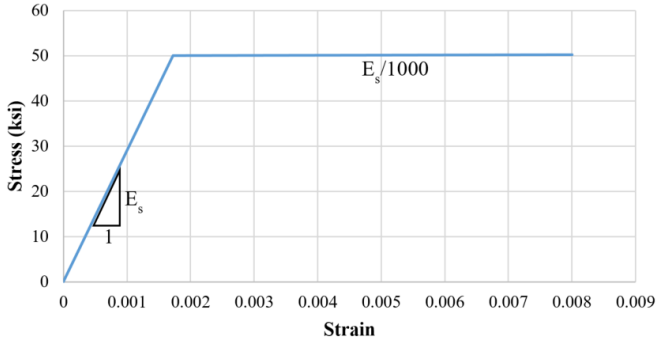

Figure 81. Selected stress-strain diagram for concrete

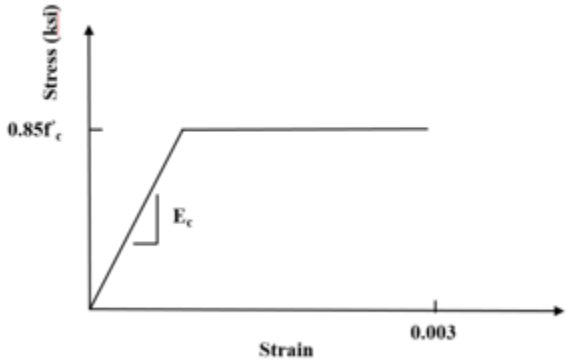

Group I FEA Results

Test Run #3 was selected as a representative example to illustrate the FEA output and make a comparison between the analysis and test results. The test represented a stiff supporting floor beam, had bolted connections between the stringer and floor beam, and was loaded in one single span. Figure 82 and Figure 83 show lateral deflection and element normal stress contours, respectively. Analysis results are compared against test data at Locs. 3 and 10 (Figure 84 to Figure 87). Analysis results are generally comparable to test data. For illustration purposes, Figure 88 shows lateral deflection plots when the stringer is loaded on both spans. Similar plots for other test runs are provided in Appendix III.

Figure 82. Lateral deflection contour, Test Run #3

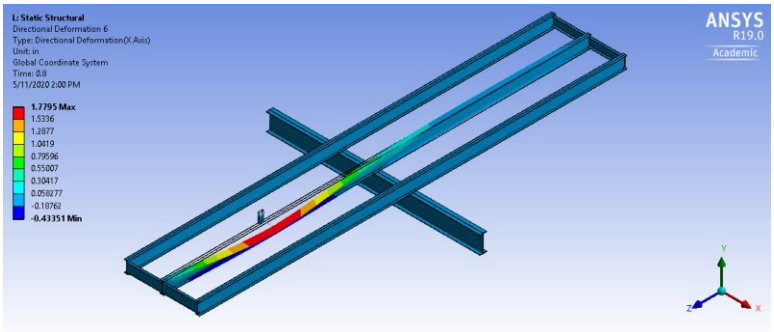

Figure 83. Normal stress contour, Test Run #3

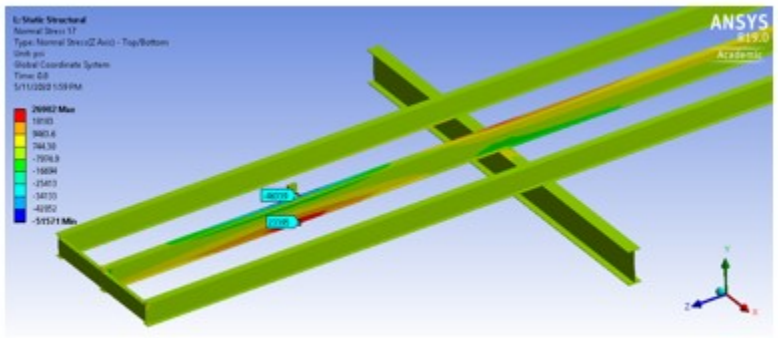

Figure 84. Comparison of FEA and measured vertical deflections, Test Run #3

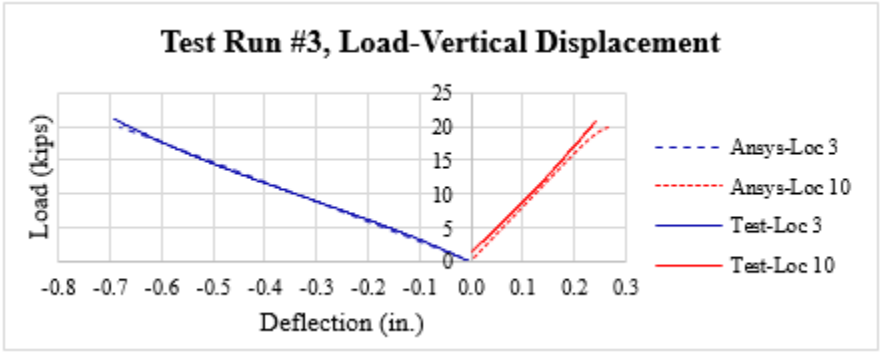

Figure 85. Comparison of FEA and measured lateral deflections, Test Run #3

Figure 86. Comparison of Loc. 3 normal stresses between analysis and test data, Test Run #3

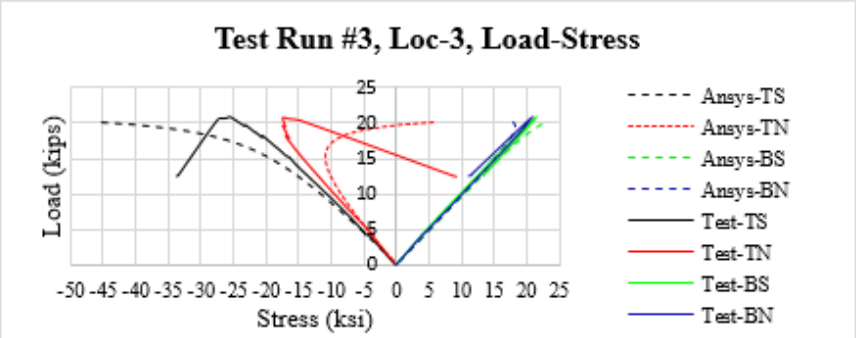

Figure 87. Comparison of Loc. 10 normal stresses between analysis and test data, Test Run #3

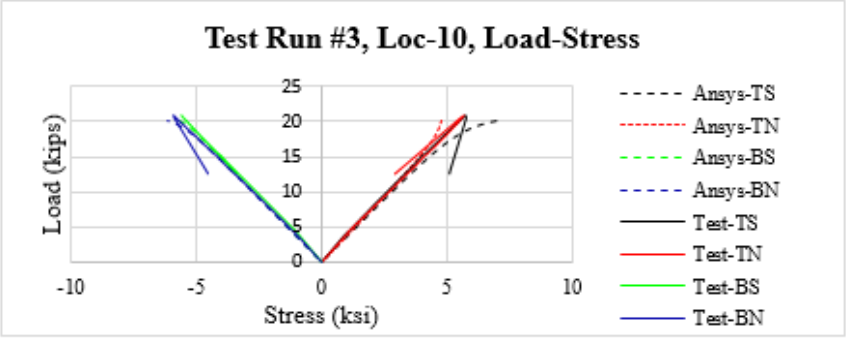

Figure 88. Comparison of FEA and measured lateral deflections, Test Run #4

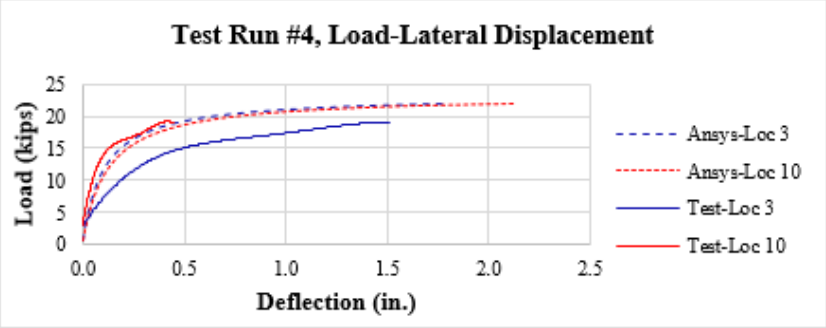

Group II FEA Results

Test Run #15 was selected as a representative example comparing FEA and test results. The test represented a stiff supporting floor beam and had unbolted connections between the stringer and floor beam. Steel diaphragms were provided at a quarter span from the interior supports. Figure 89 shows the deflection contour subject to loading at one span only. The analysis results were compared with the test data, including the vertical and

lateral deflections, and stresses at Locs. 3 and 10 (Figure 90 to Figure 93). Similar plots of other test runs are provided in Appendix III. The analysis results are generally comparable with the test data.

Figure 89. Deformation contour, Test Run #15, one span loaded

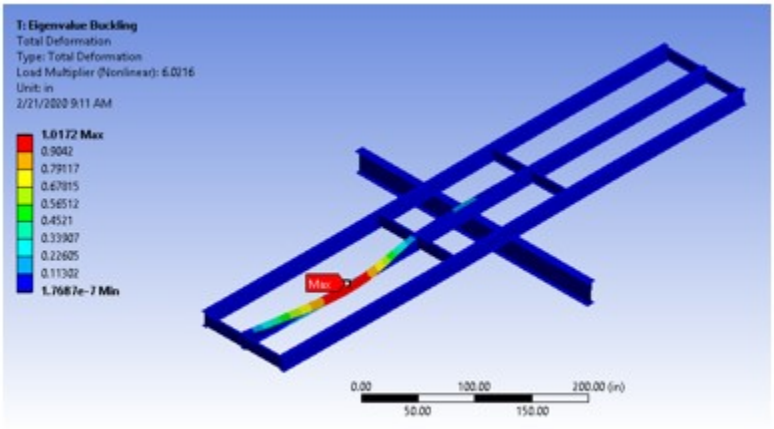

Figure 90. Comparison of FEA and measured vertical deflections, Test Run #15

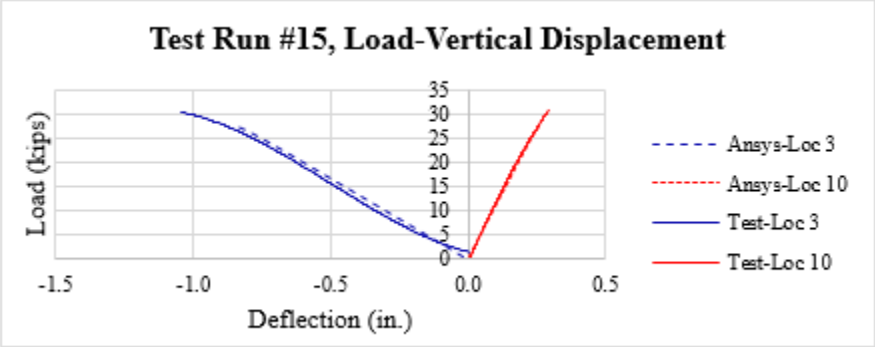

Figure 91. Comparison of FEA and measured lateral deflections, Test Run #15

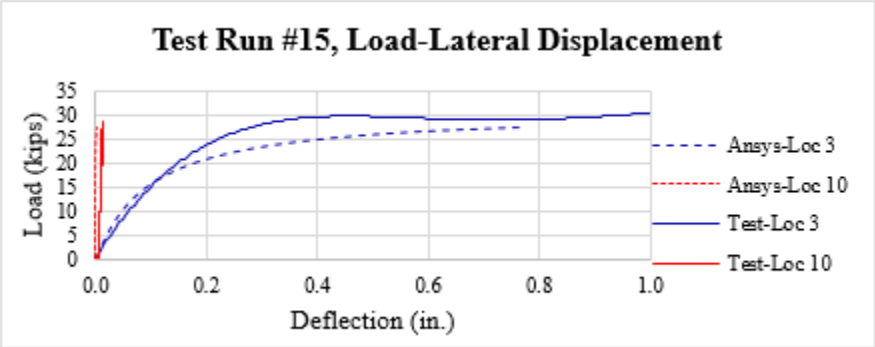

Figure 92. Comparison of Loc. 3 stresses between analysis and test data, Test Run #15

Figure 93. Comparison of Loc. 10 stresses between analysis and test data, Test Run #15

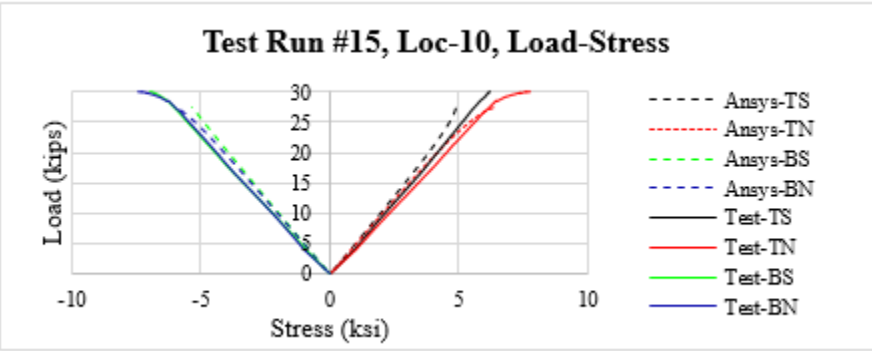

Group III FEA Results

Test Run #33 was selected as a representative example comparing FEA and test results. The test represented a stiff supporting floor beam and had bolted connections between the stringer and floor beam. The stringer top flanges were braced by timber ties and C-clamps

at the midspans and over the floor beam. Figure 94 shows the FEA model subject to loading at both spans. Figure 95 and Figure 96 present the contours of vertical and lateral deflections, respectively. The analysis results are compared with the testing data, including the vertical and lateral deflections, and stresses at Locs. 3 and 10 (Figure 97 to Figure 100). The analysis results are generally comparable with the testing data. Similar plots of other test runs are provided in Appendix III.

Figure 94. FEA model, Test Run #33

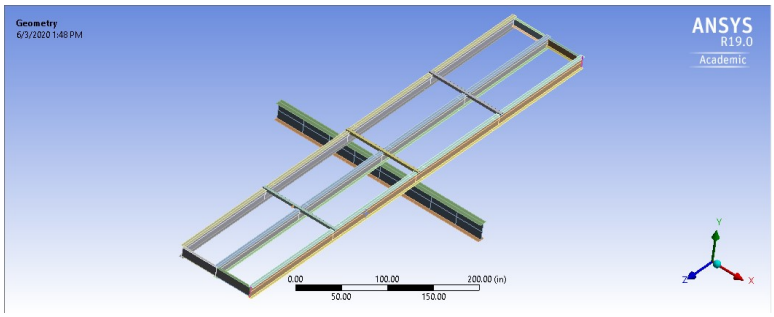

Figure 95. Vertical deflection contour, Test Run #33

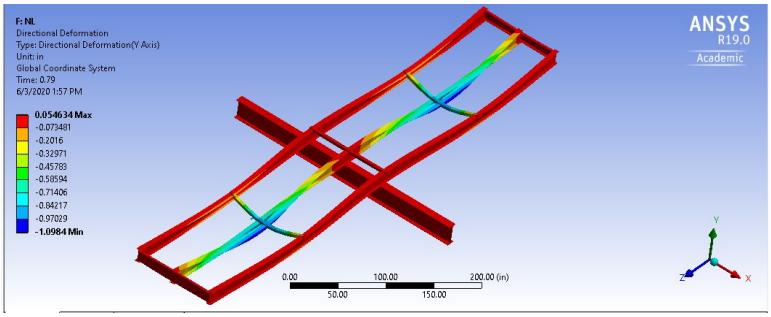

Figure 96. Lateral deflection contour, Test Run #33

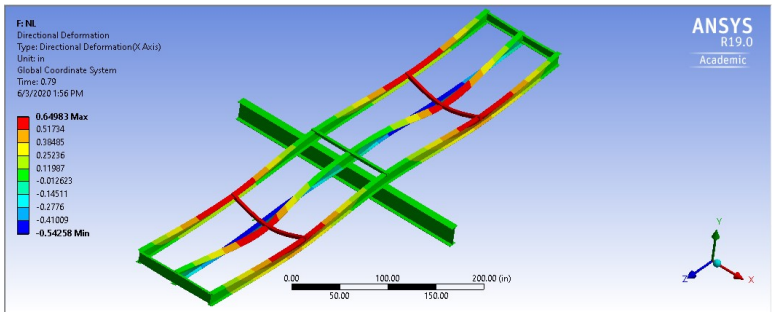

Figure 97. Comparison of FEA and measured vertical deflections, Test Run #33

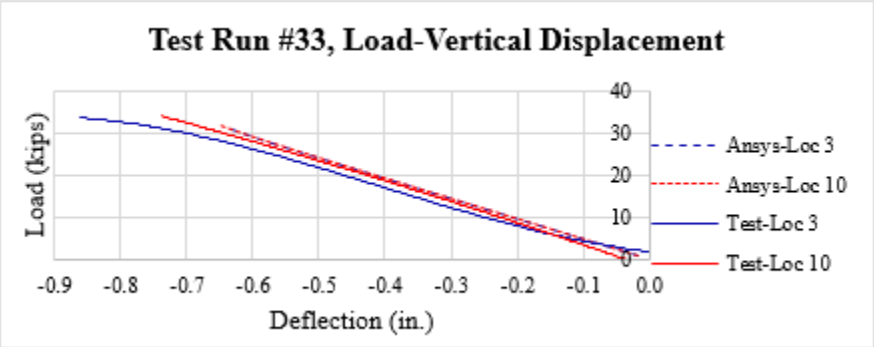

Figure 98. Comparison of FEA and measured lateral deflections, Test Run #33

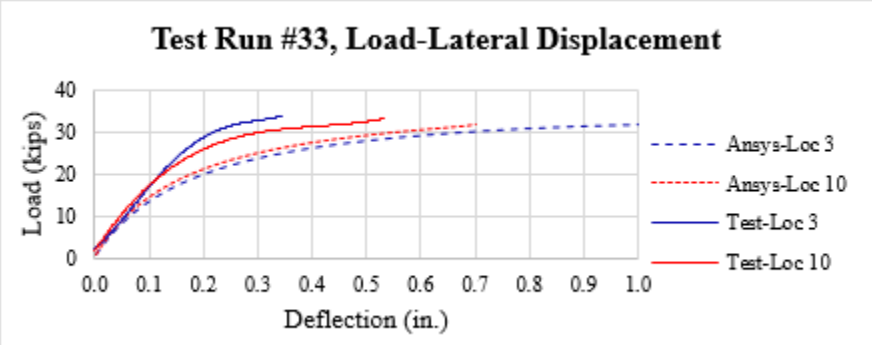

Figure 99. Comparison of Loc. 3 normal stresses between analysis and test data, Test Run #33

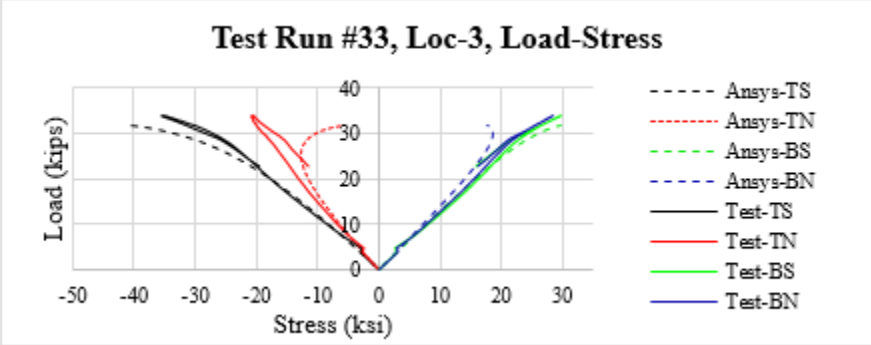

Figure 100. Comparison of Loc. 10 normal stresses between analysis and test data, Test Run #33

Group IV Test Results – Non-composite Concrete Slab

Figure 101 and Figure 102 document placement of deck reinforcement and the concrete, respectively.

Table 22 summarizes the test runs involving non-composite deck. These test runs accounted for rigid and flexible floor beam, and bolted and unbolted connections between the stringers and floor beam. Some of the test runs such as #57, 69, and 81 were loaded to approximately 80 kips, while the others were loaded to the maximum loading capacities. A majority of the test runs were subject to loading at the midspan near Loc. 3, except for Test Runs #45 and 46. In Test Run #45, two of three tests, Failure 3 and Failure 2, were loaded near Loc. 10 or across the full deck width near Locs. 3, 13, and 17. In Test Run #46, both spans were loaded near Locs. 3 and 10. Results of various test runs are reported, including applied loads, vertical and lateral deflections, and stresses at critical locations. Tests that are reported were selected because they can represent the structural behavior of the system.

Figure 101. Deck reinforcement

Figure 102. Deck concrete at completion of pour

Table 22. List of test runs with non-composite deck

Test Run No.		Floor beam relative stiffness	Stringer to floor beam connection	Load location, maximum applied load	
				Location	Maximum load
57		Rigid	Bolted	Loc. 3	Approx. 80 K
45	Failure 1		Unbolted	Loc. 3	Up to maximum
	Failure 2			Locs. 3, 13 & 17	Up to maximum
	Failure 3			Loc. 10	Up to maximum
46		Rigid	Unbolted	Locs. 3 and 10	Up to maximum
81		Flexible	Bolted	Loc. 3	Approx. 80 K
69			Unbolted	Loc. 3	Approx. 80 K

Test Run #57

Test Run #57 is reported first because it was the first test in Group IV and it served as a baseline for comparison purpose. It included a stiff floor beam and stringer bottom flanges were bolted to the floor beam. A vertical load up to approximately 80 kips was applied at midspan of the interior stringer. Figure 103 details how load was applied and Figure 104 shows measured load-vertical deflection plots at Locs. 3 and 10. Load-lateral deflection plots are illustrated in Figure 105 and results indicate that the lateral deflections are minimal. Load-normal stress plots for each strain gauge location at Locs. 3, 6, and 7 are shown in Figure 106 to Figure 117 and results indicate that the stresses attributable to the out-of-plane bending and warping torsion are negligible. Each figure plots total stresses calculated from the gauge readings and various stress components discussed in the aforementioned section.

Figure 103. Test Run #57 load application

Figure 104. Test #57 applied load vs. measured vertical deflections, Locs. 3 and 10

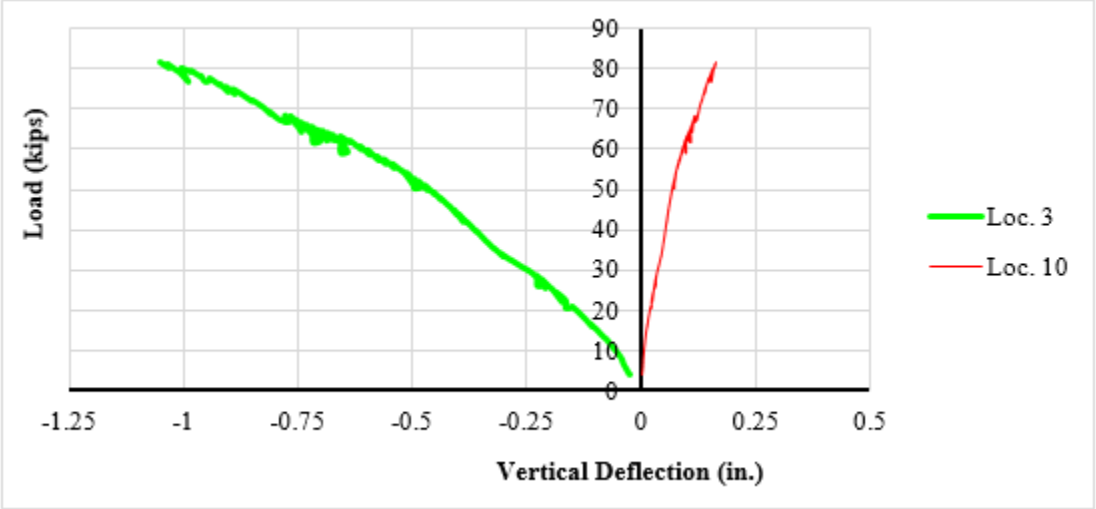

Figure 105. Test #57 applied load vs. measured lateral deflections, Locs. 3 and 10

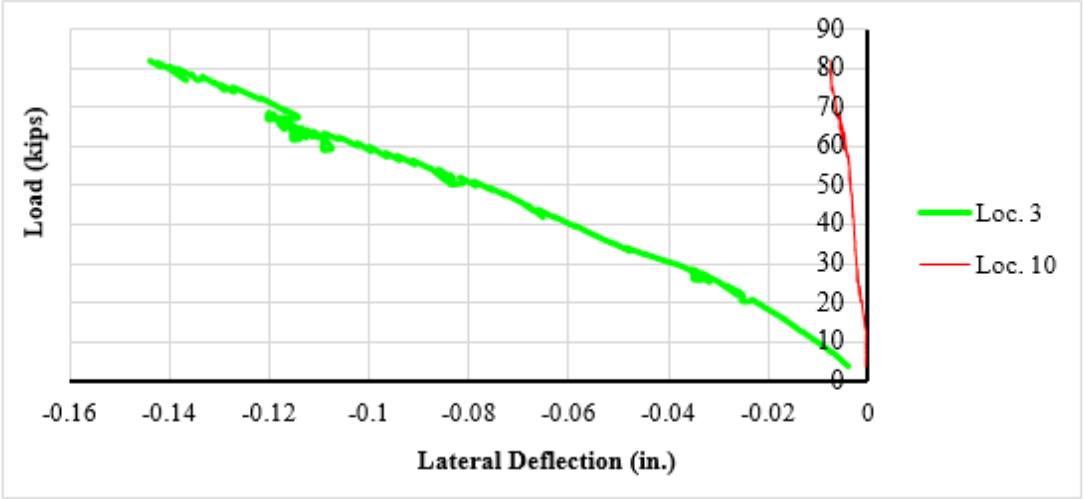

Figure 106. Test #57 applied load vs. normal stresses, Loc. 3 TN

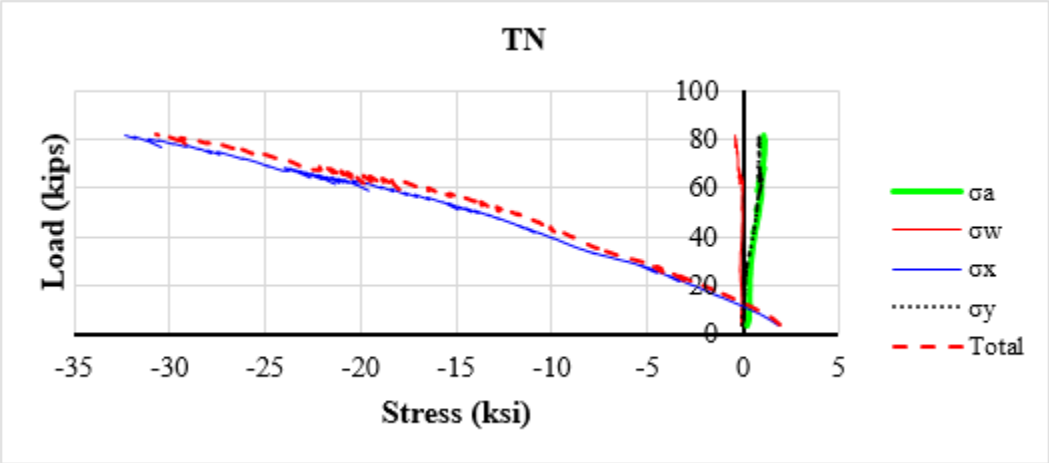

Figure 107. Test #57 applied load vs. normal stresses, Loc. 3 TS

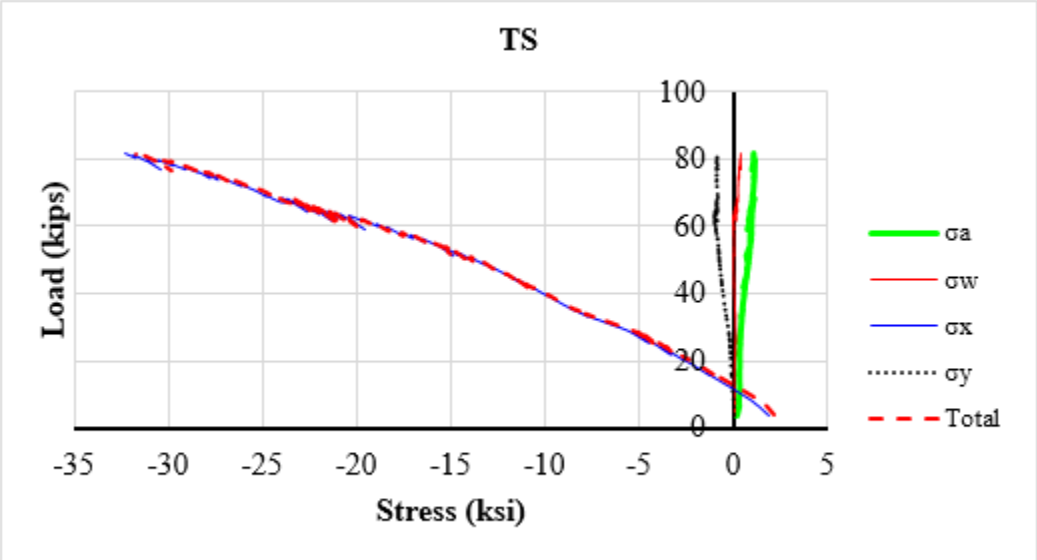

Figure 108. Test #57 applied load vs. normal stresses, Loc. 3 BN

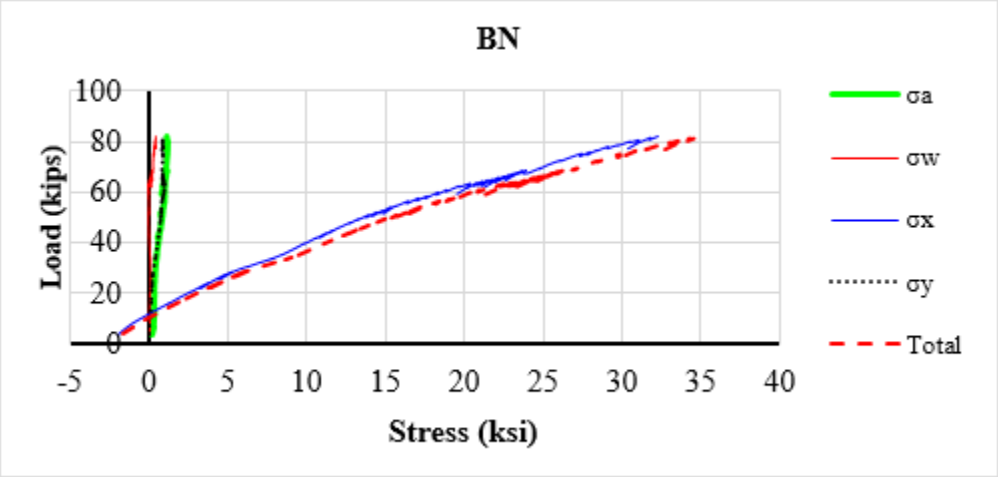

Figure 109. Test #57 applied load vs. normal stresses, Loc. 3 BS

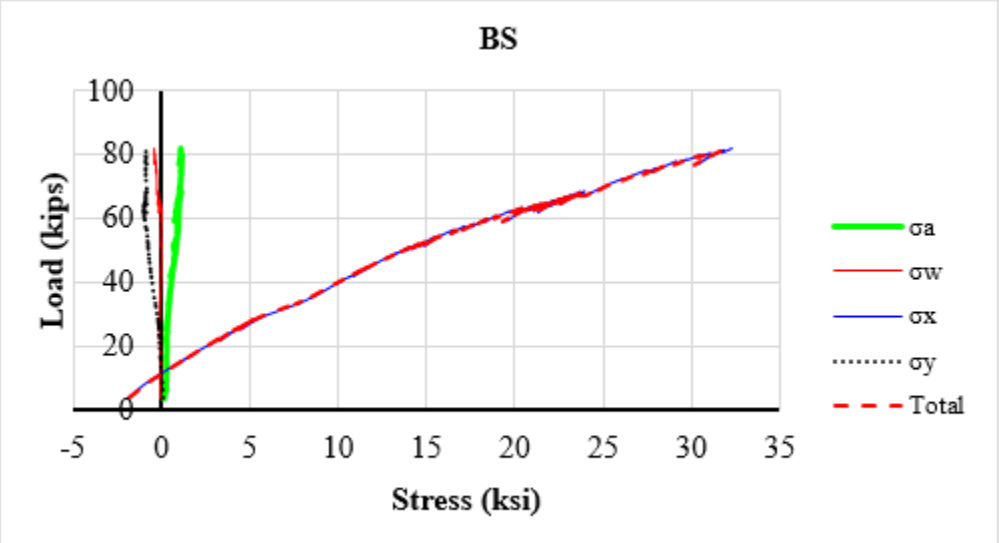

Figure 110. Test #57 applied load vs. normal stresses, Loc. 6 TN

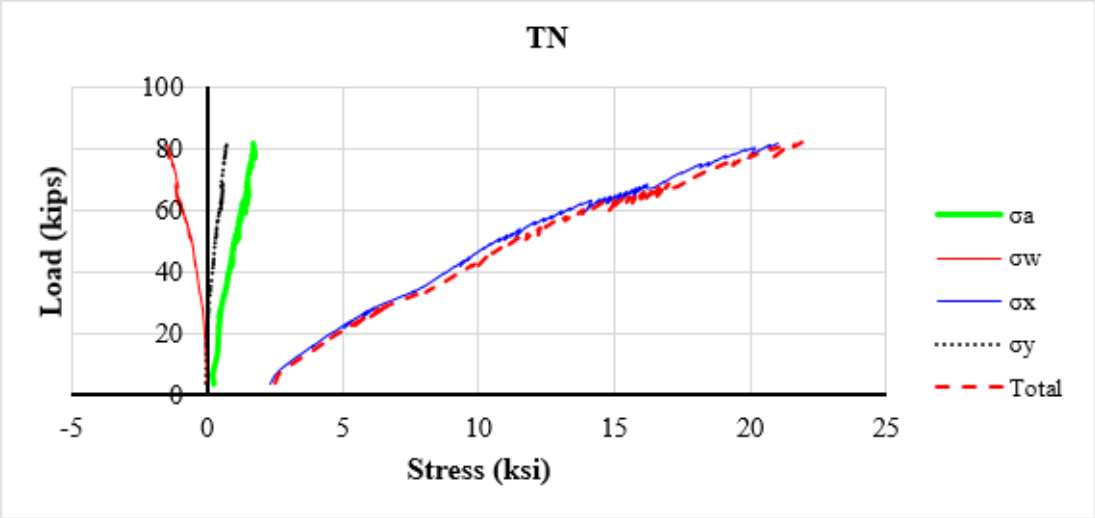

Figure 111. Test #57 applied load vs. normal stresses, Loc. 6 TS

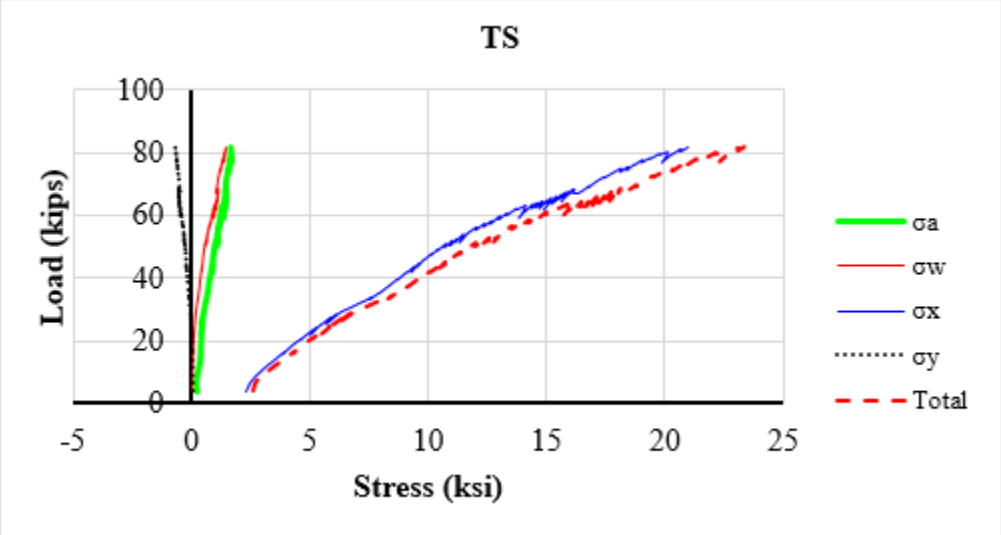

Figure 112. Test #57 applied load vs. normal stresses, Loc. 6 BN

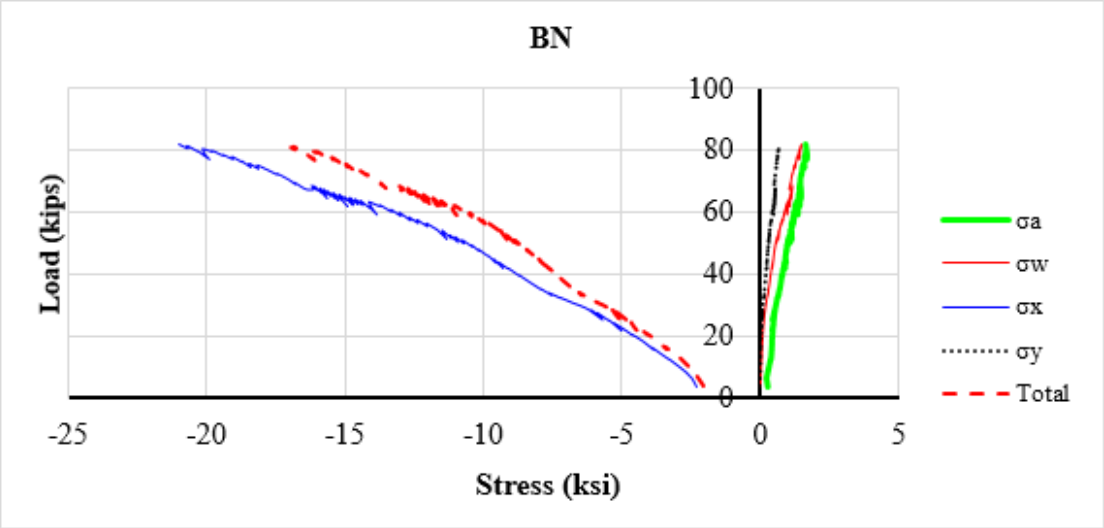

Figure 113. Test #57 applied load vs. normal stresses, Loc. 6 BS

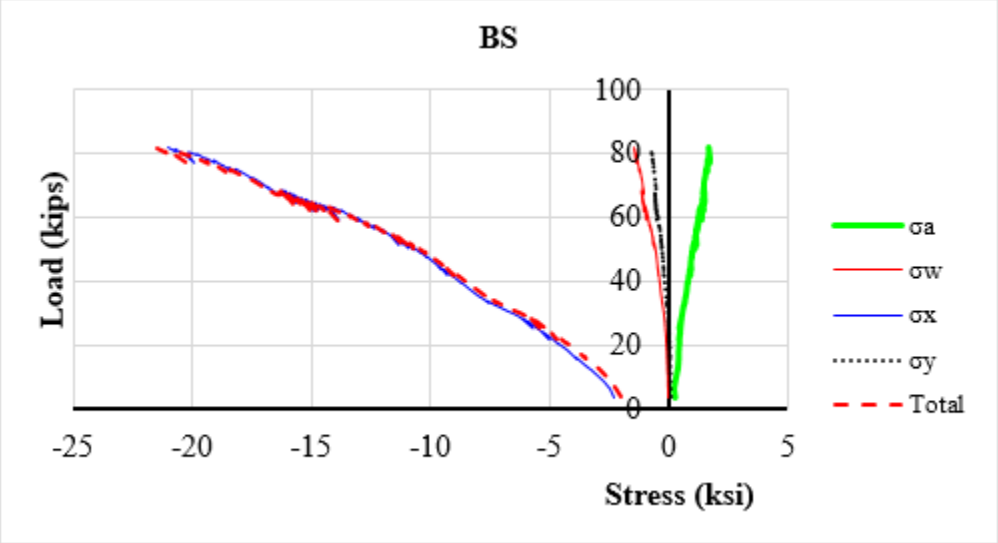

Figure 114. Test #57 applied load vs. normal stresses, Loc. 7 TN

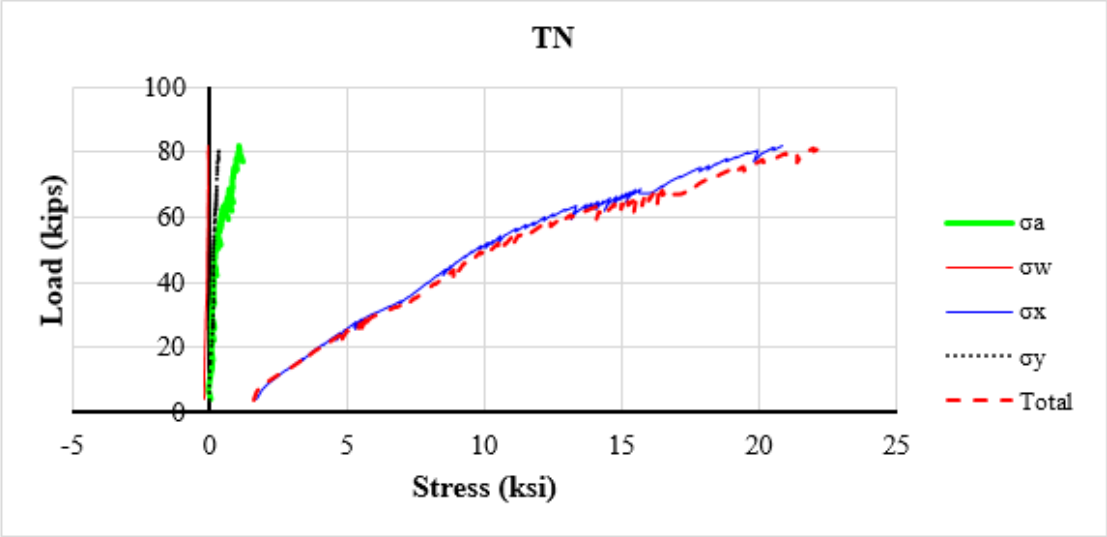

Figure 115. Test #57 applied load vs. normal stresses, Loc. 7 TS

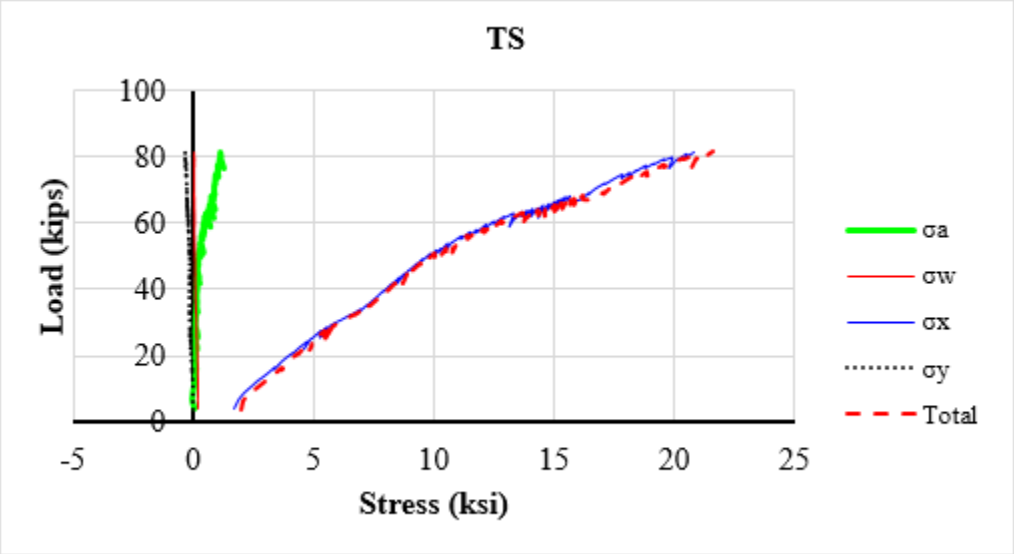

Figure 116. Test #57 applied load vs. normal stresses, Loc. 7 BN

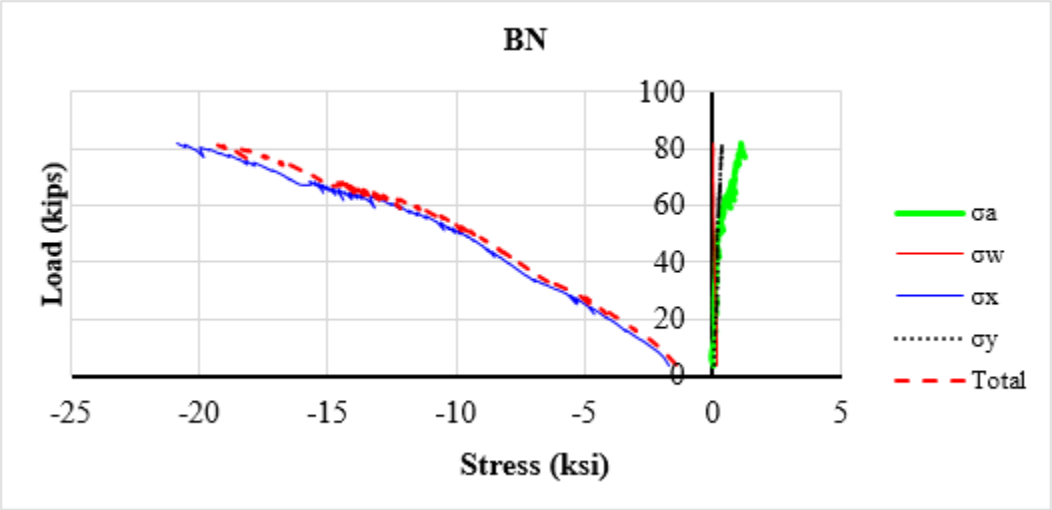

Figure 117. Test #57 applied load vs. normal stresses, Loc. 7 BS

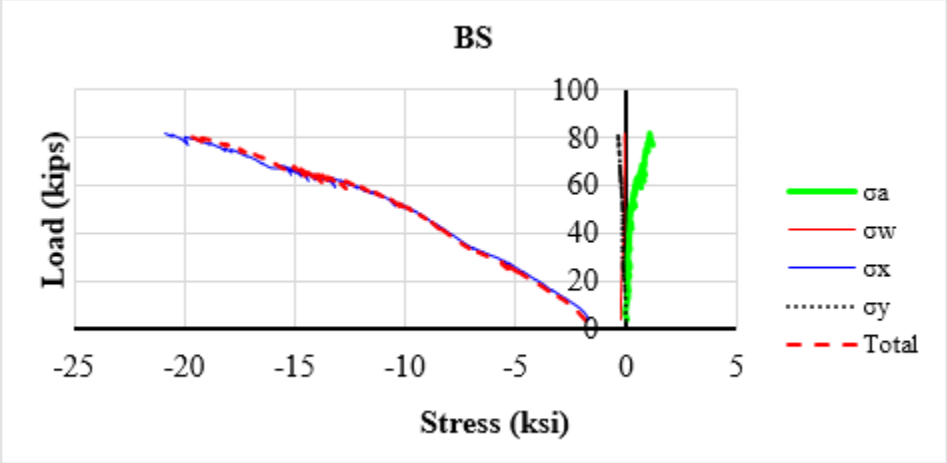

Comparison among Test Runs #57, 45, 81, and 69 Data

Test Runs #57, 45 (Failure 1), 81, and 69 were loaded at Loc. 3 and accounted for various floor beam relative stiffness and stringer to floor beam connection conditions (Table 23). Load-vertical deflection, load-lateral deflection, and load-stress plots at critical locations were compared for these test runs to an applied load up to approximately 80 kips. These comparisons are completed to study the effects due to the floor beam relative stiffness and stringer to floor beam connection conditions (Figure 118 to Figure 127). As predicted, maximum vertical deflections increased substantially with a flexible floor beam. Tests where stringers were not bolted to the floor beam produced slightly increased maximum vertical deflections when compared to bolted cases, irrespective of floor beam

relative stiffness. Figure 128 to Figure 130 provide strain diagrams at interior stringer Locs, 3, 6, and 7 at a load of around 80 kips. It can be observed that neutral axis locations remain constant for the tests. Strains at the stringer top and bottom flanges are not entirely the same, indicating existence of small axial strains as result of possible friction between the stringers and deck.

Table 23. Test Run #57, 45, 81, and 69

Test Run No.	Floor beam relative stiffness	Stringer to floor beam connection
57	Rigid	Bolted
45		Unbolted
81	Flexible	Bolted
69		Unbolted

Figure 118. Applied load vs. measured vertical deflections, Test Run #57, 45, 81, and 69, Locs. 3 and 10

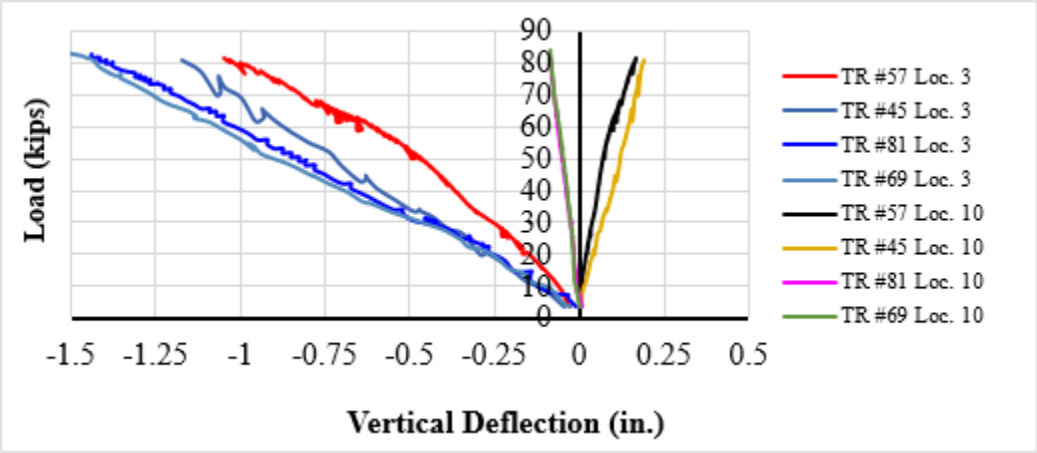

Figure 119. Applied load vs. measured lateral deflections, Test Run #57, 45, 81, and 69, Locs. 3 and 10

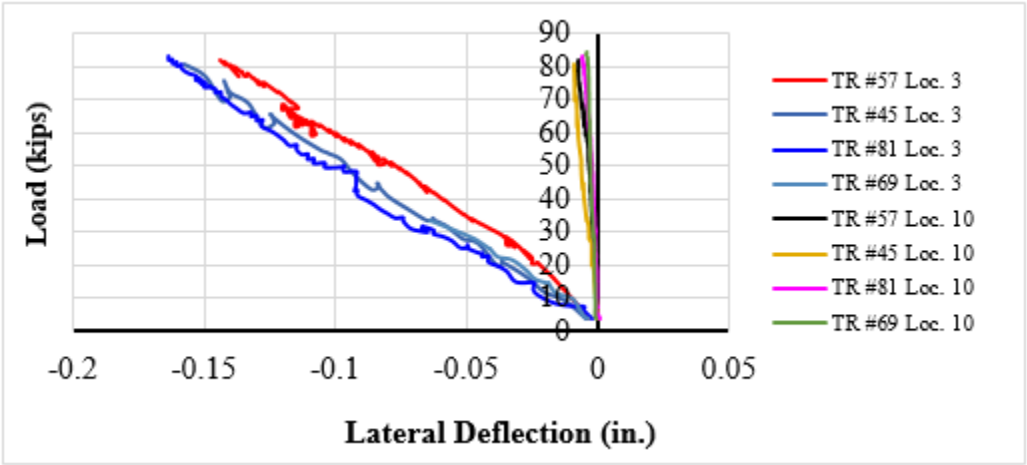

Note: Lateral deflection of TR #69 at Loc. 3 not recorded after load exceeded 33.4 kips, LVDT slipped.

Figure 120. Load-strain plots, Test Run #57, 45, 81, and 69, Loc. 3 TN and TS (load at Loc. 3)

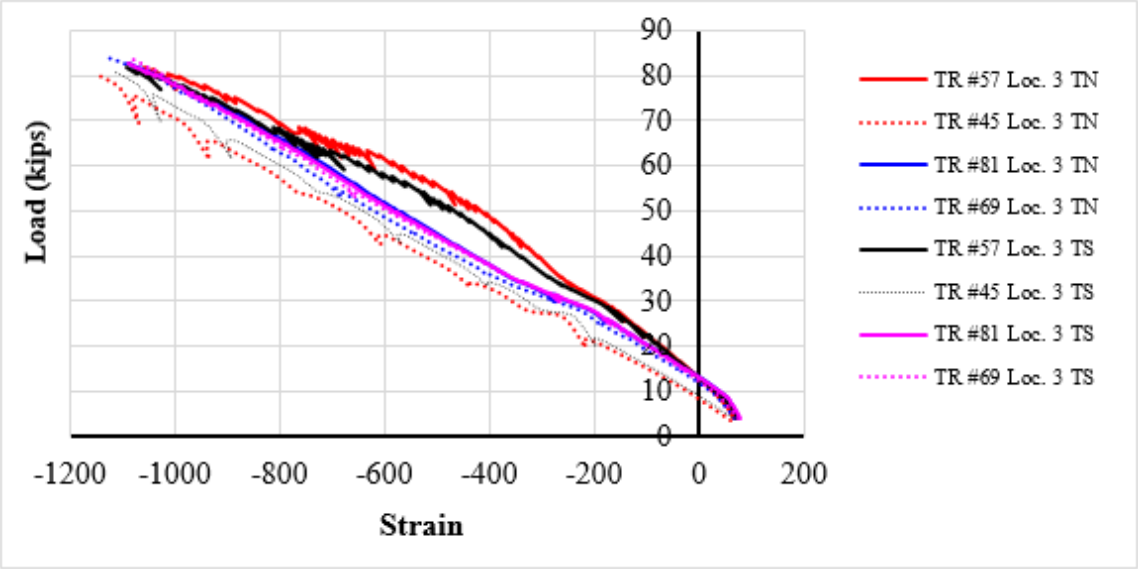

Figure 121. Load-strain plots, Test Run #57, 45, 81, and 69, Loc. 3 BN and BS (load at Loc. 3)

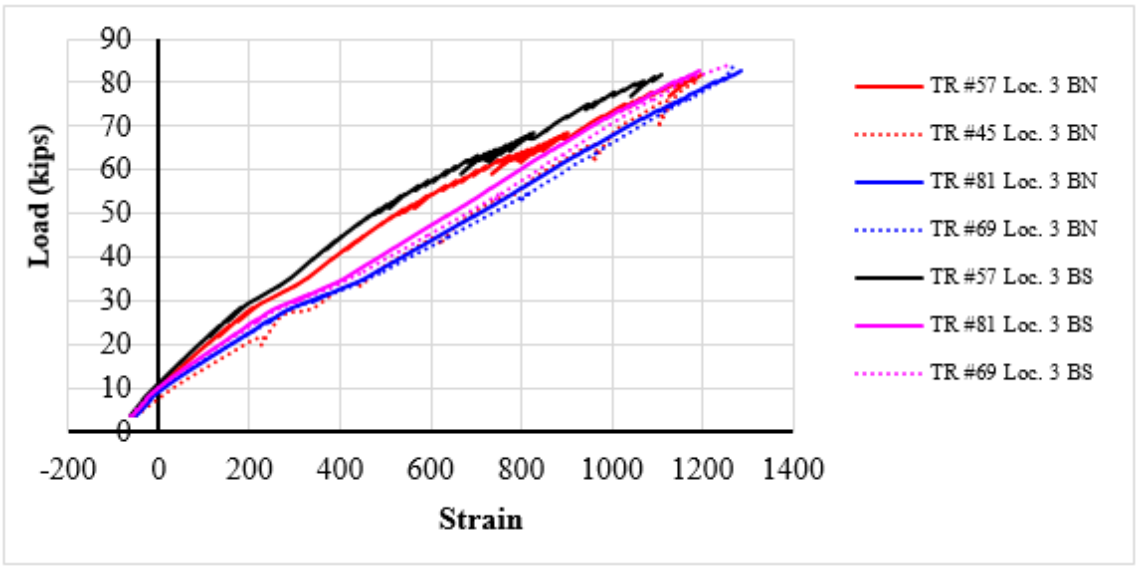

Figure 122. Load-strain plots, Test Run #57, 45, 81, and 69, Loc. 6 TN and TS (load at Loc. 3)

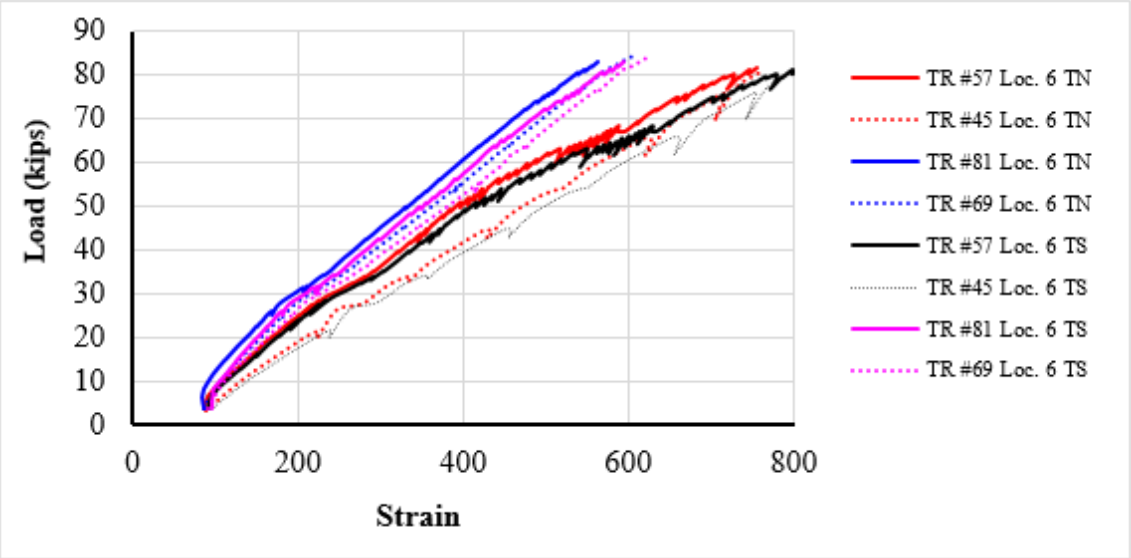

Figure 123. Load-strain plots, Test Run #57, 45, 81, and 69, Loc. 6 BN and BS (load at Loc. 3)

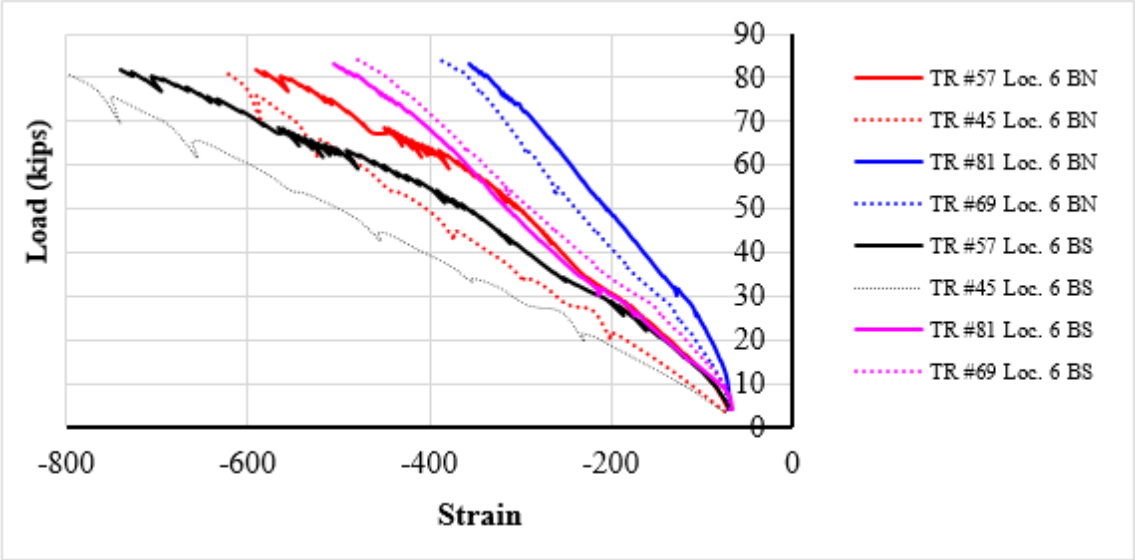

Figure 124. Load-strain plots, Test Run #57, 45, 81, and 69, Loc. 7 TN and TS (load at Loc. 3)

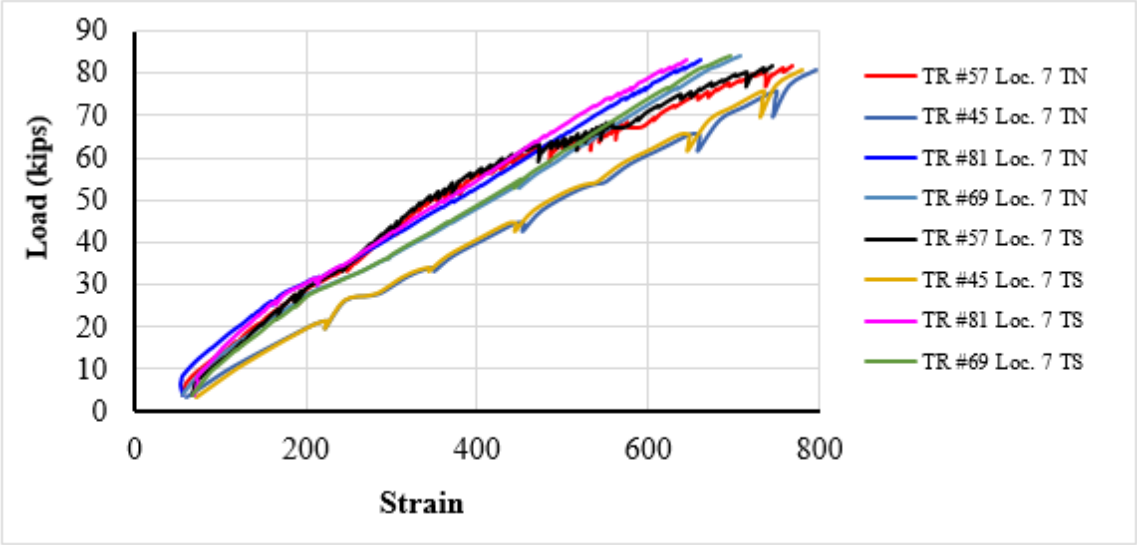

Figure 125. Load-strain plots, Test Run #57, 45, 81, and 69, Loc. 7 BN and BS (load at Loc. 3)

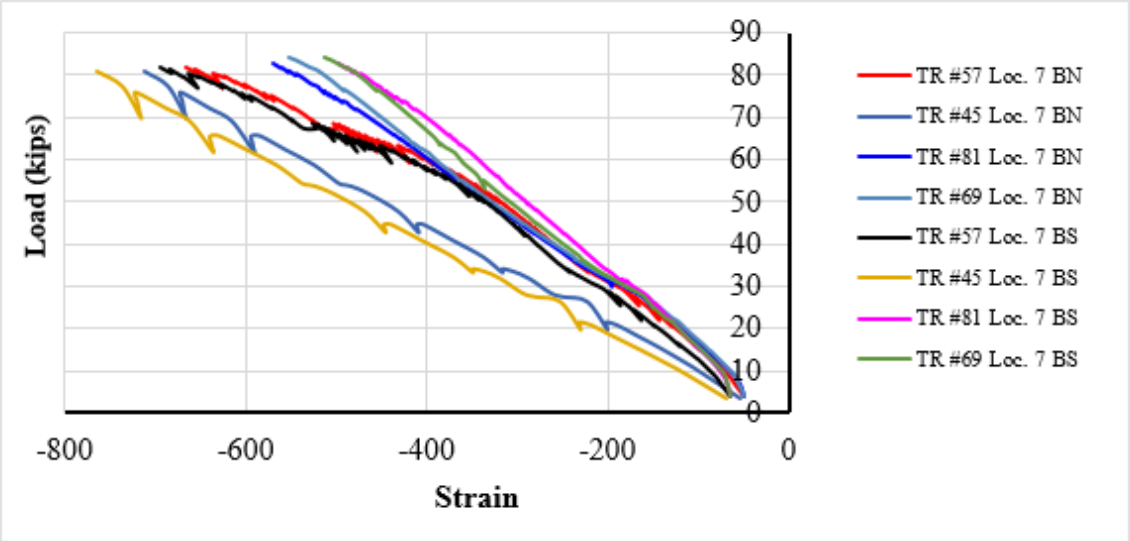

Figure 126. Load-strain plots, Test Run #57, 45, 81, and 69, Loc. 10 TN and TS (load at Loc. 3)

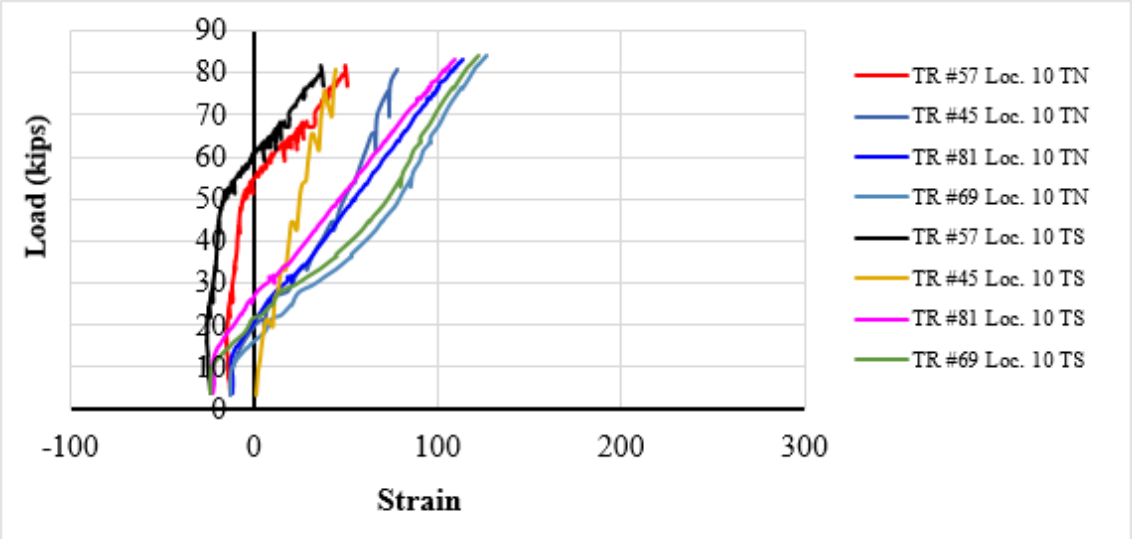

Figure 127. Load-strain plots, Test Run #57, 45, 81, and 69, Loc. 10 BN and BS (load at Loc. 3)

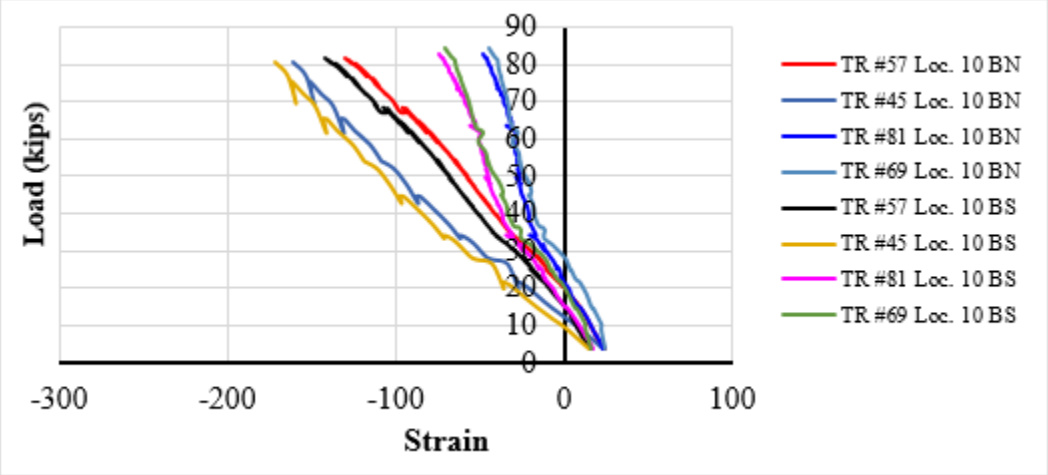

Figure 128. Strain distribution at Loc. 3 due to 80 kips (load at Loc. 3)

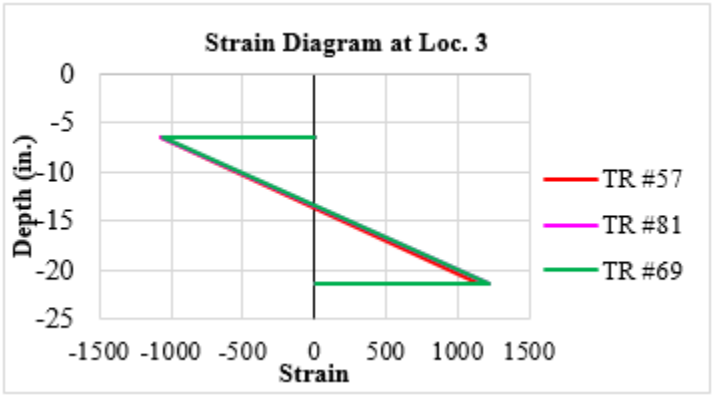

Figure 129. Strain diagrams at Loc. 6 due to 80 kips (load at Loc. 3)

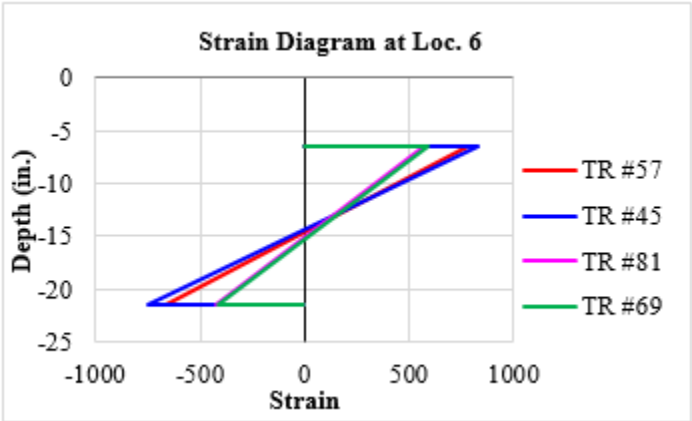

Figure 130. Strain diagrams at Loc. 10 due to 80 kips (load at Loc. 3)

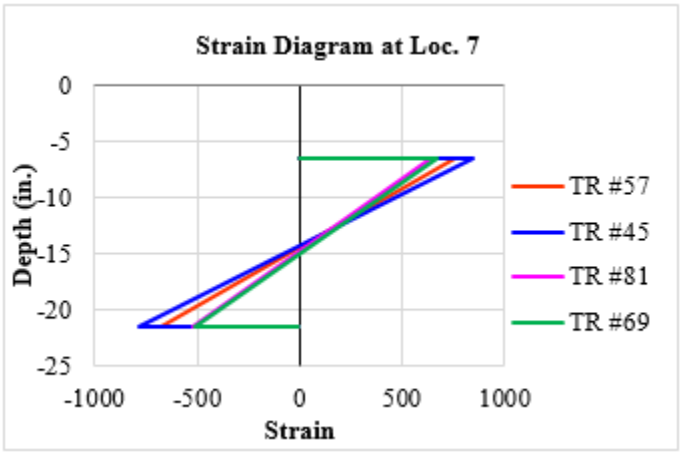

A diagram of the primary bending moment, M_x, including the deck and spreader beam weights, is plotted at an applied load of 80 kips in Figure 131. Interior stringer vertical bending moments, M_x, were determined from measures strains at critical sections along the stringer and compared to elastic analysis from RISA-3D at this applied load level. These comparisons were completed to study the effect of the floor beam relative stiffness and stringer to floor beam connection conditions. Findings indicate that, in addition to the analyses results nearly matching measured values:

1. Strains and M_x in Test Run #45 (rigid/unbraced) are noticeably larger than Test Run #57 (rigid/braced).
2. Strains and M_x in Test Run #69 (flexible/unbraced) are slightly larger than Test Run #81 (flexible/braced) under the same loading.
3. Maximum positive M_x in Test Run #81 (flexible/braced) are larger than Test Run #57 (rigid/braced) under the same loading. Similarly, maximum negative M_x in Test Run #81 (flexible/braced) are smaller than Test Run #57 (rigid/braced) under the same loading.
4. Nearly same M_x is observed in Test Run #81 (flexible/braced) and Test Run #69 (flexible/unbraced).

Figure 131. Measured and modeled interior stringer M_x diagrams at an applied load of 80 kips

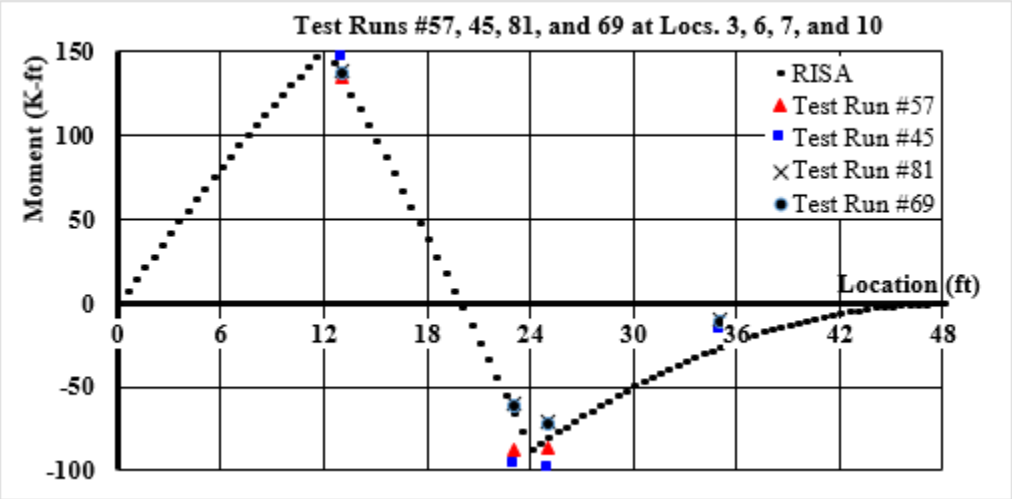

Test Run #45 Failure 3 (Load at Loc. 10)

This test run was conducted by applying a vertical load at Loc. 10. Figure 132 shows load location and a plan view of the test is illustrated in Figure 133. The load-vertical deflection and load-lateral deflection plots are shown at Locs. 3 and 10 in Figure 134 and Figure 135, respectively. Figure 136 to Figure 139 illustrate the load-stress plots at Loc. 10, including the total stress and stress components at various gauge locations such as TN, TS, BN, and BS. Similar plots are provided in Figure 140 to Figure 143 for Loc. 7 and in Figure 144 to Figure 147 for Loc. 6. The total stress at each location is nearly the same as the primary bending stress, indicating that the weak-axis bending and warping torsion stresses are negligible. Load-stress plots are other representative locations are presented in Appendix V. Strain diagrams at Locs. 10 and 7 subject to various loads are provided in Figure 148 and Figure 149, respectively.

Figure 132. Test Run #45 Failure 3 setup (load at Loc. 10)

Figure 133. Test Run #45 plan view

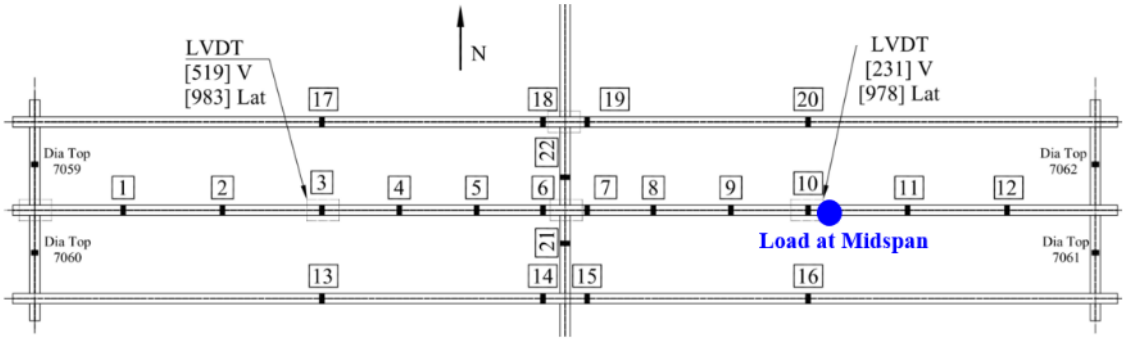

Figure 134. Test Run #45 applied load vs. measured vertical deflections, Locs. 3 and 10 (load at Loc. 10)

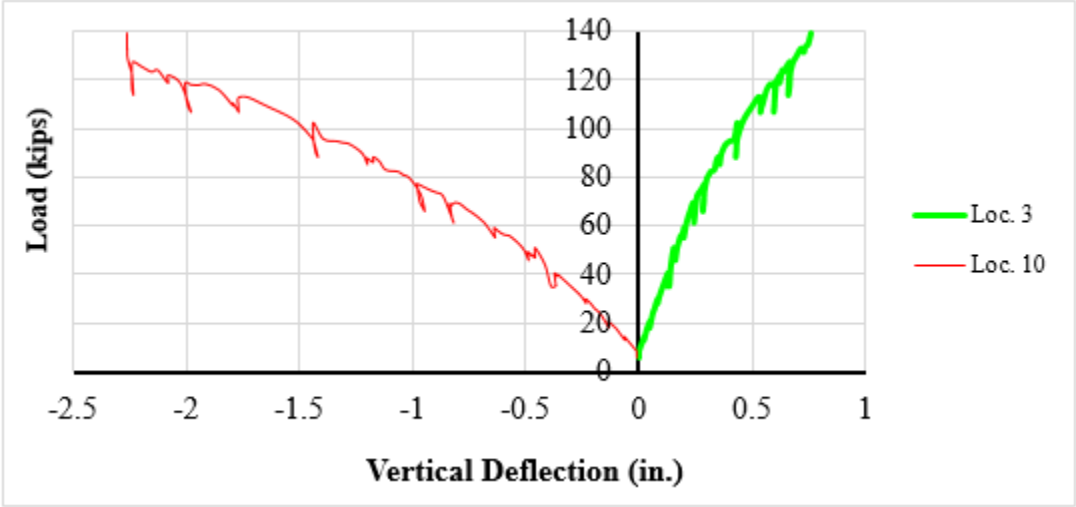

Figure 135. Test Run #45 applied load vs. measured lateral deflections, Locs. 3 and 10 (load at Loc. 10)

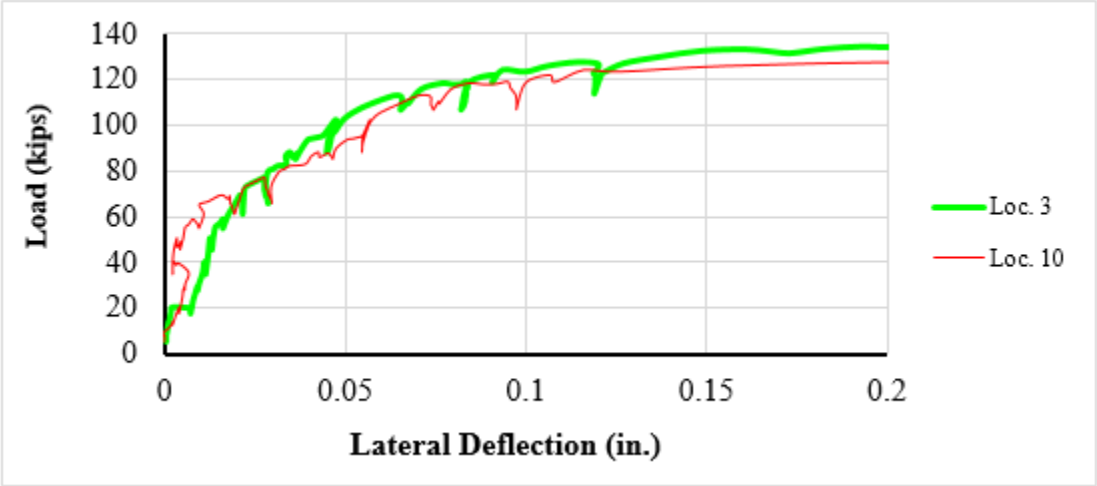

Figure 136. Test Run #45 applied load vs. normal stress components, Loc. 10 TN (load at Loc. 10)

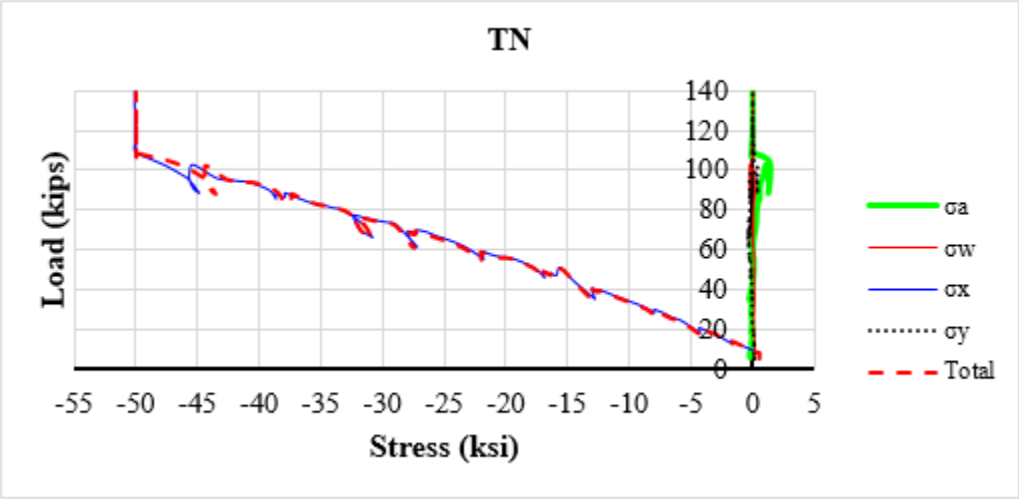

Figure 137. Test Run #45 applied load vs. normal stress components, Loc. 10 TS (load at Loc. 10)

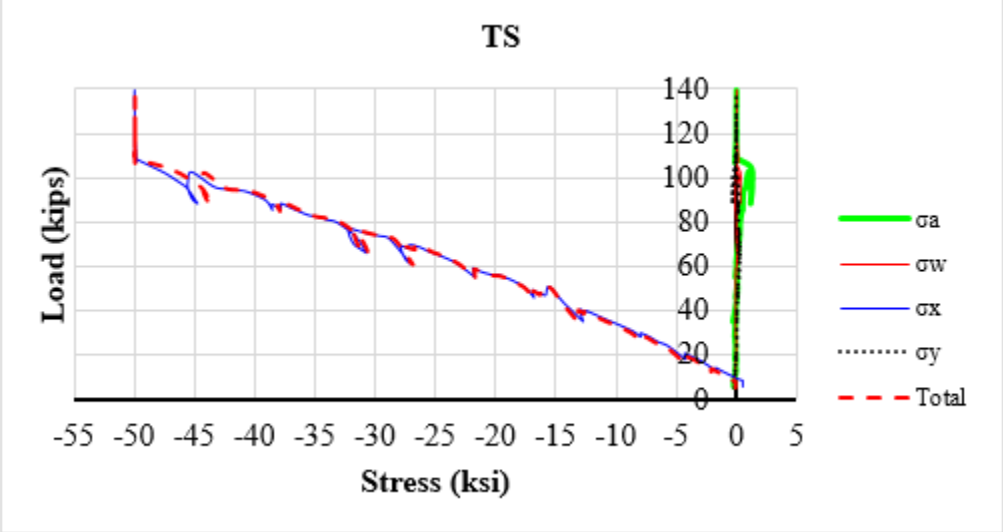

Figure 138. Test Run #45 applied load vs. normal stress components, Loc. 10 BN (load at Loc. 10)

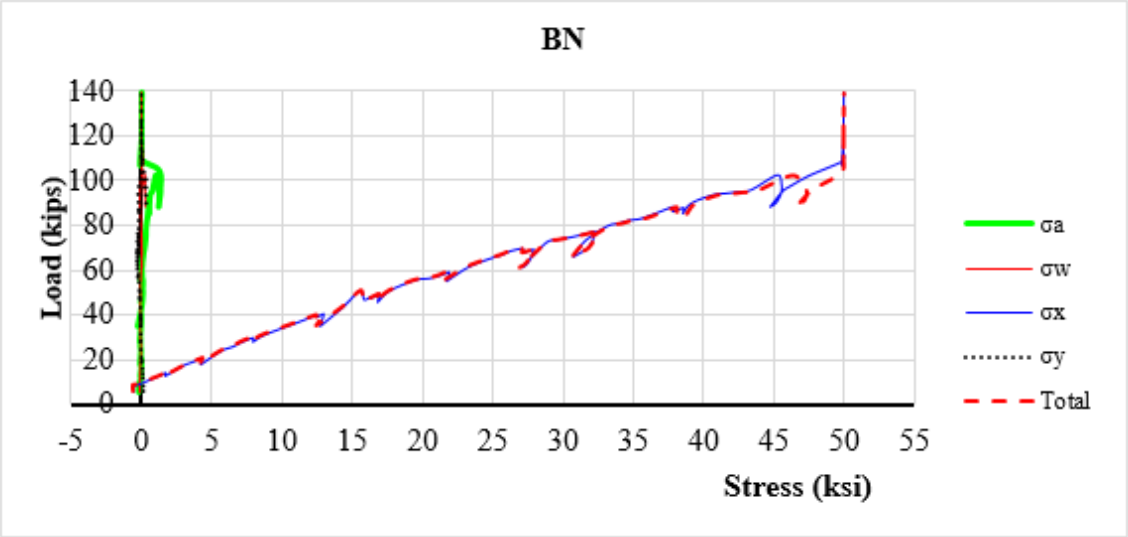

Figure 139. Test Run #45 applied load vs. normal stress components, Loc. 10 BS (load at Loc. 10)

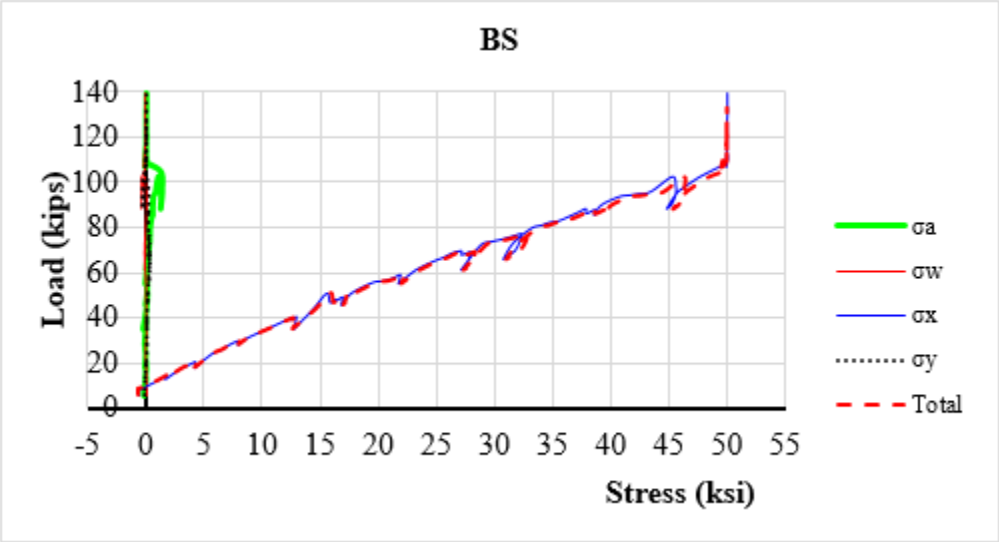

Figure 140. Test Run #45 applied load vs. normal stress components, Loc. 7 TN (load at Loc. 10)

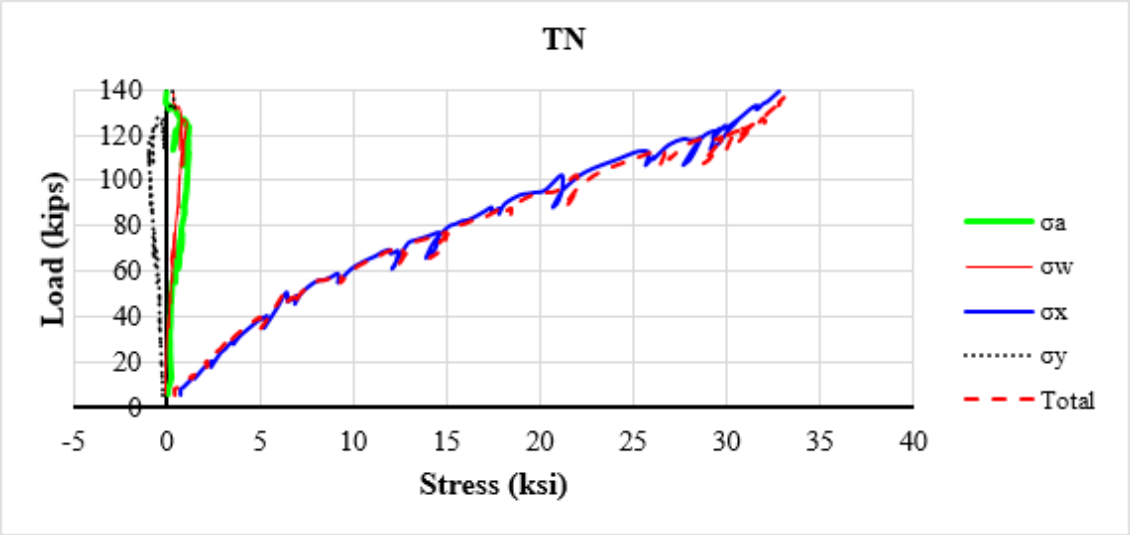

Figure 141. Test Run #45 applied load vs. normal stress components, Loc. 7 TS (load at Loc. 10)

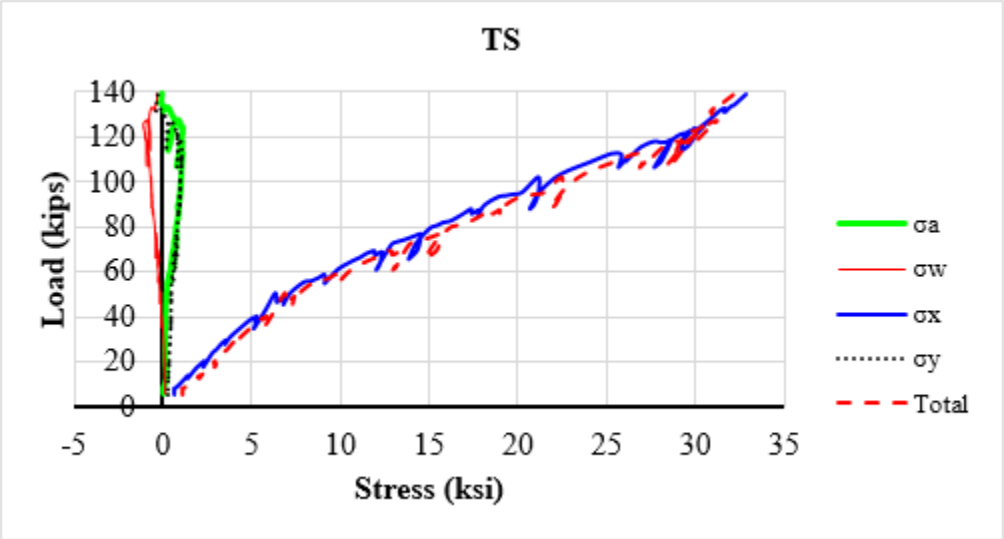

Figure 142. Test Run #45 applied load vs. normal stress components, Loc. 7 BN (load at Loc. 10)

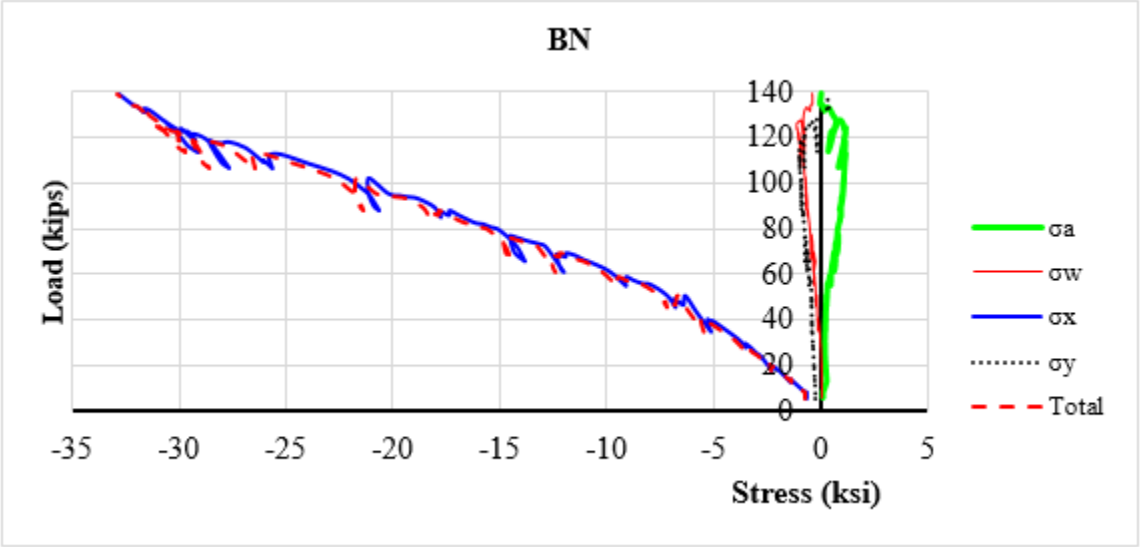

Figure 143. Test Run #45 applied load vs. normal stress components, Loc. 7 BS (load at Loc. 10)

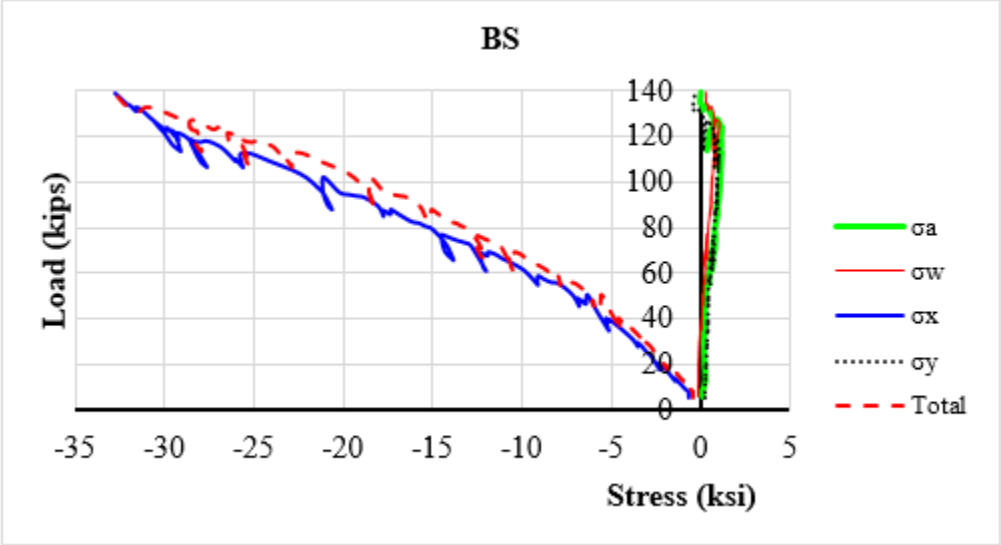

Figure 144. Test Run #45 applied load vs. normal stress components, Loc. 6 TN (load at Loc. 10)

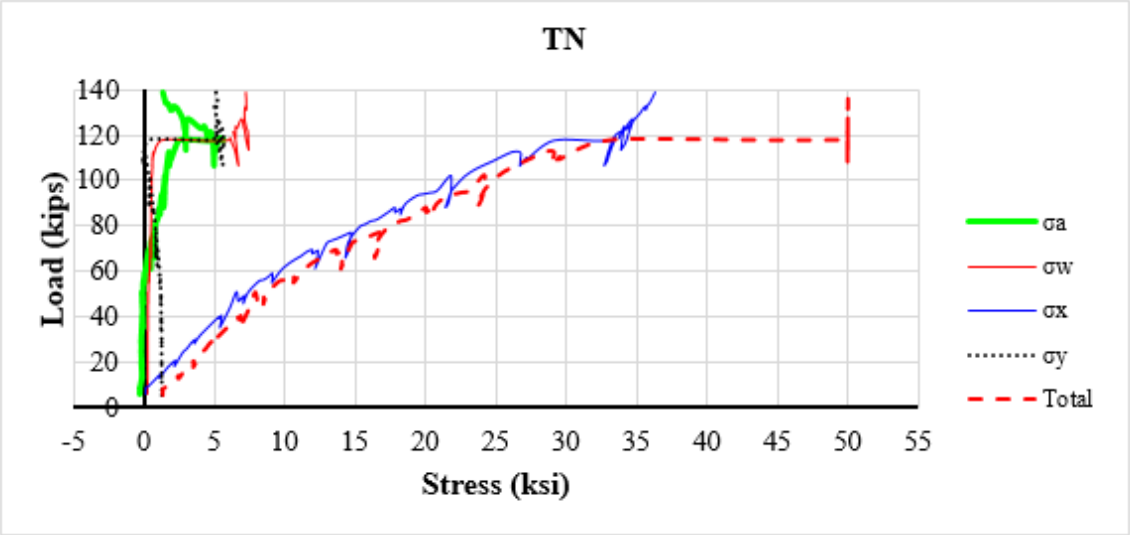

Figure 145. Test Run #45 applied load vs. normal stress components, Loc. 6 TS (load at Loc. 10)

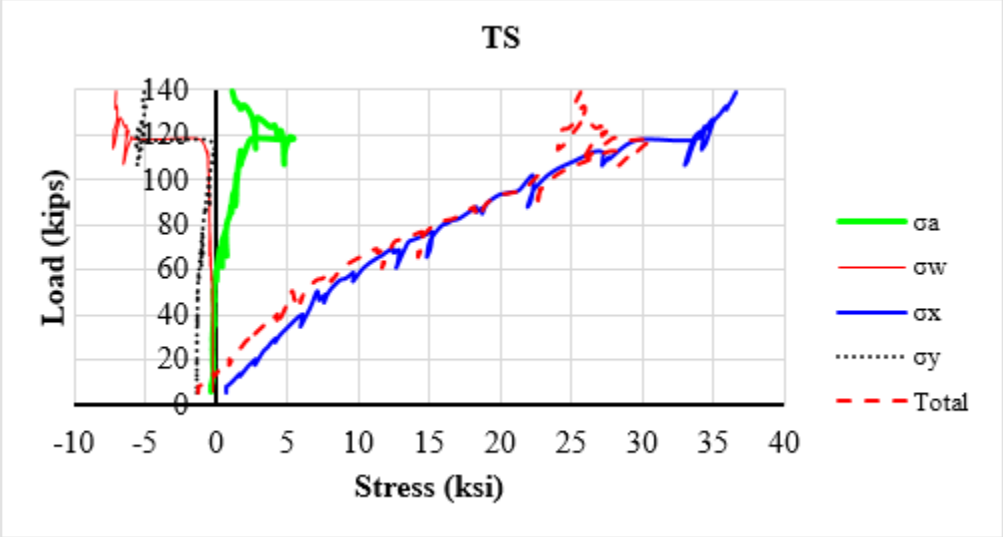

Figure 146. Test Run #45 applied load vs. normal stress components, Loc. 6 BN (load at Loc. 10)

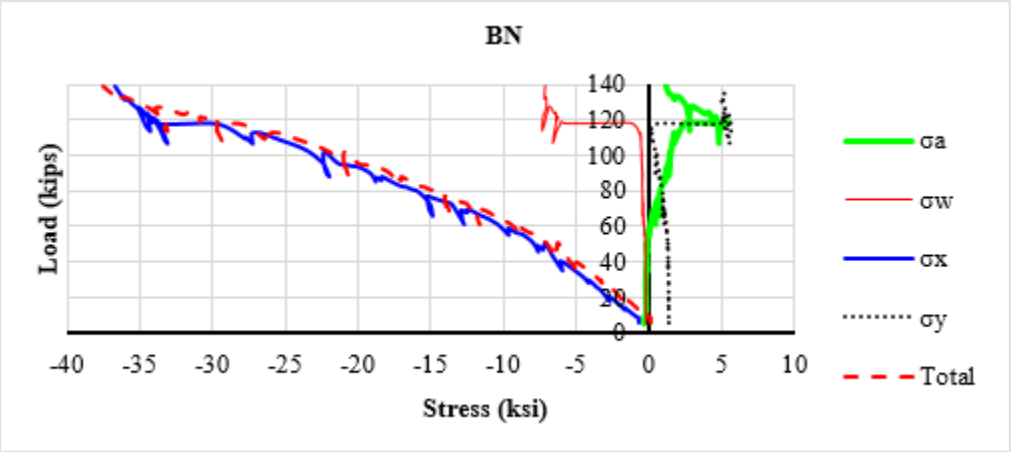

Figure 147. Test Run #45 applied load vs. normal stress components, Loc. 6 BS (load at Loc. 10)

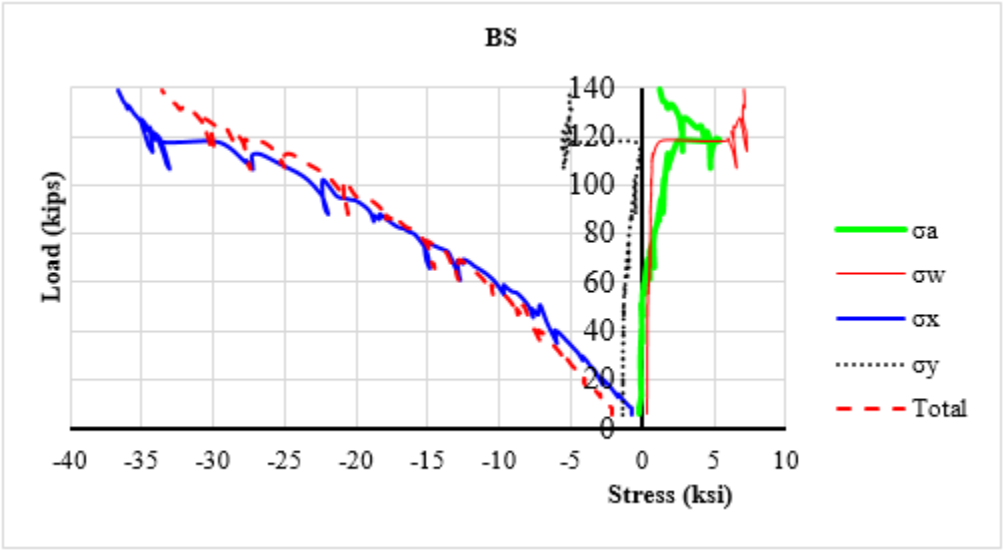

Figure 148. Strain diagram, Loc. 10 (load at Loc. 10)

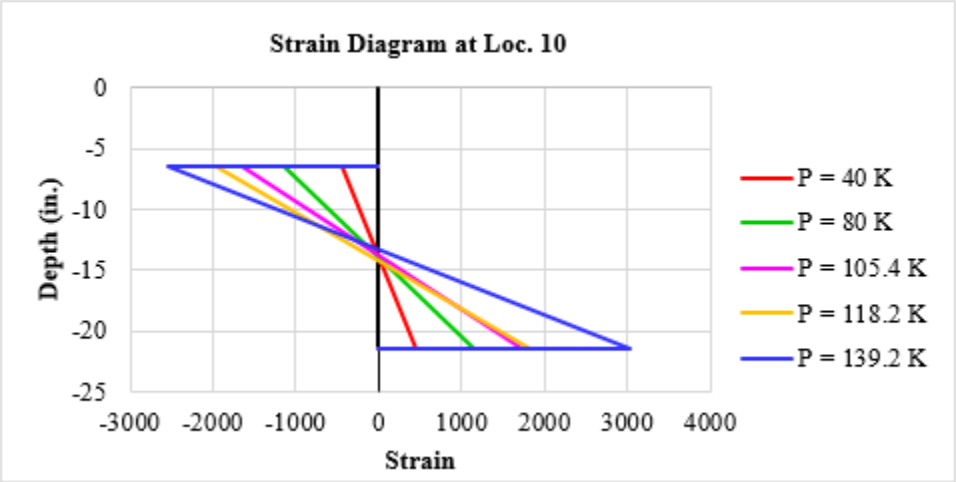

Figure 149. Strain diagram, Loc. 7 (load at Loc. 10)

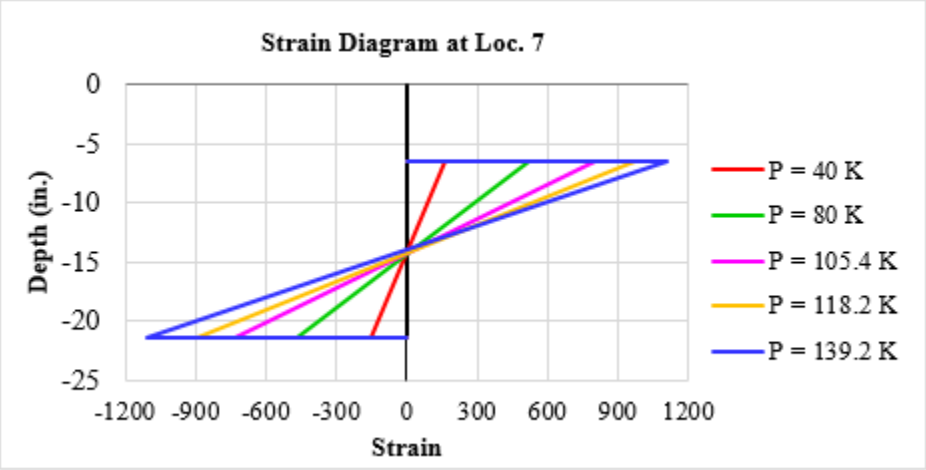

Figure 150 and Figure 151 compare primary bending moments, M_x, from RISA-3D elastic analyses and test data at applied loads of 139.2 kips (peak load) and 118.2 kips, respectively. Elastic analyses were completed assuming distribution factors of 0.36 and 0.42 at Loc. 10, respectively. Distribution factors were determined by comparing M_x at the interior stringer with that of the whole system. These figures show that M_x from the analyses largely matches M_x from the tests. When *AASHTO LRFD Bridge Design Specifications* are followed for an unbraced length of 24 ft. and a moment gradient factor of one, the flexural resistance of the stringer is 45.1 kip-ft. Calculated flexural strengths at Loc. 6 from the testing data are 151 kip-ft. and 122.9 kip-ft. at 139.2 kips and 118.2 kips, respectively (Table 24). As a result, calculated gradient factors, C_b, are 3.35 and

2.73, respectively. Because Loc. 6 exhibited LTB when the applied load reached 118.2 kips, a gradient factor of 2.73 is recommended.

Figure 150. Measured and modeled interior stringer M_x diagrams at an applied load of 139.2 kips (peak load)

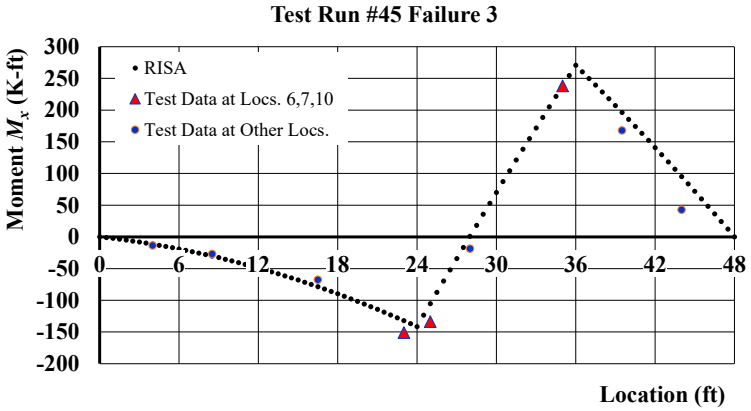

Figure 151. Measured and modeled interior stringer M_x diagrams at an applied of 118.2 kips

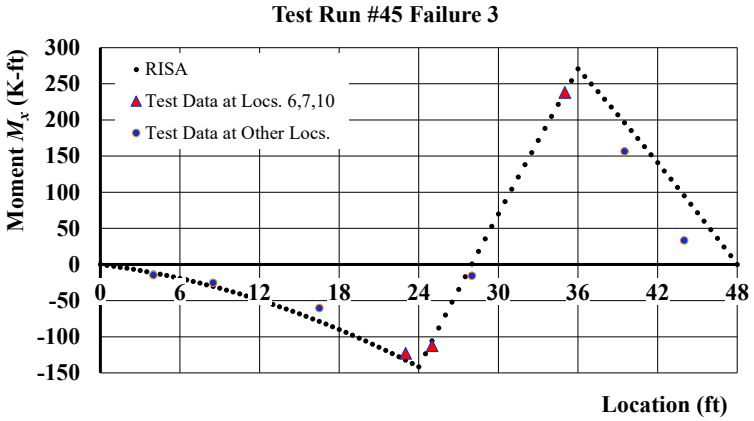

Table 24. Calculated moment gradients, Test Run #45 Failure 3

Applied load (kips)	Measured flexural strength at Loc. 6 (Kip-ft.)	Calculated gradient factor, C_b
139.2	151.0	3.35
118.2	122.9	2.73

Figure 152 depicts the exterior stringers after testing. The deck exhibited visible bending and the largest deflection occurred under the interior stringer (Figure 153). Because the deck was designed to act non-compositely, the end of the deck slipped by approximately ¼ in. longitudinally at an end support (Figure 154).

Figure 152. Exterior stringers after testing

Figure 153. Deck after testing

Figure 154. Relative slip at end support

Test Run #45 Failure 2

The vertical load was applied at midspan (near Loc. 3) across the full deck width through the spreader beam in this test run. Plots of load-vertical deflection, load-lateral deflection, and load-strain at the critical sections are provided in Appendix V. Comparison of strains near the floor beam (e.g., Locs. 7, 15, and 19 in

Figure 155 155) is provided in Figure 156 to Figure 158 among the three stringers. Stress plots between the two exterior stringers are more comparable than that of TR #45 Failure 3 because the spreader beam is in contact with the full deck width. Load distribution of the interior stringer at the midspan of the loaded span is slightly lower than that of the exterior stringers. Figure 159 shows the strain diagram at Loc. 3 in the deck and stringer, which indicates the existence of unintended friction between the stringer and deck.

Figure 155. Layout of locations for strain comparison

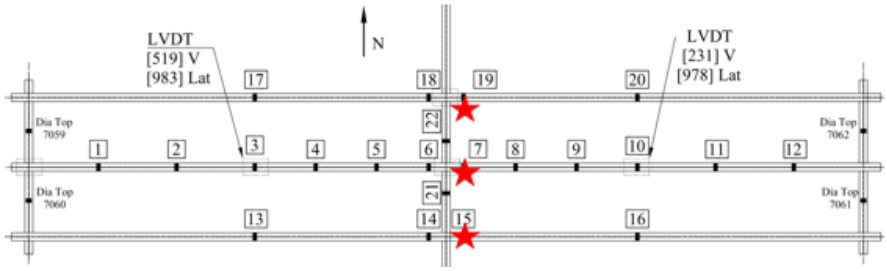

Figure 156. Comparison of strains at TN (load near Loc. 3)

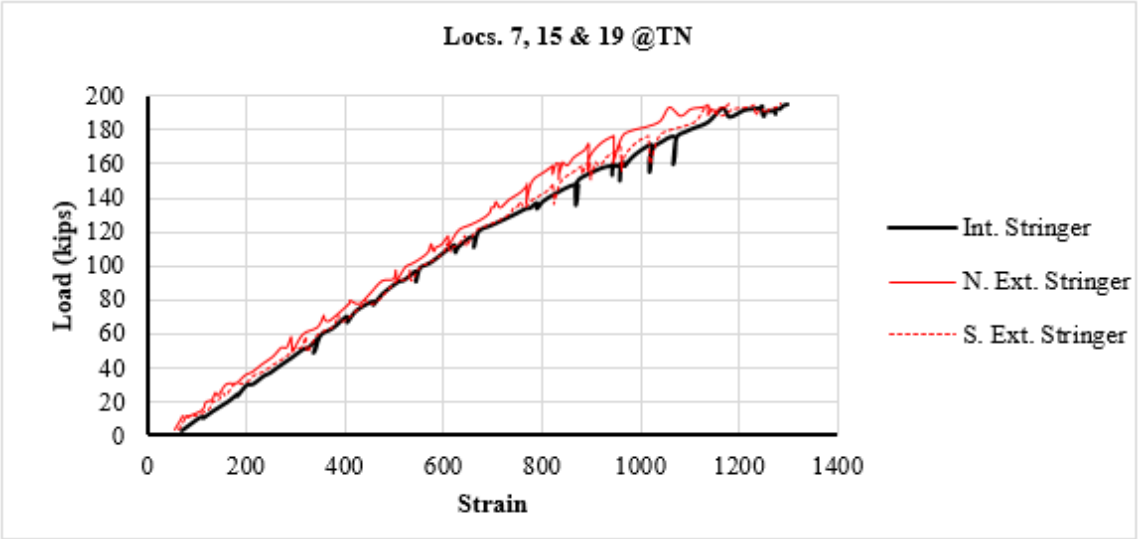

Figure 157. Comparison of strains at TS (load near Loc. 3)

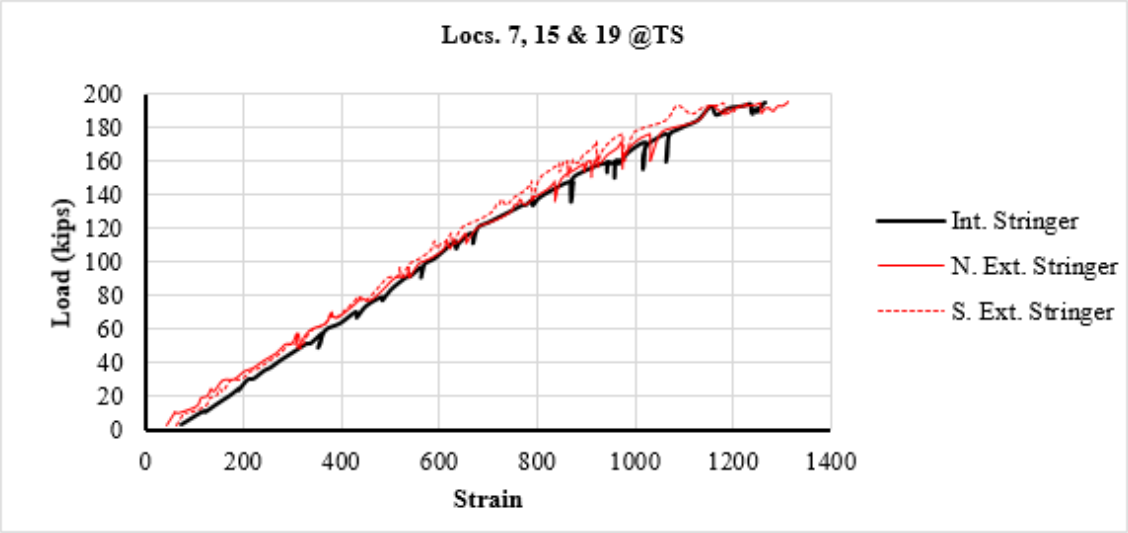

Figure 158. Comparison of strains at BN (load near Loc. 3)

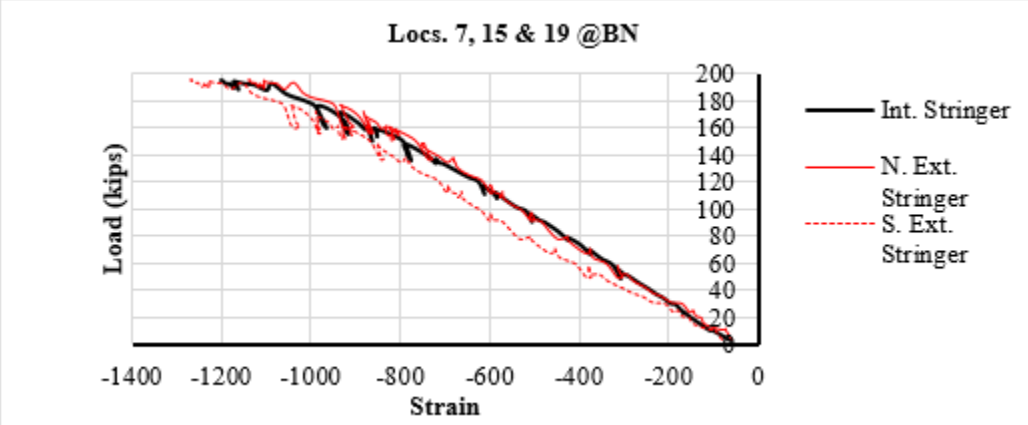

Figure 159. Strain diagram at Loc. 3 (load near Loc. 3)

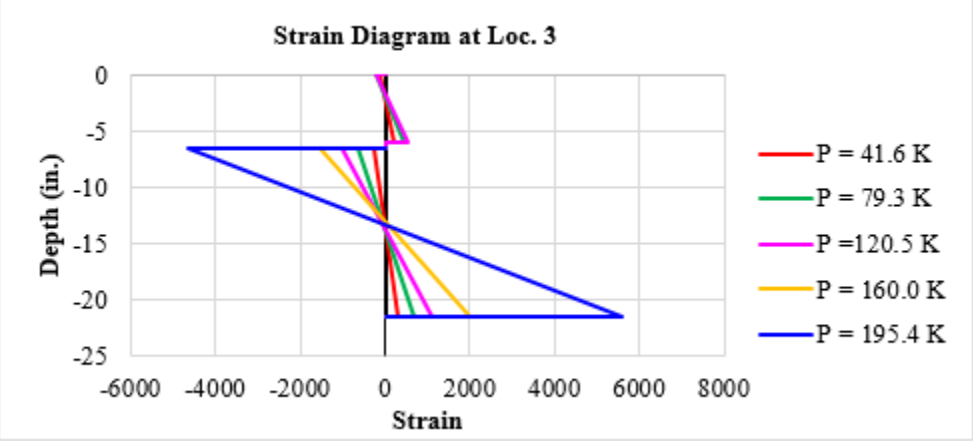

Figure **160** 160 illustrates the M_x diagram subject to an applied load of 170.1 kips using a calculated distribution factor of 0.25 per Loc. 3. The calculated flexural strength at Loc. 7 using the testing data is 116.2 Kip-ft., which corresponds to a gradient factor of C_b = 2.58.

Figure 160. Moment M_x due to an applied load of 170.1 kips

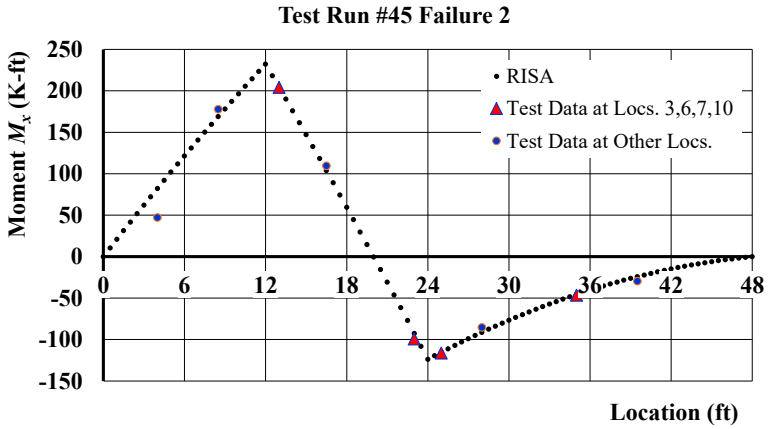

Concrete Deck Lateral Support

Lateral support provided by the non-composite concrete deck was evaluated by comparing Test Run #1, 13, and 45. Differences among the tests are summarized in Table 25. Figure 161 to Figure 166 present load-vertical deflection, load-lateral deflection, and load-longitudinal strain plots at the critical sections for these tests. A distribution factor of 0.43, determined based on the ratio of M_x in the interior stringer over M_x in the system, was used for TR #45 Failure 3. When compared to TR #1, increased capacity for TR #13 is caused by bracing provided by the intermediate diaphragm even though it is located near the contraflexure point. Lateral support provided by the non-composite deck is also apparent due to increased capacity for TR #45 Failure 3.

Photos of the deck soffit are provided in Figure 167 after TR #45 Failure 3 was completed. A number of critical locations are presented, including the interior stringer near Loc. 3, exterior stringers near Locs. 13 and 17, and interior stringer near Loc. 10. The concrete haunches (0.44 in. thick and 3 in. wide) near loading locations exhibited appreciable spalling or cracking, indicating that the concrete haunches were engaged to provide the lateral bracing effect.

Table 25. Test Run #1, 13, and 45, one span loaded

Test Run No.	Description of boundary conditions		
	Interior support at center stringer	Top flange of stringer bracing	Bottom flange of stringer bracing
1	Rigid	No deck and unbraced	Unbraced
13	Rigid	No deck and steel diaphragms @ L/8 from interior support	Unbraced
45 – Failure 3	Rigid	Non-composite concrete deck	Unbraced

Figure 161. Test Run #1, 13, and 45 applied load vs. measured vertical deflections, Locs. 3 and 10

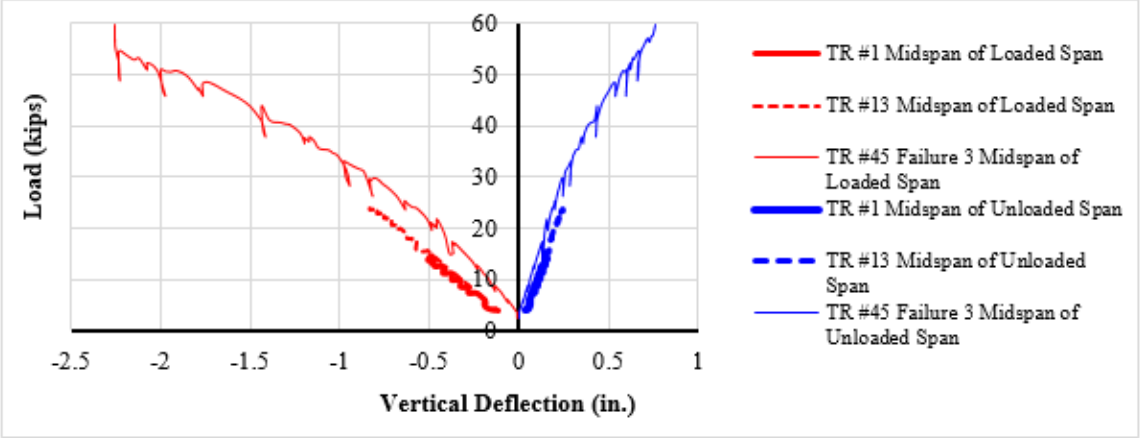

Figure 162. Test Run #1, 13, and 45 applied load vs. measured lateral deflections, Locs. 3 and 10

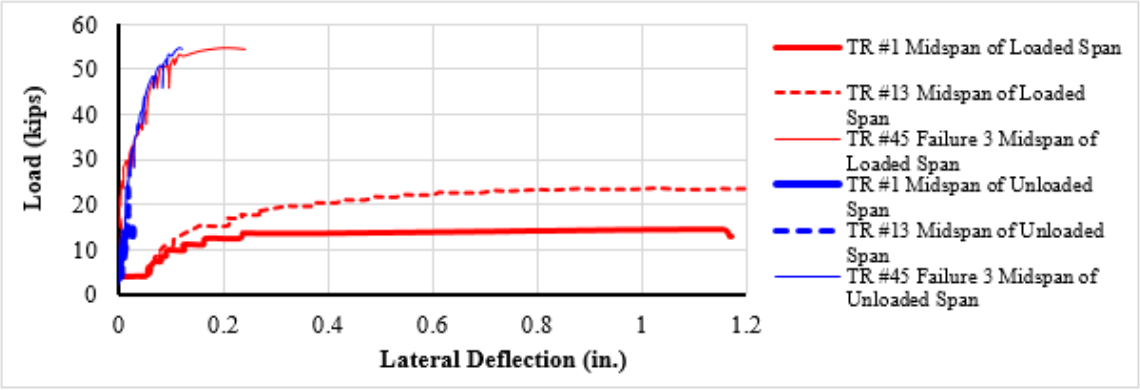

Figure 163. Test Run #1, 13, and 45 load-strain plots at stringer top, near midspan of the loaded span

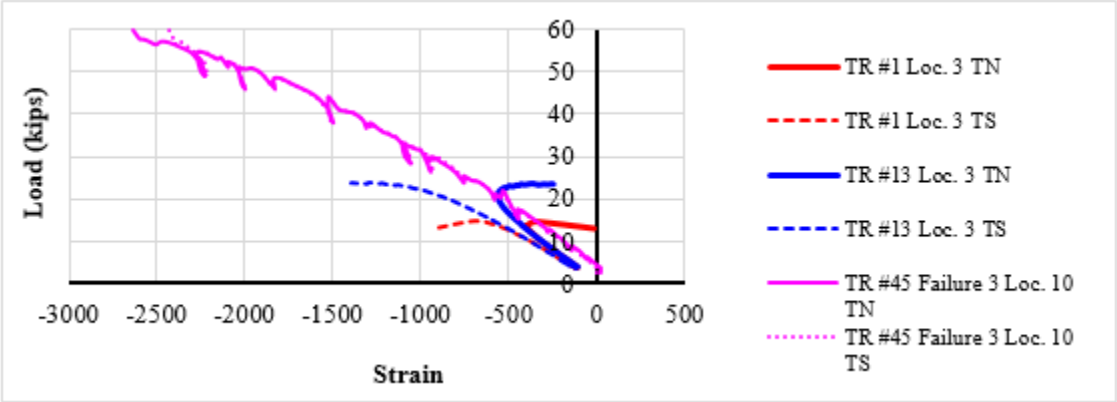

Figure 164. Test Run #1, 13, and 45 load-strain plots at stringer bottom, near midspan of the loaded span

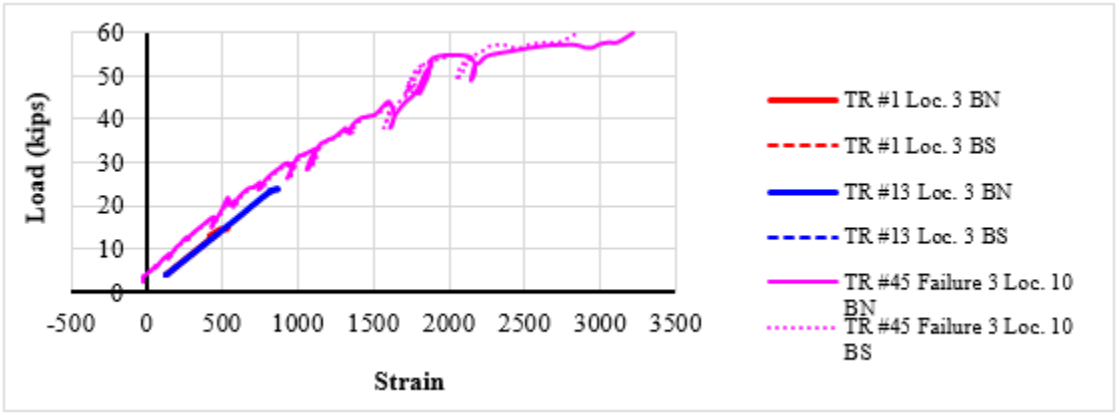

Figure 165. Test Run #1, 13, and 45 load-strain plots at stringer top, near floor beam of the unloaded span

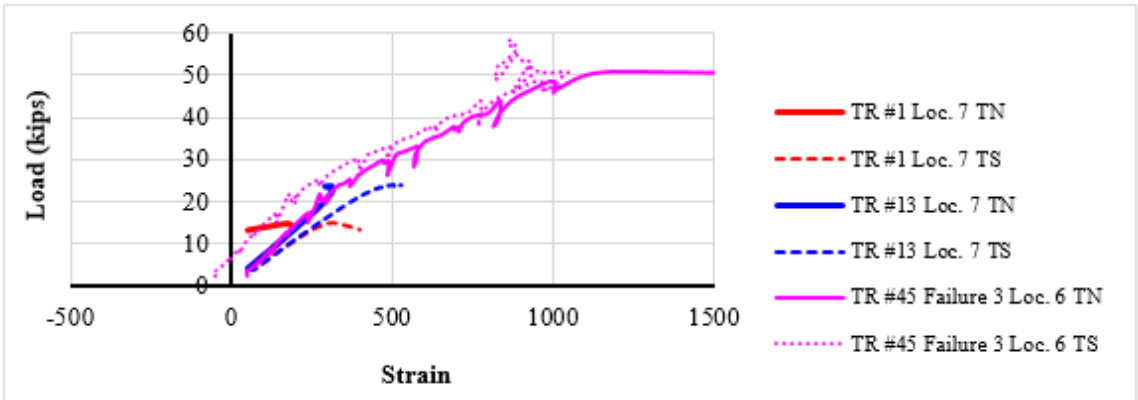

Figure 166. Test Run #1, 13, and 45 load-strain plots at stringer bottom, near floor beam of the unloaded span

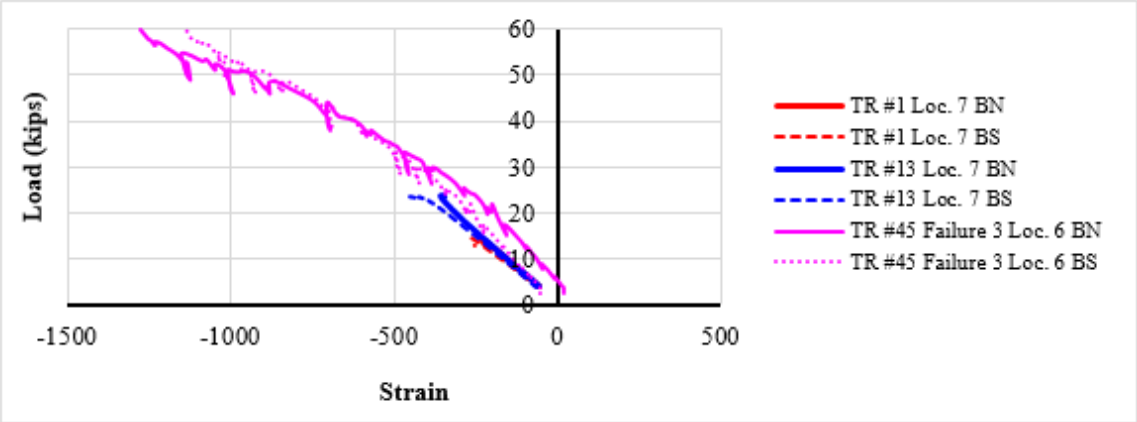

Figure 167. Deck soffit at various locations after testing

(a) Interior stringer near Loc. 3

(b) Exterior stringers near Locs. 13 &17

(c) Interior stringer near Loc. 10

FEA, Test Run #45 Failure 3 (Load near Loc. 10)

The FEA model includes the non-composite deck and can account for concrete cracking and crushing. Modeled behavior was calibrated against measured results. When a frictional coefficient of 0.1 was assumed between the stringer and deck, FEA results agreed reasonably well with test data. Figure 168 and Figure 169 are vertical deflection contours subject to a peak load of 128.1 kips in the stringers and deck, respectively. Figure 170 shows lateral deflection contours, and Figure 171 and Figure 172 present longitudinal stress contours in the stringers and deck. Comparisons between analysis and test results are provided in Figure 173 to Figure 177. Comparisons show that the FEA predicted peak load is slightly lower than that from the test, indicating that the FEA model can conservatively simulate overall behavior.

Figure 168. Stringer vertical deflection contour, Test Run #45 Failure 3

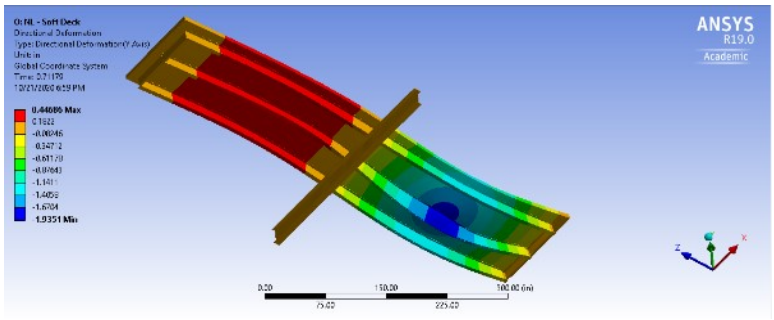

Figure 169. Deck vertical deflection contour, Test Run #45 Failure 3

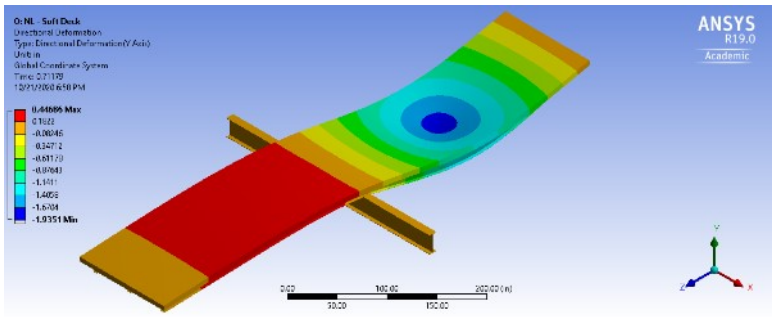

Figure 170. Lateral deflection contour, Test Run #45 Failure 3

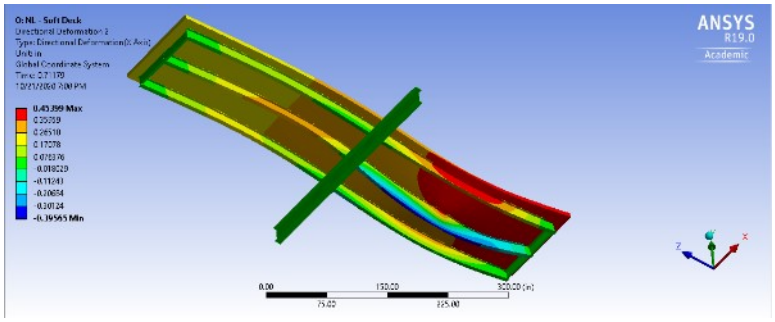

Figure 171. Stringer longitudinal normal stress contour, Test Run #45 Failure 3

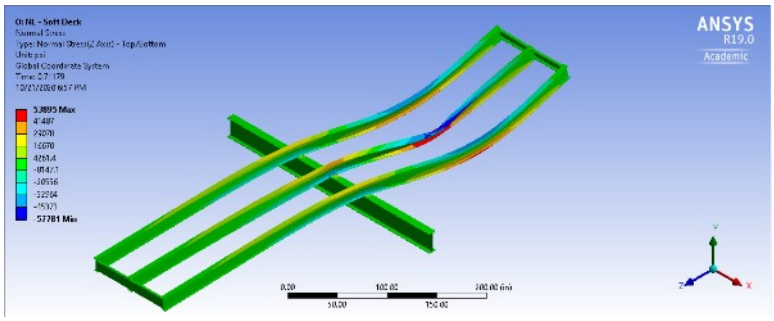

Figure 172. Deck longitudinal normal stress contour, Test Run #45 Failure 3

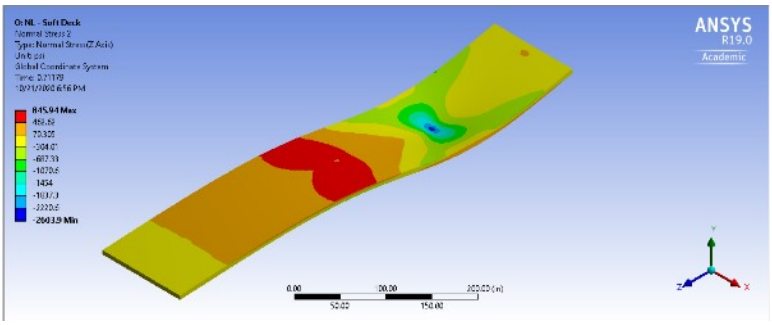

Figure 173. Comparison of FEA and measured vertical deflections, Test Run #45 Failure 3

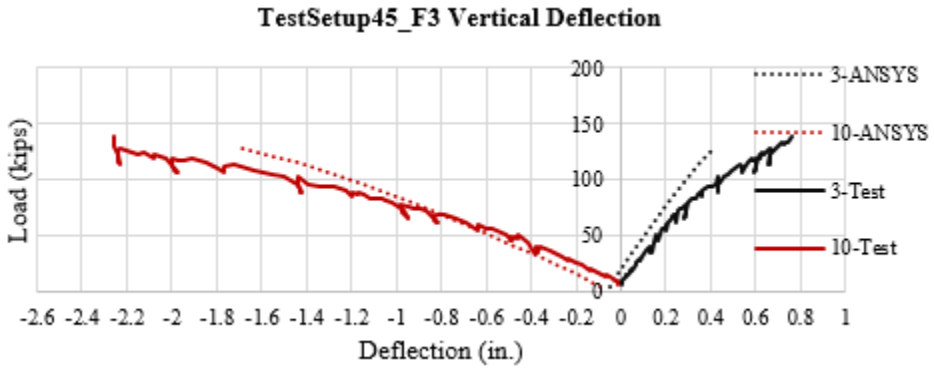

Figure 174. Comparison of FEA and measured lateral deflections, Test Run #45 Failure 3

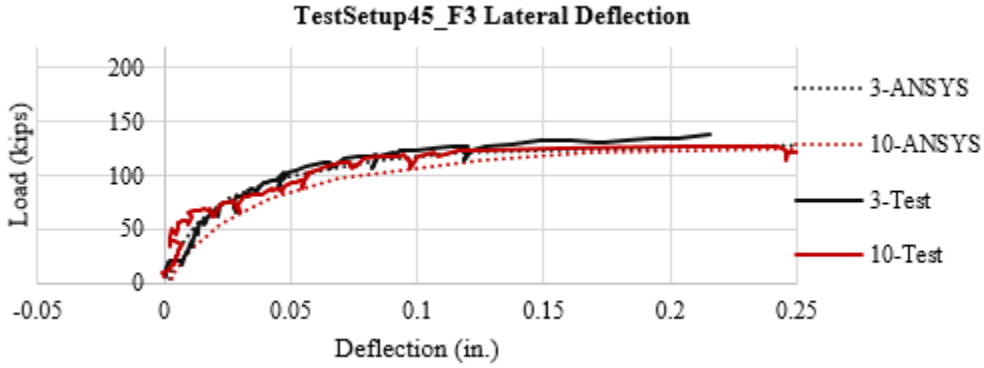

Figure 175. Comparison of FEA and measured axial strains, Loc. 10, Test Run #45 Failure 3

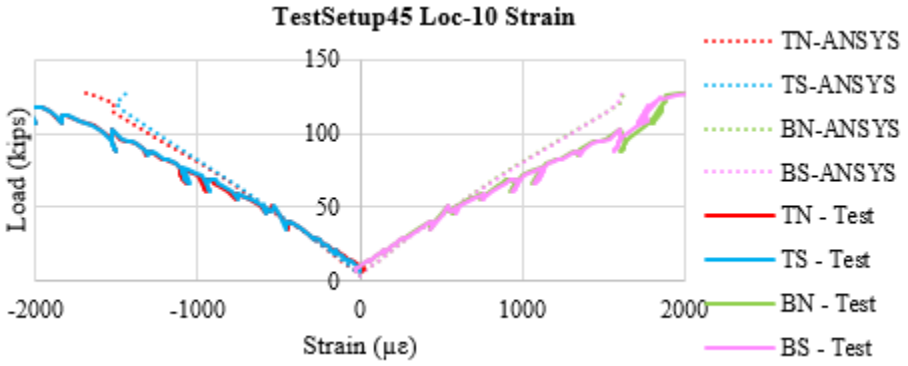

Figure 176. Comparison of FEA and measured axial strains, Loc. 6, Test Run #45 Failure 3

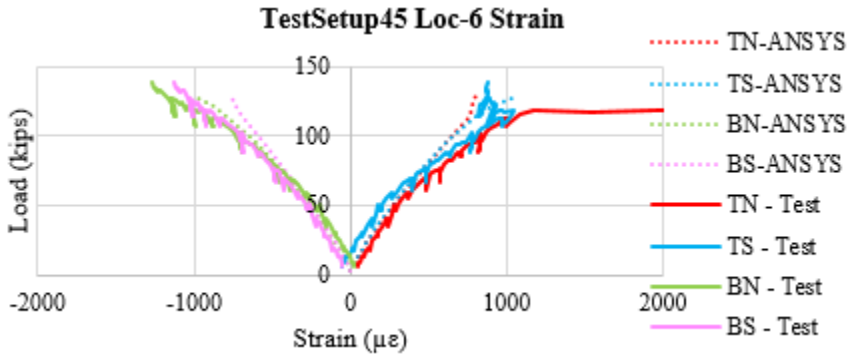

Figure 177. Comparison of FEA and measured axial strains, Loc. 7, Test Run #45 Failure 3

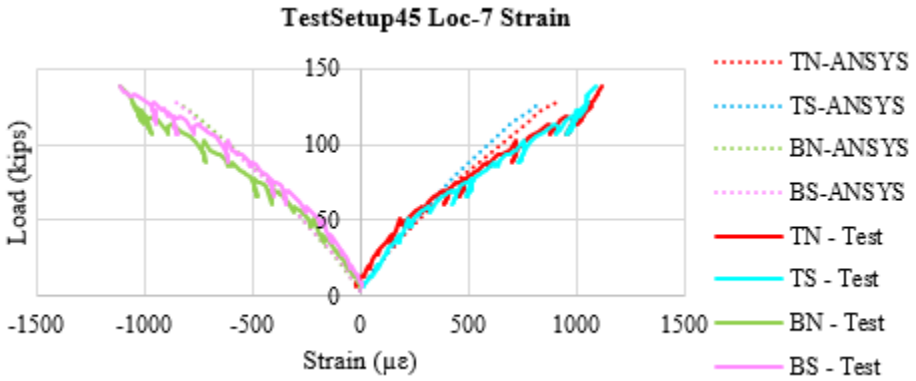

FEA of Representative Bridges

To evaluate the effect of various parameters (e.g., geometry and materials) on LTB strength and moment gradient factors, the representative bridges provided by the DOTD were modeled using FEA. The FEA models were constructed using techniques that matched the calibrated models. Example results for Bridge No. 201810 are presented. The two-span bridge contains C12x25 end diaphragms, W21x68 stringers, and W33x141

floor beams, all of which were manufactured using Grade 33 steel. Each span is 28 ft. long and includes three lines of stringers. The stringers are spaced at 5 ft.- 6 in., and the concrete deck is 16 ft.- 6 in. wide and 7 in. thick. It is assumed that #4 top and bottom deck reinforcement is spaced at 8 in. in both directions and additional #5 bars provided over the floor beam are spaced at 8 in. Rigid interior supports are assumed at the floor beam and the stringers are unbolted to the floor beam.

Non-linear buckling analyses were conducted for two load cases: 1) loading centered at midspan of one span; and 2) loading centered at midspan of both spans. Two vertical loads spaced at 4 ft. longitudinally were applied at one/both locations to match a design tandem. Each vertical load corresponds to an axle load of the design tandem, and the loads are applied to the interior stringer directly. FEA results for the first load case are presented in Figure 178 to Figure 184. Figure 178 and Figure 179 are vertical and lateral deflection contours. The normal stress contour is provided in Figure 180. Load-vertical and load-lateral deflection plots are illustrated in Figure 181 and Figure 182, respectively. Load-longitudinal strain plots for the interior stringer at midspan and at the floor beam are provided in Figure 183 and Figure 184. Each vertical load reaches a maximum of 133.5 kips for the first load case. FEA results for the second load case are presented in Figure 185 to Figure 191. Each vertical load reaches a maximum of 128.6 kips for the second load case. Both load cases show that critical positive and moment sections reach the plastic moment when the peak load is reached. Analyses of another representative bridge provided by DOTD are provided in Appendix VII.

Figure 178. Vertical deflection contour, single span loaded

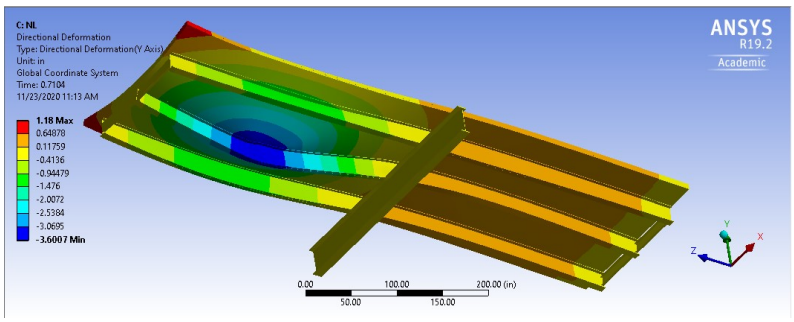

Figure 179. Lateral deflection contour, single span loaded

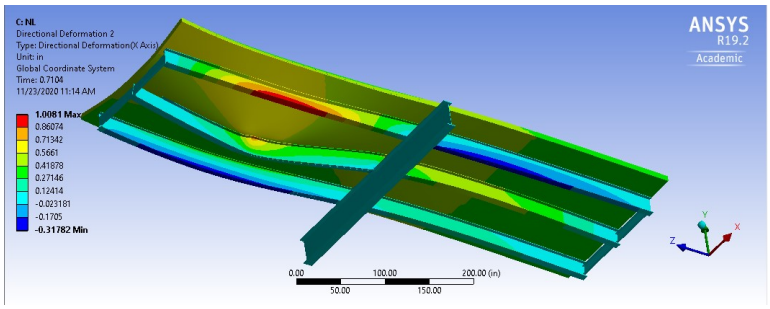

Figure 180. Stringer longitudinal stress contour, single span loaded (deck removed for clarity)

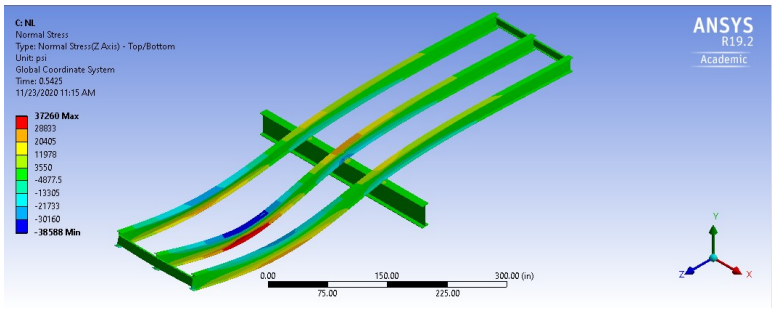

Figure 181. Load-vertical deflection plot, single span loaded

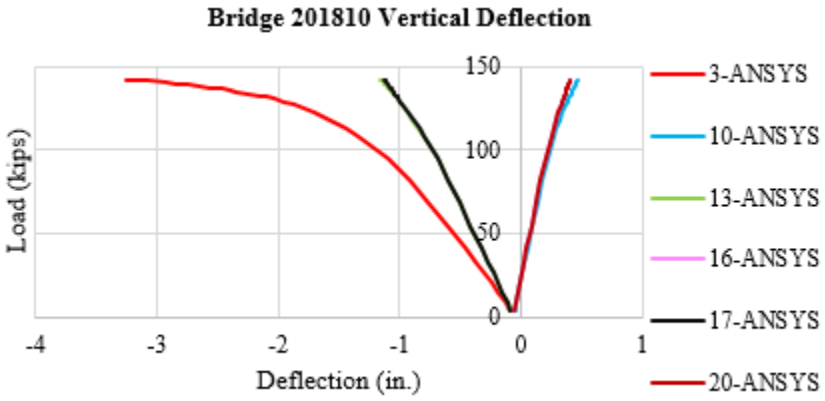

Figure 182. Load-lateral deflection plots, single span loaded

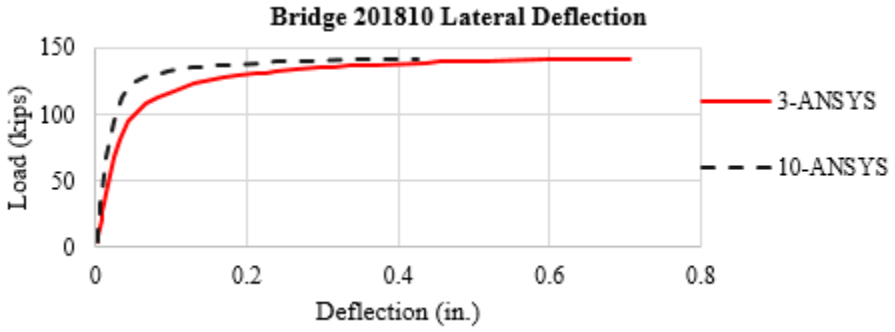

Figure 183. Load-strain plots at Loc. 3, single span loaded

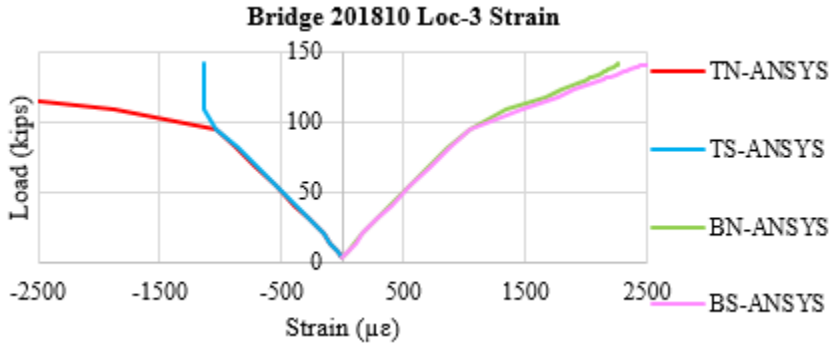

Figure 184. Load-strain plots at Loc. 7, single span loaded

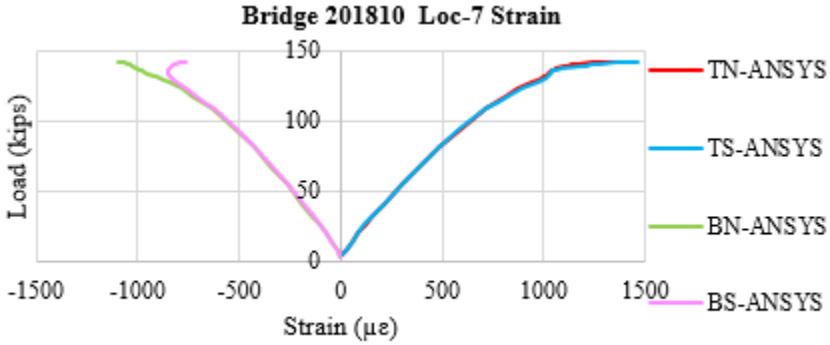

Figure 185. Vertical deflection contour, both spans loaded

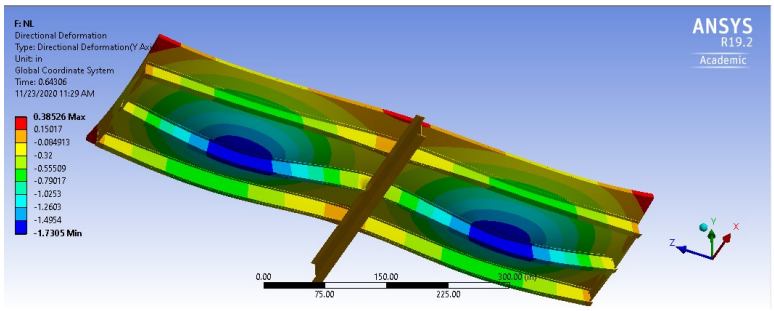

Figure 186. Lateral deflection contour, both spans loaded

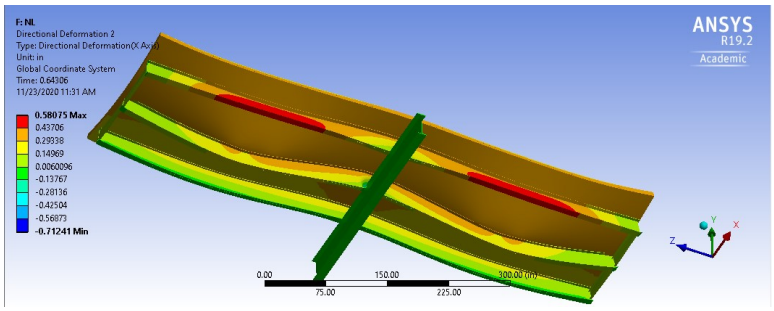

Figure 187. Stringer longitudinal stress contour, both spans loaded (deck removed for clarity)

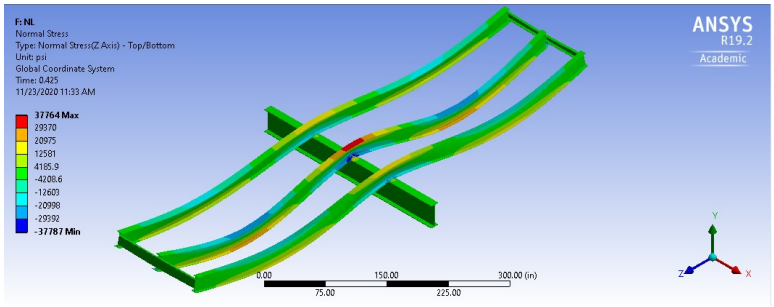

Figure 188. Load-vertical deflection plots, both spans loaded

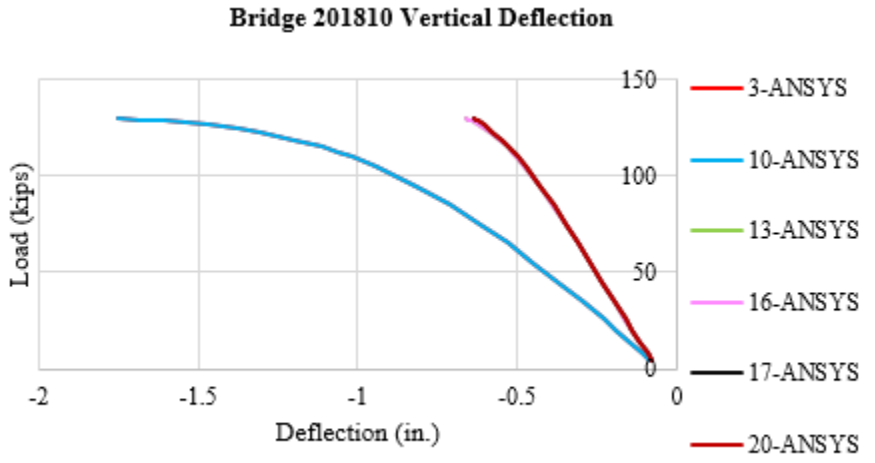

Figure 189. Load-lateral deflection plots, both spans loaded

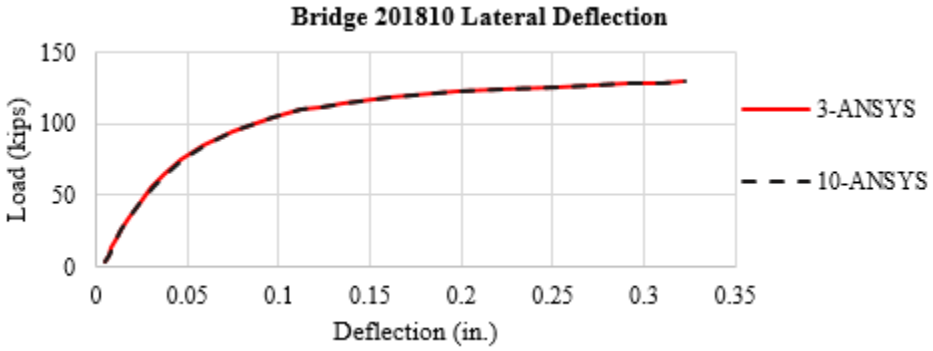

Figure 190. Load-strain plots at Loc. 3, both spans loaded

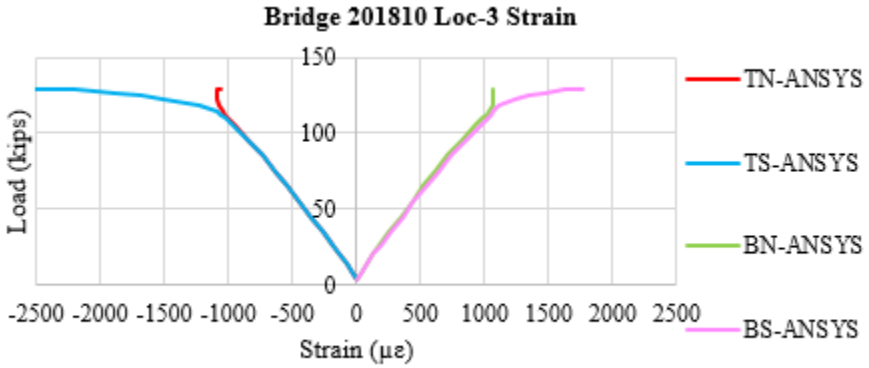

Figure 191. Load-strain plots at Loc. 7, both spans loaded

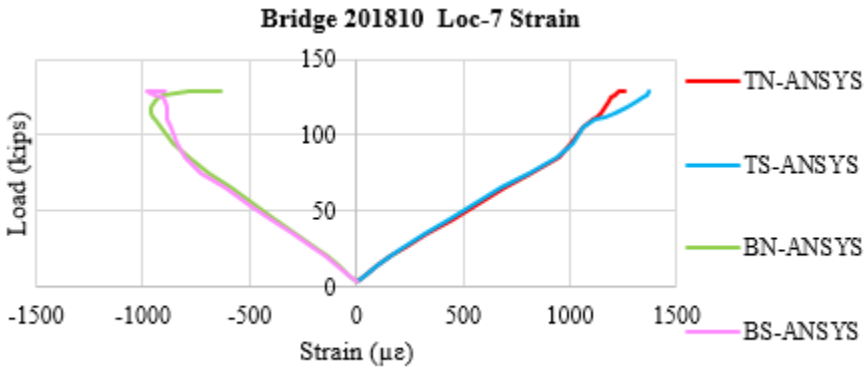

Discussion of Results

Multiple lab tests were conducted to study LTB resistance of continuous stringers with a non-composite deck. The tests helped assess bracing effects provided by the deck and allowed for evaluating effects of floor beam relative stiffness and stringer-to-floor beam connection conditions on LTB. The test data were analyzed to capture axial, primary and out-of-plane bending, and warping torsion normal stress components. FEA models were calibrated against test results to allow for simulating stringer behavior while accounting for various parameters, including rigid and flexible interior (floor beam) supports, and various loading conditions. FEA was shown to provide comparable results with the test data and predict stringer flexural strength.

Lab Testing Findings

Testing data indicated friction occurred between the stringer and deck. Lateral support provided by the deck was identified as significant when Group IV test results were compared to those from the other test groups. When one span was loaded, the unloaded span was subject to negative moment and stringers were unbraced. Stringer top flanges were in tension and laterally supported by the deck, which limited lateral movement and twisting, and therefore, increased flexural strength. The critical stringer positive moment section for the non-composite deck tests reached its yield or plastic moment capacity, while the critical negative moment section was shown to experience moment gradients best represented using C_b between 2.34 and 2.73. When both spans were loaded, the interior stringer was predicted to eventually reach plastic moment at both critical negative and positive moment sections. Detailed test and FEA results are provided in Appendix VII.

Previous research demonstrated that an inflection point cannot be treated as a bracing location unless physical bracing is provided. Lab tests completed herein verified these findings. Also, some researchers determined that even if no mechanical connection is provided between the deck and the stringers, friction may still be adequate to develop the required deck stiffness and act as a lateral brace under wheel load, which they felt justified use of a half span as the unbraced length [22]. Group IV testing results, however, showed that the interior stringer still slightly moved laterally. Therefore, using a half span as unbraced length is not suggested. The full span is recommended as the unbraced length irrespective of stringer-to-floor beam connection conditions.

Moment Gradient Factor

Comparisons between measured flexural strengths and those predicted using the *AASHTO LRFD Bridge Design Specifications* were completed to identify the moment gradient factor. As a result of these comparisons, the equation proposed by Yura and Helwig (2010) is recommended:

$$C_b = 3.0 - \frac{2}{3}\left(\frac{M_1}{M_0}\right) - \frac{8}{3}\left[\frac{M_{CL}}{(M_1+M_0)^*}\right] \quad (29)$$

Using the equation above gives comparable moment gradient factors to those obtained from lab testing (Table 26).

Table 26. Moment gradient factor summary

Test Run	C_b, *tests*	C_b, *Yura and Helwig (2010)*
#45 Failure 1	2.34	2.24
#45 Failure 2	2.58	2.13
#45 Failure 3	2.73	2.07
#46	4.91	5.17

Load Rating

A summary of rating factors (RFs) for the representative bridges calculated using AASHTO LRFD, AISC, and Yura and Helwig (2010) equations is provided (Table 27). RFs were calculated using moment gradient factors from these three sources for HL-93 (Inventory) load at the strength I limit state. Using the moment envelope approach, controlling exterior and interior span moment gradient factors were determined and are listed in the table below. Rating factors are significantly higher when the Yura and Helwig equation is used.

Table 27. Summary of moment gradient and rating factors

Bridge No.	C_b			*RF*		
	AASHTO LRFD	AISC	Yura and Helwig	AASHTO LRFD	AISC	Yura and Helwig
610065	1.07	1.20	2.40	0.33	0.41	1.00
300330	1.06	1.21	2.41	0.57	0.68	1.21
200830	1.00	1.16	2.31	0.52	0.63	1.14
201810	1.05	1.25	2.31	0.45	0.58	1.06
001715	1.00	1.18	2.27	0.09	0.13	0.37

The research team attempted to develop a factor that allowed for envelope moments to reasonably approximate concurrent moments. A continuous bridge was considered consisting of three equal spans varying from 20 to 35 ft. each, with moments determined at an interval of 5 ft. C_b ratios, which represent ratios of concurrent to envelope moments at strength I limit state, are shown in Figure 192. The plot accounts for a variety of live loads, including two design tandems, a single design tandem, a design truck, and lane load. The dead loads include stringer and deck self-weights. Assumed stringer spacings were 6.0, 7.5, and 9.0 ft. and were shown to barely affect the C_b ratios. The figure shows that C_b ratios varied from 1.22 to 1.68 for an interior span and from 1.54 to 2.51 for an exterior span. Therefore, a factor of 1.15 was conservatively recommended to take advantage of the concurrent moment approach in lieu of a more refined analysis.

Figure 192. C_b ratios between the concurrent moment and moment envelope approaches

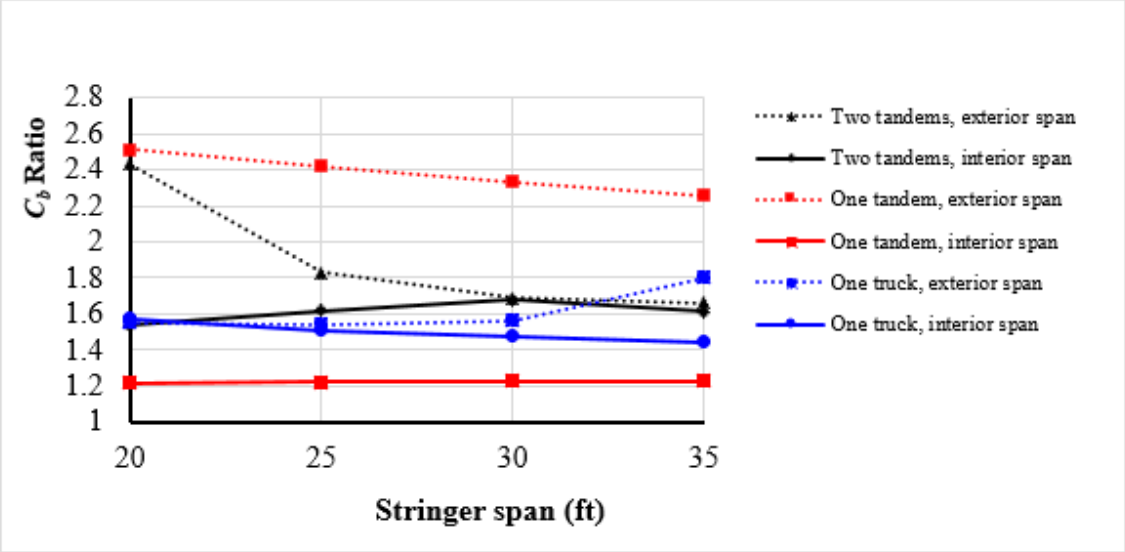

Conclusions and Recommendations

When continuous stringers are load-rated using AASHTOWare Bridge Rating™ analysis software, C_b is determined following the *AASHTO LRFD Bridge Design Specifications*, which may not properly account for bracing effects provided by a non-composite deck and could underestimate available flexural strength. This project was conducted to assess the LTB resistance of continuous stringers and to develop a new approach for rating the stringers using more accurate C_b values.

Full-scale lab testing was performed to examine LTB resistance of a two-span structure that included three lines of continuous stringers. Various bracing types and locations, including steel diaphragms, timber ties, and a non-composite concrete deck, were tested to experimentally establish their effect on LTB resistance. Bolted and unbolted conditions were investigated at the intersection of the stringer and supporting floor beam flanges, and rigid and flexible floor beam conditions were evaluated. Finite element models were calibrated to match lab testing results and non-linear buckling analyses were conducted of representative bridges supplied by the DOTD.

The following conclusions were drawn from the study:

1) The positive moment section of a stringer was observed to be fully braced by the concrete deck. Therefore, the non-composite plastic moment may be used for stringer nominal strength for load rating. The negative moment section, however, should account for LTB resistance subject to various loads. The stringer moment gradient factor can be determined using the equation proposed by Yura and Helwig (2010), which was also included in the Commentary C-F1-5 of the *AISC Specification for Structural Steel Buildings* (2016) [29]:

$$C_b = 3.0 - \frac{2}{3}\left(\frac{M_1}{M_0}\right) - \frac{8}{3}\left[\frac{M_{CL}}{(M_1+M_0)^*}\right] \qquad (29)$$

2) It is recommended to use the full span length as the unbraced length to determine the stringer's flexural strength regardless of whether the stringer bottom flange is braced by the floor beam.

3) The bracing effect provided by the non-composite deck was shown to significantly increase stringer LTB resistance, which results in a moment gradient factor appreciably larger than 1.0 and increases load rating factors. The moment gradient factor can be manually computed, and load-rating factors refined for critical load cases should BrR not provide sufficient rating factors.

4) If the moment envelope approach due to HL-93 (Inventory) loads at the strength limit state results in unacceptable rating factors, C_b can be increased by 15% to take advantage of the concurrent moment approach unless a refined analysis is conducted.

5) Should the stinger be connected to a flexible floor beam; it is conservative to conduct the load rating assuming a rigid interior support. If a refined analysis is necessary, the floor beam can be modelled as a beam element to directly account for its flexural stiffness.

Acronyms, Abbreviations, and Symbols

Term	Description
AASHTO	American Association of State Highway and Transportation Officials
ft.	foot (feet)
in.	inch(es)
LTRC	Louisiana Transportation Research Center
LTB	Lateral torsional buckling
C_b	Moment gradient factor
DOTD	Louisiana Department of Transportation and Development
L	Length of span
L_b	Unbraced length
RF	Rating factor
LRFD	Load and resistance factor design
MBE	Manual of bridge evaluation
DC	Dead load effect due to structural components and attachments
DW	Dead load effect due to wearing surface and utilities
LL	Live load effect
P	Permanent loads other than dead loads
IM	Dynamic load allowance
Φ_C	Condition factor
Φ_S	System factor
Φ	LRFD resistance factor
C	Capacity
γ_{DC}	LRFD load factor for structural components and attachments
γ_{DW}	LRFD load factor for wearing surfaces and utilities
γ_P	LRFD load factor for permanent loads other than dead loads
γ_{LL}	Evaluation live load factor
R_n	Nominal member resistance
LADV	Louisiana Design Vehicle Live Load
F_{max}	Maximum potential compression-flange flexural resistance
F_{yr}	Compression-flange stress at the onset of nominal yielding within the cross section

Term	Description
F_{yc}	Specified minimum yield strength of a compression flange
L_r	Limiting unbraced length to achieve the onset of nominal yielding in either flange under uniform bending
L_p	Limiting unbraced length to achieve the nominal flexural resistance M_p under uniform bending
R_b	Web load-shedding factor
R_h	Hybrid factor
M_{max}	Maximum potential flexural resistance based on the compression flange
HL-93	LRFD design live load
F_{nc}	Nominal flexural resistance of a member
NRL	Notional Rating Load
F_y	Specified minimum yield strength of steel
FLB	Flange lateral buckling
f_1	Stress without consideration of lateral bending at the brace point opposite to the one corresponding to f_2, calculated as the intercept of the most critical assumed linear stress variation passing through f_2 and either f_{mid} or f_0, whichever produces the smaller value of C_b
f_2	Largest compressive stress without consideration of lateral bending at either end of the unbraced length of the flange under consideration, calculated from the critical moment envelope value
f_0	Stress due to the factored loads without consideration of flange lateral bending at a brace point opposite to the one corresponding to f_2
M_A	Absolute value of moment at quarter point of the unbraced segment
M_B	Absolute value of moment at center of the unbraced segment
M_C	Absolute value of moment at three-quarter point of the unbraced segment
M_p	Plastic moment
M_u	Moment due to the factored loads
M_r	Factored flexural resistance
E_s	Elastic modulus of steel
E_c	Elastic modulus of concrete
I_y	Moment of inertia about the minor principal axis of the cross section
I_x	Moment of inertia about the major principal axis of the cross section

Term	Description
C_w	Warping torsional constant
S_x	Elastic section modulus about the x-axis
J	St. Venant torsional constant

References

[1] DOTD, *Bridge Design and Evaluation Manual*, 2019.

[2] AASHTO, *Manual for Bridge Evaluation*, Second Edition, with 2011, 2013, 2014, 2015, and 2016 Interim Revisions, Washington, D.C., 2016.

[3] AASHTO, *LRFD Bridge Design Specifications*, Eighth Edition, Washington, D.C, 2017.

[4] M. Ravindra and T. Galambos, "*Load and Resistance Factor Design for Steel*," vol. 104(9), pp. 1337-1353, 1978.

[5] M. Salvadori, "*Lateral Buckling of I-Beams*," *Transactions of the American Society of Civil Engineers,* vol. 120, no. 1, pp. 1165-1177., 1955.

[6] AISC, *Steel Construction Manual*, Fifteenth Edition, Chicago, IL, 2017.

[7] P. Kirby and D. Nethercot, *Design for Structural Stability*, Halsted Press, 1979.

[8] CSA, Canadian Standards Association. *Canadian Highway Bridge Design Code* S6-14, 2014.

[9] Standards Australia, AS4100 Steel Structures. Sydney, Australia, 1998.

[10] British Standard Institution (BSI), BS5950-1 Structural Use of Steelwork in Buildings – Part1, Code of Practice for Design Rolled and Welded Sections, England, 2000.

[11] Japan Society of Civil Engineers, *Standard Specifications for Steel and Composite Structures*, Tokyo, 2007.

[12] A. López, D. Yong and M. Serna, "*Lateral-Torsional Buckling of Steel Beams: A General Expression for the Moment Gradient Factor*," in *In Proceedings of the International Colloquium on Stability and Ductility of Steel Structures*, September 2006.

[13] L. Subramanian and D. White, "*Reassessment of the Lateral Torsional Buckling Resistance of Rolled I-Section Members: Moment Gradient Tests*," *Journal of Structural Engineering,* vol. 143, no. 4, 2016.

[14] D. White, "*Unified Flexural Resistance Equations for Stability Design of Steel I-Section Members: Overview*," *Journal of Structural Engineering,* vol. 134, no. 9, pp. 1405-1424, 2008.

[15] D. White and S. Jung, "*Unified Flexural Resistance Equations for Stability Design of Steel I-Section Members: Uniform Bending Tests*," *Journal of Structural Engineering,* vol. 134, no. 9, pp. 1450-1470, 2008.

[16] D. White and Y. Duk Kim, "*Unified Flexural Resistance Equations for Stability Design of Steel I-Section Members: Moment Gradient Tests*," *Journal of Structural Engineering,* vol. 134, no. 9, pp. 1471-1486, 2008.

[17] T. Helwig, K. Frank and J. Yura, "*Lateral-Torsional Buckling of Singly Symmetric I-Beams*," *Journal of Structural Engineering,* vol. 123, no. 9, pp. 1172-1179, 1997.

[18] M. Salvadori, "*Lateral Buckling of Eccentrically Loaded I-Columns*," *Transactions of the American Society of Civil Engineers,* vol. 121, no. 1, pp. 1163-1178, 1956.

[19] E. Wong and R. Driver, "*Critical Evaluation of Equivalent Moment Factor Procedures for Laterally Unsupported Beams*," *Engineering Journal,* vol. 47, no. 1, 2010.

[20] J. Yura, "*Bracing for Stability—State-of-the-Art. In Restructuring: America and Beyond*," *ASCE,* pp. 88-103, April 1995.

[21] J. Yura and T. Helwig, "*Buckling of Beams with Inflection Points*," in *Proceedings, Annual Stability Conference*, 2010.

[22] J. Yura, B. Phillips, S. Raju and S. Webb, "*Bracing of Steel Beams in Bridges*," The University of Texas at Austin, 1992.

[23] J. Yura, "*Fundamentals of Beam Bracing*," *Engineering Journal-American Institute of Steel Construction,* vol. 38, no. 1, pp. 11-26, 2001.

[24] S. Vegesna and J. Yura, "*An Ultimate Load Test to Study Bracing Effects of Bridge Decks*," Interior for Transportation Research, University of Texas, 1992.

[25] R. Kissane, "*Lateral Restraint of Non-composite Beams*," New York State Department of Transportation, Engineering Research and Development Bureau, 1985.

[26] D. Linzell, D. Nevling, A. Kollias and J. Laman, "*Experimental and Numerical Response of a 1915 Riveted Through-Girder Bridge*," *Transportation Research Record: Journal of the Transportation Research Board,* vol. 1814 , pp. 127-134, 2002.

[27] R. Ziemian, *Guide to Stability Design Criteria for Metal Structures*, John Wiley & Sons, 2010.

[28] B. Johnston, *Guide to Stability Design Criteria for Metal Structures*, John Wiley & Sons, 1976.

[29] AISC, *Specification for Structural Steel Buildings*, 2016.

To obtain a copy of the appendix or a PDF version with both the report and appendix, please contact project manager and Senior Structures Research Engineer Walid Alaywan, Ph.D., P.E., at (225) 767-9106 or walid.alaywan@la.gov.

This public document is published at a total cost of $200.
29 copies of this public document were published in this first printing at a cost of $200. The total cost of all printings of this document including reprints is $200. This document was published by Louisiana Transportation Research Center to report and publish research findings as required in R.S. 48:105. This material was duplicated in accordance with standards for printing by state agencies established pursuant to R.S. 43:31. Printing of this material was purchased in accordance with the provisions of Title 43 of the Louisiana Revised Statutes.